Dissertation for the degree
of Doctor Scientiarum
Ellen Mengshoel Brevik

Small compounds for targeted radiotherapy

DEPARTMENT OF CHEMISTRY
FACULTY OF MATHEMATICS
AND NATURAL SCIENCES
UNIVERSITY OF OSLO 03/2007

Series of dissertations submitted to the
Faculty of Mathematics and Natural Sciences, University of Oslo.
No. 634

ISSN 1501-7710

Cover: Inger Sandved Anfinsen.
Printed in Norway: AiT e-dit AS, Oslo, 2007.

Produced in co-operation with Unipub AS.
The thesis is produced by Unipub AS merely in connection with the
thesis defence. Kindly direct all inquiries regarding the thesis to the copyright
holder or the unit which grants the doctorate.

Unipub AS is owned by
The University Foundation for Student Life (SiO)

Summary

This thesis describes efforts in synthesising and investigating new tumour-seeking agents for targeted radiotherapy of malignant melanomas and bone-related cancers. The concept of targeted radiotherapy is presented, and selection criteria for therapeutic radionuclides are discussed. Emphasis has been given to the heavier radiohalogens (radioiodine isotopes and ^{211}At) and their labelling chemistry.

Three classes of melanoma-seeking agents have been treated; phenothiazines, cysteaminylphenols and benzamides. Stannylated derivatives of the two latter groups were successfully synthesised and radiohalogenated, resulting in six potential melanoma-seeking agents labelled with radioiodine or ^{211}At. Melanoma affinity and *in vivo* stability were investigated in mice bearing the human melanoma xenografts HHMSX (pigmented) or SESX (non-pigmented). Four derivatives showed high stability to enzymatic dehalogenation *in vivo*, but only the radioiodinated benzamide [^{125}I]IMBA demonstrated promising tumour accumulation and retention in the melanoma models. The results supports previous suggestions of using [*I]IMBA in scintigraphic imaging of pigmented and non-pigmented melanomas. [*I]IMBA may also have a future in scintigraphic imaging of other cancers expressing a high density of sigma-receptors.

The bone-seeking iodobisphosphonate [*I]HIPEBA was labelled with ^{123}I, and its potential for clinical applications in humans was investigated in young pigs. Initial pharmacokinetic properties were studied using dynamic and static gamma-camera imaging, showing superior bone uptake and negligible renal excretion of [^{123}I]HIPEBA compared to ^{99m}Tc-MDP. Estimated radiation doses in humans indicated similar radiotherapeutic properties for [^{131}I]HIPEBA and ^{153}Sm-EDTMP. Hence, [*I]HIPEBA is a promising candidate for diagnostic imaging and targeted radiotherapy of osseous lesions, and further evaluations in humans are justified.

The thesis gives an extended overview of the work, presenting additional experiments and results to those described in the papers.

List of papers

I E. M. Brevik, E. Årstad, P. Hoff.
An improved synthesis of an ^{125}I- and ^{211}At-labelled benzamide for melanoma imaging. Proceedings of the 14th Radiochemical Conference, Mariánské Lázně 14–19 April 2002, Czech Republic. *Czech. J. Phys.* **53** (2003), Suppl.A A725–A729

II E. M. Brevik, E. Årstad, P. Hoff.
Synthesis and biodistribution of *N*-(2-diethylaminoethyl)-3-[^{211}At]astato-4-methoxybenzamide for targeted radiotherapy of malignant melanoma.
Manuscript. *To be submitted to Melanoma Research.*

III E. M. Brevik, E. Årstad, F. O. Levy, P. Hoff.
Evaluation of ^{125}I- and ^{211}At-labelled benzamides for targeting of σ_1-receptors in an amelanotic melanoma xenograft.
Manuscript. *To be submitted to Melanoma Research.*

IV E. M. Brevik, K. H. Holm, D. S. Wilbur, D. K. Hamlin, P. Hoff.
Syntheses and preliminary biodistribution studies of radioiodinated cysteaminylphenol derivatives for malignant melanoma.
Manuscript. *To be submitted to Nuclear Medicine and Biology.*

V E. M. Brevik, A. Skretting, S. Bruheim, T. Bach-Gansmo, E. Årstad, P. Hoff.
Pharmacokinetic properties and bone surface uptake of 1-hydroxy-(*m*-[^{123}I]iodophenyl)ethylidene-1,1-bisphosphonic acid (^{123}I-HIPEBA) in pigs: implications for targeted radiotherapy.
Manuscript. *To be submitted to Nuclear Medicine Communications.*

Acknowledgements

The present work was carried out at the Nuclear Chemistry group, Department of Chemistry, University of Oslo, in collaboration with scientists at the Norwegian Radium Hospital and Department of Radiation Oncology, University of Washington, Seattle, USA. The study was initiated as part of a master degree. Post-graduate work was made possible through a grant from the Norwegian Research Council which is greatfully acknowledged.

I would like to express my gratitude and thanks to my supervisors Professor Per Hoff, for initiating this doctoral thesis and allowing me to pursue my diverse ideas (whether fruitful or not), and Chief scientist Kjetil H. Holm, for your chemical expertise, enthusiasm and dedication in solving the obstacles which emerged during organic syntheses.

I deeply appreciate the contributions from Professor Arne Skretting, for your expertise and guidance in medical physics and nuclear medicine, and Professor D. Scott Wilbur, for your great hospitality, interesting discussions and inspiring enthusiasm for this project.

Thanks are also due to:
Don K. Hamlin, for your friendship and helpfulness in every way. Erik Årstad, for including me in the bisphosphonate project and for accurate and quick guidance. Skjalg Bruheim and staff at the Norwegian Radium Hospital, for all help and assistance with the animal experiments. Kurt Allan Krobert, my right-hand and instructor in pharmacology. Eivind Atle Olsen, for production of ^{211}At at the OCL cyclotron.

I am greatful to collegues and fellow students in the Nuclear Chemistry group, in particular Håvar, Liv and Jorolf, for your friendship and support over many years.

Thanks to my family and friends, for reminding me of life outside Blindern and for backing me up in doing this "cancer stuff".

Finally, my profound gratitude goes to Håvar and Eirik, for your endless love, support and patience.

Ellen Mengshoel Brevik

Contents

Part I

INTRODUCTION

Chapter 1

Introduction

The prognosis of surviving cancer has improved over the years. However, only 50 % of Norwegian patients are alive five years post-diagnosis [1]. Hence, development of more efficient cancer treatments is a major challenge in cancer research.

Successful curative therapy requires complete removal or destruction of malignant cells. However, for many malignancies there are no effective treatment for patients with extensive metastatic spread of the disease. Advances and research in alternative and improved treatment methods for metastatic cancer disease are highly required.

Systemic targeted radiotherapy is a promising modality for treatment of disseminated cancers. The concept is based on selective irradiation of malignant cells by means of radionuclides attached to "tumour-seeking" molecules. Interest in this treatment modality has increased over the years due to new developments of available radionuclides and carrier molecules.

In this thesis focus has been on developing new radiopharmaceuticals for targeted radiotherapy of two different forms of cancer where standard treatment modalities have failed or have had limited success. *Part I* presents therapeutic radionuclides for targeted radiotherapy, with emphasis on radioiodine isotopes, the α-emitter astatine-211 and their labelling chemistry. *Part II* presents the efforts in developing new radiohalogenated melanoma-seeking agents for diagnosis and targeted radiotherapy of metastatic malignant melanomas. *Part III* concentrates on the investigation of a radioiodinated bisphosphonate with potential in palliative treatment and targeted radiotherapy of osteosarcoma and bone metastases.

Chapter 2

Background

2.1 Targeted radiotherapy of cancer

When tumours or metastases cannot be removed by surgery, the conventional therapeutic approach is external beam radiotherapy and chemotherapy. However, these treatments show low selectivity for cancer cells and tumour tissues, and might be damaging or cytotoxic to healthy tissues when applied at curative levels.

An attractive alternative is to exploit a biological or chemical characteristic of the specific cancer or the affected tissue. In favourable cases, molecules with affinity for a specialised biological feature may function as specific, "tumour-seeking" agents (e.g. antibodies, antibody fragments, peptides, small molecules with tumour affinity). Targeted radiotherapy involves such agents incorporating a suitable therapeutic radionuclide, ideally giving site-specific radiation treatment of the primary tumour and its metastases while producing minimal radiation damage to surrounding normal tissues [2]. Thus, the choice of carrier molecule and radionuclide must be adjusted to the type of tumour or metastasis with regard to biological properties, size, geometry and localisation relative to dose-limiting organs.

2.2 Therapeutic radionuclides and radiobiology

Important criteria in the choice of suitable therapeutic radionuclides include physical, chemical, biological and economical aspects. Methods for rapid and specific labelling chemistry producing radioactive agents with a chemically stable label are crucial. The half-life of the radionuclide must allow time for chemistry, purification, logistics and maximal (intra)cellular retention when distributed *in vivo*. The energy deposition of the emitted radiation must be considered, and the daughter nuclide(s) should have properties minimising the radiation burden to healthy tissues. The selection of therapeutic radionuclides is furthermore limited

by cost and availability [3].

After considering these restrictions, a suitable therapeutic radionuclide is essentially chosen due to the quality of the emitted radiation expressed by the linear energy transfer (LET). In terms of causing a biological effect (irreparable damages to DNA, cell death), the focus is set on ionising radiation from radionuclides emitting charged particles [4]. Particles with high ionisation densities (high LET-values) have a direct interaction with tissue, inducing irrepairable double strand breaks in DNA. This effect is optimal for particles having a LET-value about 100 keV/μm, i.e. when the distance between ionising events along the particle track coincides with the distance between the strings of the DNA double helix [5]. Particles with low LET-values predominantly have an indirect interaction with tissue caused by radiation-induced radicals. Thus, the probability of inducing irreparable double strand breaks in DNA is strongly reduced. However, the effect of low-LET radiation depends not only on the applied radiation dose, but also on dose rate, number of dose fractions, the cell cycle and the use of radioprotectors and radiosensitisers [5].

Clinical radionuclide therapy has so far been limited to a few β^--emitting radionuclides and a few types of tumours [2, 6].

2.2.1 Radionuclides emitting β-particles

The majority of current clinical applications in targeted radiotherapy involve the β^--emitters ^{131}I, ^{32}P, ^{90}Y and ^{89}Sr [7, 8]. The β-particles have low LET-values (range 0.2–1.0 keV/μm) and a modest relative biological effectiveness (RBE). However, β-emitters are readily available at low cost and offer a wide choice of candidates in terms of particle energies and chemical properties. The emitted β-particles have a tissue range of several millimeters (Table 2.1) and are well suited for treatment of larger tumour masses and tumours with a heterogenous uptake (through crossfire irradiation). The use of highly energetic β-particles is restricted by the radiation burden and cell damages to surrounding healthy tissues, and especially by the suppression of activity in red bone marrow.

2.2.2 Radionuclides emitting α-particles

The use of α-emitting radionuclides has a major advantage in radiotherapy of cancer. The α-particles have mean LET-values of 80–100 keV/μm, close to maximal RBE and a cell-killing efficiency independent of biological and chemical factors [5]. The high cytotoxicity and short tissue range (30–100 μm) restrict the cell-killing to a few cells surrounding the α-emitting radionuclide [9]. Thus, a carrier molecule incorporating a suitable α-emitter might induce a radiotherapeutic effect on tiny clusters of cancer cells, micrometastases and single-cell diseases, minimising the radiation doses to red bone marrow and healthy tissues.

Table 2.1: Data on some potential radionuclides for targeted radiotherapy.

Nuclide	**Half-life**	**Decay mode**[a]	**E_β max (MeV)**	**E_α max (MeV)**	**γ-energy (keV)**[b]	**Mean particle tissue range**
^{32}P	14.26 d	β^-	1.7	-	-	$\sim$ 3.0 mm
^{89}Sr	50.5 d	β^-	1.5	-	(909)	$\sim$ 2.4 mm
^{90}Y	64.1 h	β^-	2.3	-	(2186)	$\sim$ 3.6 mm
^{117m}Sn	13.6 d	e^-	-	-	159	0.3 mm[c]
^{125}I	59.41 d	EC[d], e^-	-	-	35	$\sim$ 1 μm
^{131}I	8.02 d	β^-	0.6	-	364	$\sim$ 0.7 mm
^{149}Tb	4.1 h	EC, α, β^+	1.8	3.97	352	$\sim$ 28 μm[e]
^{153}Sm	46.27 h	β^-	0.7	-	103	$\sim$ 0.8 mm
^{166}Ho	26.8 h	β^-, e^-	1.9	-	81	$\sim$ 3.2 mm
^{177}Lu	6.71 d	β^-	0.5	-	208	$\sim$ 0.5 mm
^{186}Re	89.25 h	β^-, EC	1.1	-	137	$\sim$ 1.1 mm
^{188}Re	16.98 h	β^-	2.1	-	155	$\sim$ 3.4 mm
^{211}At	7.22 h	EC, α	-	5.87	(687)	55–80 μm
^{212}Bi	60.6 min	β^-, α	2.3	6.05	727	50–90 μm[e]
^{213}Bi	45.59 min	β^-, α	1.4	5.87	440	50–90 μm[e]
^{223}Ra	11.43 d	α	-	5.72	269	$<$ 100 μm
^{224}Ra	3.66 d	α	-	5.69	241	$<$ 100 μm
^{225}Ac	10.0 d	α, e^-	-	5.83	100	$<$ 100 μm[e]
^{227}Th	18.7 d	α, e^-	-	6.04	236	$<$ 100 μm[e]
^{255}Fm	20.1 h	α, sf, e^-	-	7.02	(81)	$\sim$ 100 μm[e]

[a] EC = electron capture, e^- = conversion electrons, β^- = electron emission, β^+ = positron emission, α = alpha emission, sf = spontaneous fission.

[b] Intensities <1 % are given in brackets.

[c] Conversion electrons emitted by ^{117m}Sn are monoenergetic (0.13 MeV).

[d] Abundance of Auger-electrons >100 %.

[e] The α-particle range.

Only a few α-emitters are suitable for targeted radiotherapy of cancer, e.g. ^{211}At, ^{212}Bi, ^{213}Bi, ^{223}Ra, ^{224}Ra, ^{225}Ac, ^{227}Th, ^{255}Fm and ^{149}Tb (Table 2.1) [9, 10]. Among these, only ^{211}At, ^{212}Bi, ^{213}Bi and ^{223}Ra have been extensively evaluated *in vivo* for use in cancer therapy. The bismuth-isotopes are bound to chelating agents by complexation [11, 12], while ^{223}Ra simply is used as $^{223}RaCl_2$ [13]. Astatine is chemically quite similar to iodine and can be incorporated into an aromatic compound by covalent bonding [14–16]. The isotope ^{211}At has been regarded as the most promising and versatile α-emitter studied for radiotherapy of cancer so far [3, 15].

2.2.3 Radionuclides emitting low-energy electrons

Other therapeutical alternatives are radionuclides emitting Auger- or low-energy conversion electrons (Table 2.1). These particles are characterised by a high ionisation density over a very short range in tissue; $\sim$0.3 mm for conversion electrons and subcellular ($\sim 1\,\mu$m) for Auger-electrons [2, 17–19]. Thus, a maximal radiobiological effect is obtained when the Auger-electron emitters are located within the nuclei of cancer cells.

A future possibility in targeted radiotherapy is to combine the efficient single-cell killing properties of α-particles and DNA-associated Auger-emitters, with β-particles eliminating larger malignancies mainly by crossfire irradiation.

2.2.4 Radionuclide pairs for imaging and radiotherapy

The dosimetry of radionuclide therapy depends on quantitative *in vivo* uptake measurements of the therapeutic agents. Pre-therapy imaging, particularly positron emission tomography (PET), can improve the accuracy of such estimates provided that two radionuclides of the same element are used successively for imaging and radiotherapy. Examples of such radionuclide pairs for PET-imaging/radiotherapy are ^{83}Sr/^{89}Sr, ^{86}Y/^{90}Y and ^{124}I/^{131}I. The radionuclide ^{64}Cu is also very interesting as it combines β^+-, β^-- and Auger-electron emissions in its decay [7].

2.3 Radiohalogens

Several radiohalogens are important in the development of new radiopharmaceuticals aiming at diagnostic imaging or radiotherapy [16]. Radiohalogens emitting high yields of photons with an energy of 100–400 keV (e.g. ^{123}I) may be used in single photon emission computed tomography (SPECT). The positron-emitting radiohalogens ^{18}F, ^{75}Br, ^{76}Br and ^{124}I are interesting for PET-imaging [20], while radiohalogens emitting α-particles, β^--particles or

Auger-electrons have properties suitable for radiotherapeutic applications. In this thesis, the radionuclides ^{123}I, ^{124}I, ^{125}I, ^{131}I and ^{211}At deserve special attention.

2.3.1 Important radioiodine isotopes

The ^{123}I ($t_{1/2}$ 13.2 h) decays through electron capture with emission of 159 keV γ-rays, resulting in almost optimal gamma-camera performance in SPECT. This radionuclide also emits Auger-electrons, thus it may be an attractive candidate for radiotherapeutic applications.

The ^{124}I ($t_{1/2}$ 4.15 d) disintegrates by electron capture and emission of up to 2.13 MeV β^+-particles. The radionuclide benefits from a longer half-life than most standard PET-isotopes, but high-energy positrons might result in loss of spatial resolution in PET-images compared to ^{18}F. Emission of high-energy γ (>603 keV) may be a limiting factor for clinical applications.

The ^{125}I ($t_{1/2}$ 59.41 d) disintegrates by electron capture, emitting 35 keV γ and conversion electrons. The emission of Auger-electrons makes ^{125}I an interesting radionuclide for micro-tumour therapy, but the physical half-life is too long for clinical applications. Hence, this radionuclide is mainly used preclinically due to its easy handling and storage.

The ^{131}I ($t_{1/2}$ 8.02 d) disintegrates by β^--decay (0.6 MeV) with a main accompanying γ-energy of 364 keV. The radionuclide is considered suitable for therapeutic applications, but it is not ideal for imaging purposes due to the radiation dose caused by the emitted β^--particles. However, ^{131}I is the most commonly used radionuclide in radiotherapy, particularly in the treatment of thyroid cancers and non-malignant thyroid disorders.

2.3.2 Astatine-211

The α-emitting radionuclide ^{211}At ($t_{1/2}$ 7.22 h) disintegrates following a branched decay scheme as illustrated in Figure 2.1. In the first branch, the ^{211}At decays by emission of 5.87 MeV α-particles to ^{207}Bi ($t_{1/2}$ 31.55 y), which disintegrates by electron capture to stable

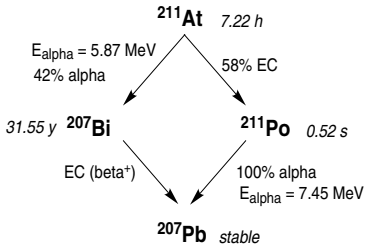

Figure 2.1: Decay scheme for ^{211}At.

^{207}Pb. The second branch involves decay by electron capture to ^{211}Po ($t_{1/2}$ 0.52 s), followed by an emission of 7.45 MeV α-particles giving stable ^{207}Pb. Hence, the mean energy of the emitted α-particles is 6.7 MeV, resulting in a mean LET value of 97 keV/μm and a tissue range corresponding to 55–80 μm from the point of decay. This high LET-value and short tissue range make ^{211}At particularly attractive for radiotherapy of micrometastatic cancers or in applications where single cells are targeted. However, diffusion of the ^{211}Po daughter might reduce the total tumour radiation dose [21]. Decay of ^{211}Po results in polonium K X-rays (77–92 keV) which enable sample-detection as well as external imaging using SPECT. The general use of astatine is limited by the lack of long-lived astatine-isotopes and few production facilities for ^{211}At.

2.4 Radiohalogen labelling chemistry

Several requirements have to be fulfilled when labelling a compound with a radionuclide. In general, the labelling chemistry should be fast, regiospecific, reproducible and give a stable, labelled product in high radiochemical yield. With short-lived radionuclides, labelling in the last reaction step is often advantageous, reducing the loss of radioactivity, time for synthesis and purification as well as exposure. The specific radioactivity of the product should normally be as high as possible (starting with no-carrier-added radionuclides), and the compound should retain its original biological properties after radiolabelling. Radiolysis has to be taken into account in the labelling procedure, particularly when using high-LET radionuclides like ^{211}At [22, 23]. The *in vivo* stability of the radiolabelled product is of paramount importance if the substance is to be used as a radiopharmaceutical. Thus, the choice of labelling method is crucial for an optimal production of a radioactive preparation.

Most radiohalogenations (except for fluorinations) are conducted as electrophilic substitution reactions. Electrophilic reactions require formation of an electrophilic radiohalogenation reagent through oxidation of halide ions:

$$X^- \rightleftarrows X^{\delta+}$$

Electrophilic halogen species can be obtained *in situ* by using various oxidising agents, e.g. chloramine-T, *tert*-butyl-hydroperoxide (TBHP), *N*-chlorosuccinimide (NCS) and *N*-iodosuccinimide (NIS) [24].

2.4.1 Direct radiolabelling of small aromatic compounds

Strongly activated aryl compounds (e.g. phenols, anilines and *N*-alkyl-anilines) are readily radiohalogenated *via* a direct electrophilic halogenation using an appropriate oxidising agent:

$$\text{Ar–H} + {}^{*}\text{X}^{\delta+}\text{–X}^{\delta-} \rightarrow \text{Ar–}{}^{*}\text{X} + \text{H–X} \qquad \text{where X = Cl, Br, I} \qquad \text{or}$$

$$\text{Ar–H} + {}^{*}\text{X}^{+}\text{–A}^{-} \rightarrow \text{Ar–}{}^{*}\text{X} + \text{H–A}$$

where *X is the radiohalogen and A is a more electronegative group than *X. The radiolabelling reaction will primarily give monohalogenated products with the radiohalogen incorporated *ortho* or *para* to the activating substituent. Direct halogenation may also be used for moderately activated aryl compounds, but the radiochemical yields might be significantly reduced due to side reactions.

Direct electrophilic radioiodinations are very common, giving aryliodides with high chemical stability [24, 25]. Direct electrophilic fluorinations, chlorinations and brominations require harsh oxidising conditions, while astatinations give products with poor stability due to weak carbon–astatine bonds [26]. For example, the phenolic ring is too activated to produce stable compounds with astatine [25]. A limitation of this labelling method is the formation of isomeric product mixtures which may be difficult to separate.

2.4.2 Indirect radiolabelling of small aromatic compounds

Radiohalogens can be labelled regiospecifically into moderately or non-activated aromatic rings using indirect labelling methods. The two most common methods include incorporation of radiohalogens *via* decomposition of aryl diazonium salts or *via* organometallic intermediates [24, 25]. For labelling reactions with radioiodine and ^{211}At, the use of organometallic precursors or compounds incorporating an organoboron cage are preferred [27].

Halodemetallations are used for regiospecific labelling of a substrate molecule at the organometallic site, giving radiohalogenated products in high radiochemical yields using mild labelling conditions and short reaction times. Different organometallic intermediates have been studied, e.g. organothallium compounds, organomercury compounds, organostannanes, organosilanes and organogermanes. The outcome of a halodemetallation is affected by the metal, chemical labelling conditions as well as steric factors [14, 24].

Halodemetallation with group 14 metals

Organometallic precursors containing a group 14 metal (Si, Ge, Sn) are advantageous when labelling with radiohalogens [14, 24, 28]. Aryltrialkylmetal precursors facilitate the no-carrier-added syntheses of radiolabelled arylhalides, described by the reaction mechanism in Figure 2.2:

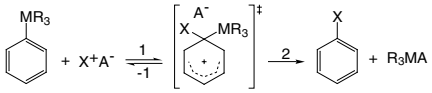

Figure 2.2: Proposed reaction mechanism of the halodemetallation using aryltrialkyl group 14 organometallic precursors, from Refs. [14, 24].

where X^+–A^- is a halonium-anion species, and M is silicon, germanium or tin. The alkyl substituent R introduces a $+I$ inductive effect[1] facilitating formation of the σ-complex intermediate, while electron release by the -MR_3 group decreases the possibility of competitive halodeprotonations. An alternative and competing reaction mechanism goes *via* a radical-ion-pair intermediate which collapses to the same σ-complex as shown in Figure 2.2 [29].

The carbon–metal bond dissociation energy and the covalent radius of the metal decrease in the order Si < Ge < Sn, resulting in increased reaction rates and increased radiochemical yields of the labelled arylhalides. While the radiochemical yield of a halodestannylation is more or less unaffected by the labelling conditions, the efficiency of a halodesilylation is influenced by the choice of solvent, oxidising agent, radionuclide, alkyl substituent R, substituent(s) on the aromatic ring and pH [14, 30]. However, high radiochemical yields may also be obtained for organosilicon compounds by optimising the labelling conditions. In general, the use of silylated compounds have an advantage due to low toxicity and greater chemical inertness during multi-step syntheses.

The required aryltrialkylmetal precursors can often be synthesised from lithiated organic compounds. Radiohalogenated derivatives are produced when treating this precursor with a radiohalogen using a mild oxidising agent.

[1]The term $+I$ is used for functional groups being electron-donating relative to hydrogen.

2.5 Structure determination of radioiodinated and astatinated compounds

Structural assignment of a radioiodinated or astatinated compound can be predicted with a good degree of certainty from the expected product of the corresponding non-radioactive iodination [24, 28]. If the starting compound contains an activated aromatic ring (e.g. phenol or aniline) and is treated with electrophilic radioiodine, the location of the radioactive label in the product is a function of the $+I$ and $+M$ effects[2] of the aromatic substituent(s) [31, 32]. If the compound is labelled by a substitution reaction, the label should appear in the place of the leaving group (e.g. in iodine for bromine exchange, iododediazonisation or iododemetallation).

These structural assignments are made on the basis of analogy with non-radioactive reactions. However, reactions with no-carrier-added radionuclides may proceed very differently due to the drastic change in ratios between reagents and the higher possibility of side effects produced by minor impurities in the reaction mixture. To analyse a radioiodinated or astatinated compound, its behaviour in various forms of chromatography is measured and compared to the non-radiolabelled, iodinated compound. Chromatographic investigations are normally performed by radio-HPLC [14, 28].

[2]The terms $+I$ and $-I$ describe field effects operating through space, solvent molecules or σ-bonds. The terms $+M$ and $-M$ describe resonance effects operating through π-electrons.

Part II

MALIGNANT MELANOMA

Chapter 3

Malignant melanoma

Malignant melanoma is the least common but most serious type of skin cancer. The incidence is increasing rapidly, and the rates are doubled every 10–20 years in countries with white populations [33]. Malignant melanoma is particularly common in Australia, New Zealand and Scandinavia, and it is the most frequent cancer type for men (age 30–54) and young women (age 15–29) in Norway [1, 34]. It is assumed that genetic susceptibility and occasional exposure to high levels of ultraviolet radiation are the most important risk factors.

Human malignant melanoma represents a difficult diagnostic and therapeutic challenge. Survival is good provided early diagnosis and surgical resection of the primary tumor when it is thin ($<$1 mm) and has no nodal spread [33]. Surgery is often accompanied by radiation therapy, chemotherapy or immunotherapy. However, malignant melanoma is characterised by an early stage metastasis for which there is no effective therapy; cancer chemotherapy has failed, immunotherapy is virtually ineffective, and the majority of malignant melanomas are resistant to radiation [35, 36]. Hence, targeted α-particle radiotherapy is an appealing treatment modality for malignant melanoma.

The development of new melanoma-seeking agents for targeted radiotherapy warrants an understanding of the biological and chemical properties characteristic for malignant melanomas.

3.1 Origin and subtypes of malignant melanoma

Malignant melanoma is a cancer predominantly originating from pigment-producing cells (nevi) in the skin. Less frequently, primary melanomas are also found in other pigmented organs, e.g. eyes (uveal melanoma). The most common types of melanoma in the skin are superficial spreading melanoma, nodular melanoma, acral lentiginous melanoma and lentigo maligna melanoma. The different types of melanoma may or may not produce the pigment

melanin. Amelanotic (non-pigmented) melanomas are rare and normally form cutaneous nodules, while melanotic (pigmented) melanomas are more common and very malignant types of cancer.

3.2 Melanogenesis

A biological uniqueness of most melanocytes and malignant melanomas is the biosynthesis of melanin. Melanin is a dark pigment of complex polymer structure which is produced in highly specialised intracellular organelles (melanosomes) in the melanocytes. Microgranules of melanin are transferred to epithelial cells and form the pigment found in hair, epidermis, eyes and in *substantia nigra* in the brain [37, 38].

The melanogenesis begins with the oxidation of tyrosine (**1**) by the enzyme tyrosinase to give the activated compound dopaquinone (**2**). Dopaquinone can react *via* two different pathways to give the pigment polymers eumelanin and pheomelanin (Figure 3.1). The high reactivity of *ortho*-quinone **2** chemically controls the early process of melanogenesis, and the availability of the protein cysteine determines the ratio of eumelanin to pheomelanin [39–41]. However, the melanogenesis is a complex process which is highly regulated by enzymes, receptors and hormones under genetic control, and where the different steps of the melanin synthesis occur spontaneously dependent on the available concentrations of H^+, metal ions, reducing agents, thiols and oxygen [42].

Melanin and many melanin-related metabolites subserve several different protective functions, e.g. photoprotection, metal binding, scavenging of toxic oxygen radical species as well as inflammatory and immune reactions [35, 37, 43, 44]. The process of melanogenesis, however, represents a potential cellular hazard due to the formation of toxic *ortho*-quinone metabolites. The *ortho*-quinones are highly reactive chemical species which undergo addition reactions with glutathione (GSH), sulphydryl (SH) enzymes such as DNA polymerase and other proteins and nucleic acids, causing cell inactivation or irreversible damages and cell death [44].

Most malignant melanomas show an enhanced biosynthesis of melanin and an increased expression of tyrosinase. Thus, the chemistry of the melanogenesis may be exploited in the development of new melanoma-seeking agents for diagnosis and therapy of this malignancy.

3.3 Sigma-receptors

Another feature of many malignant melanomas is the high expression of sigma-receptors. The sigma (σ) receptor system consists of σ_1- and σ_2-receptors, and it is unique and different from other neurotransmitter and hormone receptor families [45]. Sigma-receptors are membrane-bound proteins found in the central nervous system, liver, kidneys, lungs, gonads and ovaries,

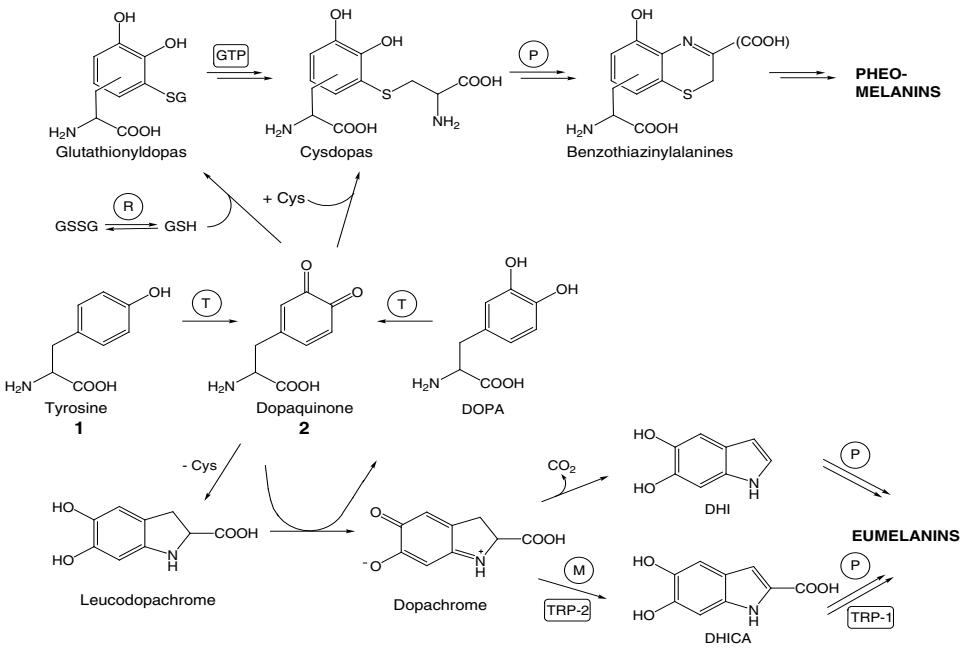

Figure 3.1: The synthesis of the melanin polymers eumelanin and pheomelanin, starting with the tyrosinase oxidation of tyrosine (**1**) to give dopaquinone (**2**). Cys = cysteine, GSH = glutathione, T = tyrosinase, M = metal ions, GTP = glutamyltranspeptidase, R = glutathione reductase, P = peroxidase, TRP-1 = DHICA oxidase, TRP-2 = dopachrome tautomerase (from Refs. [41, 43]).

as well as in certain tumour tissues [46]. Thus, sigma-receptors have been proposed as targets for selective binding of radiopharmaceuticals to cancers with an overexpression of sigma-receptors, e.g. malignant melanoma, breast cancer and prostate cancer cells [46–52]. The sigma-receptor system also provides a means to target amelanotic melanomas.

3.4 Radiolabelled melanoma-seeking agents

Random metastatic dissemination of melanoma requires a systemic treatment reaching all melanoma cells. This may be achieved using melanoma-seeking compounds carrying radionuclides with therapeutic properties (Sections 2.2–2.3).

Several melanoma-seeking radiopharmaceuticals have been developed (Table 3.1), but none has so far achieved general clinical application in treatment of malignant melanomas [53]. The main obstacles have been low selectivity for melanoma tissue and low sensitivity in scintigraphic imaging detection of metastases. Thus, development of new radiolabelled melanoma-seeking agents showing a selective uptake by the melanoma cells is critical.

There are a number of strategies for developing new melanoma-seeking agents. One approach is based on the use of tyrosinase analogues designed to maximise the generation of reactive *ortho*-quinones [44]. A selective method currently under development is based on the release of a cytotoxic agent from a prodrug during melanogenesis (melanocyte-directed enzyme-activated prodrug therapy, MDEPT) [44, 55–57]. The approaches most commonly used for developing melanoma-seeking radiopharmaceuticals are based on the incorporation of radiolabelled false precursors of melanin into the pigment polymers, or the use of radioactive agents with a general affinity for melanin [44]. Compounds that bind to melanin are numerous, while compounds incorporated in pigment polymers during melanogenesis are examplified by derivatives of phenylalanine [58, 59], cysteaminylphenol [36, 60–63] and thiouracil [64–66].

In this work focus has been on three different classes of melanoma-seeking agents, having different uptake-mechanisms and, thus, different abilities to target melanotic and amelanotic melanomas. The background for selecting phenothiazine, cysteaminylphenol and benzamide derivatives is presented in Sections 3.4.1–3.4.3.

3.4.1 Phenothiazine derivatives

In the 1950s it was found that the antipsychotic drug chlorpromazine (**3**) and several other derivatives of phenothiazine (**4**) exhibited high affinity for uveal pigment and bonded intracellulary to melanin (Figure 3.2) [67]. Thus, several derivatives with the phenothiazine structure were investigated as melanoma-seeking agents. The derivative 3,7-(dimethylamino)phenazathionium chloride (methylene blue, MTB **5**) was particularly

Table 3.1: Melanoma-seeking radiopharmaceuticals (from Refs. [53, 54]).

Uptake tests	^{32}P-phosphate
	^{3}H-DOPA
Labelled drugs	^{131}I-chloroquine
	^{131}I-chlorpromazine
Aspecific tracers	^{67}Ga-citrate
	^{57}Co-bleomycin
	^{111}In-porphyrin
	^{201}Tl-chloride
	^{99m}Tc-sestamibi
Metabolic tracers	^{123}I-methyltyrosine
	^{123}I/^{131}I-iodoquinoline derivatives
	^{123}I/^{131}I-5-iodo-2-thiouracil derivatives
	^{123}I-iodobenzamide derivatives
	^{123}I-*N*-isopropyl-*p*-iodoamphetamine (IMP)
	^{123}I/^{131}I-metaiodobenzylguanidine (MIBG)
	^{18}F-fluorodeoxyglucose (FDG)
	^{11}C-methionine (MET)
Peptides	^{111}In-pentetreotide
	^{123}I-vasoactive intestinal peptide (VIP)
	^{111}In-alpha-melanocyte stimulating hormone (MSH)
	^{212}Pb-DOTA-Re(Arg^{11})CCMSH
Monoclonal antibodies	e.g. ^{131}I-anti-p97 Mab/F(ab)$_2$ fragments
	^{99m}Tc-225.28 S F(ab)$_2$ fragments
	^{99m}Tc-NR-ML-05
	^{111}In-ZME-018
Immunoreactive agents	Radiolabelled immunoreactive cells
	^{99m}Tc-interleukin-2
	^{99m}Tc-J001X

interesting, showing very high affinity for melanin and a strong charge transfer complex with the melanin polymers resulting in a selective accumulation in pigmented melanomas [68, 69].

Link *et al.* have synthesised and evaluated radioiodinated and astatinated MTB-derivatives (**7** and **8**, Figure 3.2) as potential radiopharmaceuticals for diagnosis and radiotherapy of metastasised melanomas [68–75]. The reported results showed 95 % inhibition of tumour growth with ^{211}At-MTB in pigmented melanoma models *in vivo* [68, 72] and good sensitivity using ^{123}I-MTB or ^{131}I-MTB in scintigraphic detection of melanoma metastases in patients [73, 75]. Hence, ^{211}At-labelled MTB **8** and related thionin derivatives are promising agents for selective and efficient radiotherapy of pigmented melanoma and its metastases.

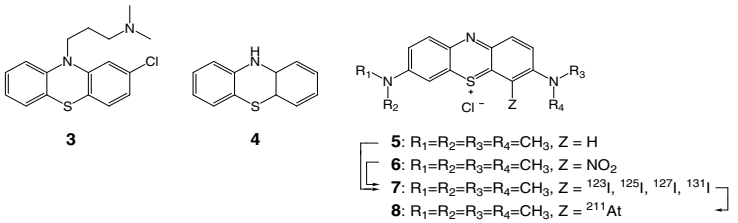

Figure 3.2: Chemical structures of chlorpromazine (**3**) and phenothiazine (**4**), and a general thionin structure representing MTB **5**, methylene green **6** and the radiohalogenated MTB-derivatives **7** and **8** previously investigated as melanoma-seeking agents.

3.4.2 Cysteaminylphenol derivatives

The enzyme tyrosinase is capable of oxidising a variety of natural and synthetic phenols, giving rise to highly reactive and cytotoxic *ortho*-quinones which may be incorporated into the melanin polymers [37, 76]. Thus, several phenolic compounds have been evaluated as chemotherapeutic agents for malignant melanoma [77], of which the 4-*S*-substituted cysteaminylphenols **9** (Figure 3.3) have been particularly promising [36, 60, 62, 63, 78–83].

Jimbow *et al.* have been leading the development of new cysteaminylphenol derivatives, evaluating their biochemistry, melanocytotoxicity and antimelanoma effects *in vitro* and *in vivo* [36, 60, 61, 78–80, 84–96]. Experiments have shown that melanin-incorporated 4-*S*-cysteaminylphenol (4-*S*-CAP **10**) inhibited tumour growth and increased the life span of mice bearing the murine B16 melanoma model [36, 78, 84, 88, 90]. The *N*-acetylated derivative *N*-acetyl-4-*S*-cysteaminylphenol (*N*-acetyl-4-*S*-CAP **11**) has demonstrated similar or better properties *in vivo*. Results with **11** have shown high melanocytotoxicity through depigmentation of black hair follicles, promising antimelanoma effects in murine B16F10 melanoma

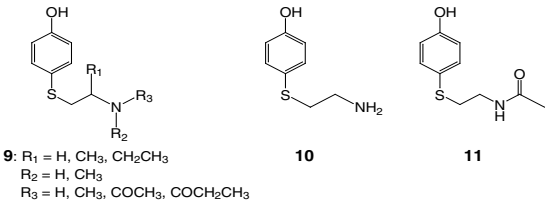

Figure 3.3: Examples of cysteaminylphenols investigated as melanoma-seeking agents.

colonies in mouse lungs and selective accumulation into murine B16 melanomas and pigmented human melanoma xenografts [36, 78, 84, 85, 87, 90]. Thus, it has been suggested that *N*-acetyl-4-*S*-CAP **11** may be a valuable model for developing radiohalogenated agents for early detection of metastasis, staging, follow-up and targeted radiotherapy of pigmented malignant melanoma [86, 93].

3.4.3 Benzamide derivatives

Radioiodinated benzamide derivatives were first studied as central nervous system D-2 dopamine receptor imaging agents [97]. By coincidence, their affinity for melanocytes was found by uveal uptake in mice [98]. The exact mechanism of benzamide accumulation in melanocytes is unknown, however, uptake has been directly linked to the biosynthesis of melanin [53, 99]. Radioiodinated benzamides also exhibit moderate to high affinity for sigma-receptors found in melanoma cell membranes [47, 49, 100, 101], but the significance of this contribution is debated [48, 99].

The melanin affinity of numerous radioiodinated benzamides have been evaluated [48, 49, 98, 100, 102–106], and the *N*-(2-dialkylaminoalkyl)-4-[*I]iodobenzamide derivatives **12** (Figure 3.4) have gained particular interest [98, 103, 107, 108]. Several derivatives of **12** have been explored in detection of melanoma metastases using SPECT, and a phase II scintigraphic clinical trial evaluating *N*-(2-diethylaminoethyl)-4-[^{123}I]iodobenzamide ([^{123}I]BZA **13**) resulted in a diagnostic sensitivity of 81 % on a lesion basis and a specificity of 100 % [107].

The introduction of an electrondonating phenyl substituent resulted in a series of new benzamides, of which the radioiodinated derivative *N*-(2-diethylaminoethyl)-3-[*I]iodo-4-methoxybenzamide ([*I]IMBA **14**) showed superior melanoma/non-target tissue dose ratios and improved contrast in scintigraphic images of pigmented and non-pigmented metastases in patients [104, 109]. It has been suggested that uptake of **14** in non-pigmented melanomas was due to the σ_1-receptor affinity of this compound (K_i = 249 ± 17 nM) [48, 109]. Thus, radiohalogenated derivatives of IMBA **14** may have a future in targeted radiotherapy of both

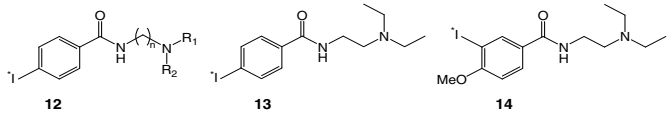

Figure 3.4: Examples of benzamides investigated as melanoma-seeking agents.

melanotic and amelanotic malignant melanomas.

3.5 Aims of study

The objective of this study was to synthesise radioiodinated and astatinated melanoma-seeking agents and evaluate their prospective use in diagnosis and targeted radiotherapy of malignant melanoma and its metastases. The specific aims:

- Synthesise derivatives of MTB **5**, *N*-acetyl-4-*S*-CAP **11** and IMBA **14** labelled with ^{125}I, ^{131}I or ^{211}At.
- Characterise *in vivo* stability and melanoma affinity of the astatinated and radioiodinated derivatives in melanoma-bearing mice.

Chapter 4

General methods

4.1 Radioactivity measurements

University of Oslo, Norway: Radioactivity measurements of radioiodinated and astatinated compounds were carried out using the radioisotope dose calibrators CRC-127R (Capintec Inc.) or VDC-304 (Veenstra Instrumenten bv.). The radioactivity content in excised organs was measured with an 1480 WIZARD automatic gamma counter (Wallac) or using a 20 % Ge-detector measuring the polonium K X-rays of the ^{211}At-daughter ^{211}Po.
University of Washington, Seattle, USA: Radioactivity measurements of the radioiodinated compounds were performed on a Capintec CRC-15R radioisotope calibrator (Capintec Inc.), and radioactivity content in tissue samples was measured in a LKB 1282 automatic gamma counter (Wallac).

4.2 Production and distillation of ^{211}At

The ^{211}At was produced at the Scanditronix MC-35 cyclotron, Oslo Cyclotron Laboratory, University of Oslo, through bombardment of stable bismuth with 29 MeV helium ions *via* the ^{209}Bi(α, 2n)^{211}At reaction. Targets were prepared by melting ^{209}Bi metal into a circular cave (diameter 25.4 mm, depth 0.50 mm) in the aluminium target backings (42 x 40 x 3 mm), and the bismuth was polished to a uniform 0.25 mm thick layer prior to use. The target backside was water-cooled during irradiation (1–2 h), and the production efficiency was ∼35 MBq ^{211}At/μAh using a beam intensity of 5-10 μA [110].

The dry-distillation method was adopted from Lindegren *et al.* [111]. The still consisted of a quartz tube inserted into a tubular oven. A custom-made teflon fitting connected the outlet of the quartz tube to the condensing unit which consisted of a PEEK-capillary loop immersed into a bath of dry-ice and ethanol (-77 °C). Any volatile astatine escaping the

condensation trap was forced through a gas wash-bottle containing aqueous $Na_2S_2O_5$ and traps with activated carbon.

The quartz tube was preheated for 1–2 h at 700–750 °C while flushing with nitrogen. The irradiated target was placed in a smaller quartz tube which rapidly was pushed into the center of the still. Astatine vapourised in the still for 1–10 min and condensed in the PEEK trap when evacuating the system. The PEEK tubing was dismounted, and astatine was recovered in 0.5 mL methanol.

The ^{211}At-distillation was conducted in a fume hood in a certificated type B laboratory using two pairs of gloves, a fresh-air mask with carbon filters (RACAL Safety Limited, UK) and a body dosimeter to monitor the radiation dose recieved from x-rays and γ-radiation. The laboratory was continuously monitored for airborne α-particles by a high sensitivity ion-chamber (LASK radon counter, Norway).

4.3 Chromatography

Analytical high-performance liquid chromatography (HPLC) is a very convenient method for rapid purification and isolation of small radiolabelled compounds. It is also an efficient tool for making preparations of radiolabelled agents for biological studies *in vivo*. If the mobile phase consists of solvents which are non-toxic or easily removed, an isolated product is simply dissolved in physiological phosphate buffered saline (20 mM, pH 7.4) and sterile filtered prior to use.

One of the radio-HPLC systems applied in this work used a general method which was applicable on a number of different compounds (Chapter 6 and Paper **IV**). It was based on separation by reversed phase radio-HPLC using a nonpolar C-18 surface modified silica column (stationary phase) and a polar, linear gradient elution system consisting of aqueous acidic acid and an increasing amount of methanol (mobile phase) [27]. The components in the mixture were separated as a function of polarity; the more hydrophilic components were eluted first, while the more lipophilic components eluted under relatively high methanol concentrations.

The other radio-HPLC system was a result of systematic studies involving ionic strength, inorganic additives and pH, and was highly optimised for separation of the radiolabelled benzamides [^{125}I]IMBA **14b** and [^{211}At]AMBA **54** (Papers **I**–**III**) [112]. The system was based on a PLRP-S 100 Å styrene-divinylbenzene column (stationary phase) and a polar mobile phase run under isocratic conditions, giving a similar elution of molecules as in reversed phase HPLC. However, the PLRP-S 100 Å column has the advantage of a broader pH stability range (pH 1–14) and a higher surface area than a C-18 column, making it particularly well suited for rapid separation of small molecules.

Detailed specifications of radio-HPLC systems, instruments and detectors are found in the respective papers (Papers **I**–**IV**).

4.4 Animals

Male and female athymic Balb/c nude mice (Balb/c nu/nu) were bred in the nude rodent facility at the Norwegian Radium Hospital (Chapter 6 and Papers **II**–**III**) or the University of Washington, Seattle, USA (Paper **IV**). The mice were kept under specific pathogen-free conditions at constant temperature (24–26 °C) and humidity (30–50 %). Sterilised food and tap water were supplied *ad libitum*. Housing and all procedures involving animals were performed according to protocols approved by the animal care and use committee at the Norwegian Radium Hospital in compliance with the National Committee for Animal Experiment's guidelines on animal welfare [113, 114], or by the University of Washington's Institutional Animal Care and Use Committee in compliance with the NIH guidelines [115]. The animals were anaesthetised as described in the respective papers (Papers **II**–**IV**).

4.5 Tumour models

The malignant melanoma xenograft lines used in this work were established in athymic mice from metastases of patients admitted to the Norwegian Radium Hospital [116, 117]. The melanoma line HHMSX is highly metastatic and melanotic (Chapter 6 and Paper **II**), while the SESX line is an amelanotic melanoma model (Paper **III**).

4.6 Statistics

Data were expressed as mean values with standard deviations (SD) where $n = 3$ or $n = 4$. Probability calculations were made by the two-tailed Student's t-test with 5 % significance limits.

Chapter 5

Phenothiazine derivatives

5.1 Introduction

In this part of the study, the aim was to synthesise new radioiodinated and astatinated derivatives of the promising phenothiazine derivative MTB **5**. Previous studies have evaluated *I- and ^{211}At-labelled MTB-derivatives with the radiohalogen located on the thionin structure. In this study, the idea was to connect the thionin structure to a chemical moiety carrying the radioactive halogen. It was assumed that this strategy would result in derivatives with the same melanoma-seeking behaviour as **5**, and perhaps increase the melanoma uptake due to an increased lipophilicity. Introduction of an appropriate leaving group should facilitate radiolabelling reactions with *I and ^{211}At. The MTB-derivative 3-dimethylamino-7-methylaminophenothiazin-5-ylium chloride (Azure B **15**, Figure 5.1) was chosen as starting agent, facilitating regiospecific reactions at the secondary amine function.

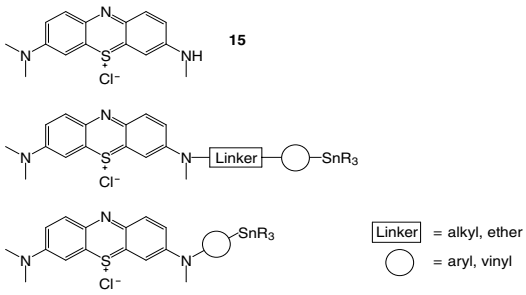

Figure 5.1: Chemical structure of Azure B **15** and general structures of the proposed target molecules with and without a linker to the trialkylstannyl moiety, respectively.

5.2 Results and discussion

In the work with Azure B **15** the main challenge was to synthesise a derivative incorporating a trialkylstannyl function. The chosen strategy was to connect **15** to a chemical moiety incorporating a trialkylstannyl leaving group, either directly or by using a linker. General structures of the proposed target molecules are depicted in Figure 5.1.

Wilbur *et al.* have described and exploited the general applicability of the stannylated aromatic activated ester Bu_3SnAr-OTFP **16** for introduction of a chemical moiety with a trialkylstannyl group through the formation of an amide bond [27, 118]. Thus, the stannylated ester **16** was synthesised following the procedures depicted in Figure 5.2. The 4-iodobenzoic acid (**17**) reacted with 2,3,5,6-tetrafluorophenol using EDC as a coupling agent to give iodide **18** (83 %). The iodinated ester was converted into **16** (33 %) using Bu_6Sn_2 in a palladium(0)-catalysed stannylation. Reaction procedures are described in Ref. [118], and spectroscopic data are summarised in Appendix C.

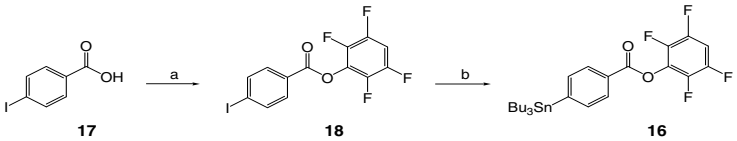

17 **18** **16**

Figure 5.2: Reaction scheme for synthesis of the iodinated activated ester **18** and the stannylated derivative **16**. Reagents and conditions: a) 2,3,5,6-tetrafluorophenol, EDC, EtOAc, rt; b) Bu_6Sn_2, $[Ph_3P]_4Pd$, toluene, reflux.

Although reported in low yield, *N*-alkylation on the secondary amine function in Azure B was assessed to be the shortest route to a derivatised analogue [119]. Thus, the first approach involved the introduction of a linker between **15** and the stannylated activated ester **16**. Feigenbaum *et al.* have reported the reaction of *N*-*tert*-butoxycarbonyl-2-chloroethylamine (**19**) and Azure B **15**, giving the intermediate **20** which decomposed to *N*-(2-aminoethyl)-Azure B **21** on heating [119]. Based on this, a synthetic approach aiming at the stannylated Azure B derivative **22**, and subsequently the radiohalogenated derivatives **23** and **24**, was suggested as indicated in Figure 5.3.

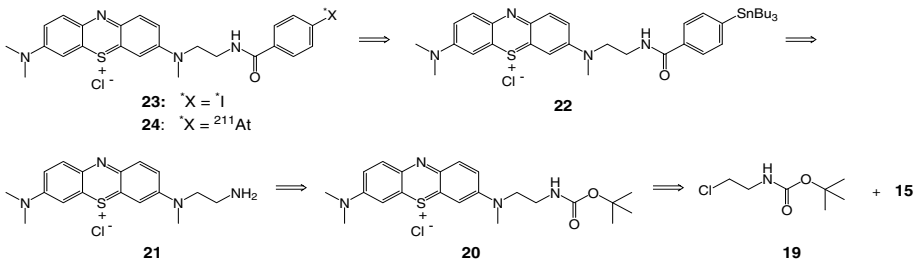

Figure 5.3: Retrosynthetic analysis of the ^{125}I- and ^{211}At-labelled Azure B derivatives **23** and **24** and the stannylated precursor **22**.

The linker reagent **19** was synthesised in 84 % yield from $(BOC)_2O$ and 2-chloroethylamine hydrochloride following the procedures of Feigenbaum *et al.* [119]. However, the subsequent reaction between **15** and **19** was in our hands not reproducible. Neither the reported product *N*-(2-aminoethyl)-Azure B **21** nor the intermediate **20** were possible to identify.

Several experiments were conducted trying to connect potential linkers or other reactive compounds to the secondary amine function of Azure B **15** (summarised in Figure 5.4), but all product mixtures obtained were complex, and proper purification and identification of the different components were not achieved.

The second approach was based on direct incorporation of a trialkylstannyl moiety to Azure B. It was suggested that **15** might react with the activated ester **16** *via* its secondary amine function, giving the stannylated amide **25** and the radiohalogenated derivatives **26** and **27** (Figure 5.5). However, once more the product mixture obtained was very complex, and the stannylated Azure B derivative **25** was not identified (Figure 5.6).

Later, another group working with Azure B experienced the same kind of problems as those mentioned above [120]. Hence, the Azure B project was abandoned, and time did not allow to pursue alternative routes to MTB-derivatives [121–123].

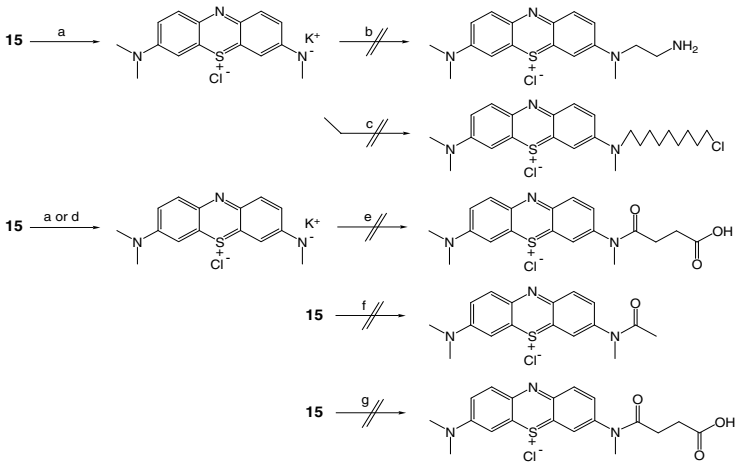

Figure 5.4: Summary of the different reactions performed in the efforts of synthesising an Azure B derivative with a linker. Reagents and conditions: a) $(CH_3)_3COK$, DMSO, rt; b) *N-tert*-butoxycarbonyl-2-chloroethylamine (**19**), Δ; c) 1-chlorodecane, rt; d) $(CH_3)_3COK$, 4-DMAP, DMSO, rt; e) Succinic anhydride, rt; f) Acetic anhydride, 4-DMAP, pyridine, rt; g) Succinic acid, Ph_3P, NCS, CH_2Cl_2, 0 °C.

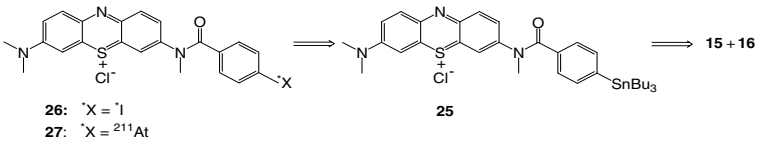

Figure 5.5: Retrosynthetic analysis of the ^{125}I- and ^{211}At-labelled Azure B derivatives **26** and **27** and the stannylated precursor **25**.

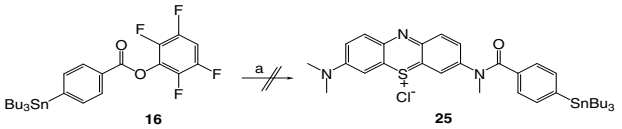

Figure 5.6: Reaction scheme for synthesis of the stannylated precursor **25**. Reagents and conditions: a) *i*) Et_3N, DMF, rt; *ii*) Azure B **15**, rt.

Chapter 6

Cysteaminylphenol derivatives

6.1 Introduction

In this part of the study, focus has been on synthesising new radioiodinated and astatinated derivatives of the promising cysteaminylphenol *N*-acetyl-4-*S*-CAP **11**. The chosen strategy was to synthesise halogenated derivatives of **11**, and derivatives with the same biologically active structure as **11** having the halogen label located on a more distant chemical moiety. It was assumed that all these derivatives would show similar melanoma-seeking behaviour as **11**. The latter group would probably show higher *in vivo* stability, as well as higher tumour accumulation due to a higher lipophilicity. However, rapid renal excretion and clearance should be expected for all cysteaminylphenol derivatives [124, 125]. The radiohalogenated derivatives **28b**, **29**, **30b** and **31** were chosen as target molecules (Figure 6.1).

It has been postulated that phenols incorporating a sulphur atom are better substrates for tyrosinase, giving rise to an increased accumulation in pigmented tissues [60, 84]. Hence, the radioiodinated tyramine homologues **32b** and **33b,c** (Figure 6.1) were pursued for comparison with the corresponding cysteaminylphenol derivatives in a pigmented melanoma model *in vivo*.

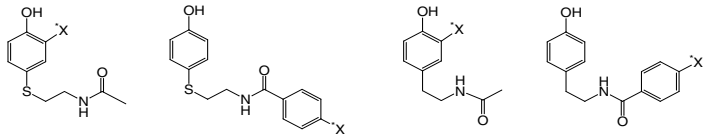

28b: *X = ^{125}I
29: *X = ^{211}At

30b: *X = ^{125}I
31: *X = ^{211}At

32b: *X = ^{131}I

33b: *X =^{125}I
33c: *X = ^{131}I

Figure 6.1: Chemical structures of the proposed target molecules **28b**–**33c**.

6.2 Chemistry

6.2.1 Synthesis

Synthetic efforts toward *N*-[2-(4-hydroxy-3-tributylstannyl-phenylsulphanyl)-ethyl]acetamide (34) and its iodo derivative 28a

In the study of melanoma-seeking cysteaminylphenol derivatives, the first target molecule chosen was the cysteaminylphenol *N*-[2-(4-hydroxy-3-iodo-phenylsulphanyl)ethyl]acetamide (**28a**) and its radiohalogenated analogues **28b** and **29** (Figure 6.2). A synthetic approach to **28b** and **29** was suggested to proceed *via* the stannylated precursor *N*-[2-(4-hydroxy-3-tributylstannyl-phenylsulphanyl)ethyl]acetamide (**34**) as depicted in Figure 6.2. The stannylated precursor might be synthesised by standard stannylation reactions from the corresponding *ortho*-halogenated cysteaminylphenols **28a** or **35**, which should be obtained by direct halogenation of **11**. Both cysteaminylphenols *N*-acetyl-4-*S*-CAP **11** and 4-*S*-CAP **10** would be synthesised following literature procedures [60, 93].

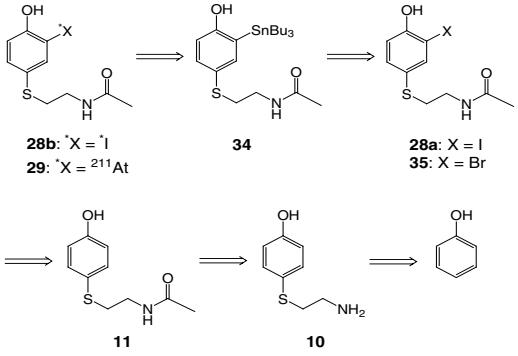

Figure 6.2: First retrosynthetic analysis of the stannylated precursor **34**.

Miura *et al.* have reported the synthesis of **10** by refluxing phenol and cystamine dihydrochloride in 47 % HBr [60]. Thus, cysteaminylphenol **10** was synthesised accordingly, followed by *N,O*-acetylation and subsequent saponification of the phenolic acetyl group to give **11** (Figure 6.3) [93]. However, the chemical yields of **10** and **11** were low (∼10 %), and subsequent direct bromination or iodination of these compounds were unsuccessful.

The next strategy suggested direct halogenation of 4-mercaptophenol (**36**) producing the dihalogenated disulphides **37** and **38**, which may be reduced to two thiols and converted into **28a** or **35** *via* the Wehrmeister reaction [126, 127]. However, analysis of the reaction product

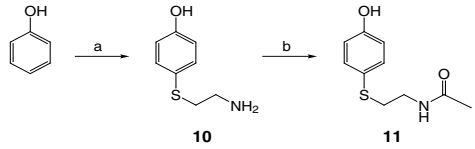

10 **11**

Figure 6.3: Literature procedure for synthesising the cysteaminylphenols **10** and **11** (Refs. [60, 93]). Reagents and conditions: a) cystamine dihydrochloride, 47 % HBr, reflux; b) *i*) Ac_2O, pyridine, rt; *ii*) NH_3, MeOH, rt.

revealed close to quantitative yields of the disulphide **39** (Figure 6.4). All attempts in introducing halogen in the aromatic ring gave very complex product mixtures and were therefore rejected. It was assumed that the halogenations did not work out as expected due to the sulphur atom interfering with the halogenation reactions. Sulphur is easily oxidised and most sulphur ethers are unsuitable as protecting groups if exposed to iodine [128]. Consequently, the synthetic approach involving direct halogenation of sulphur compounds was abandoned.

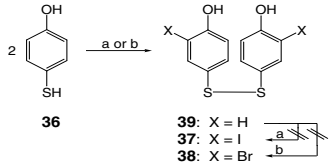

Figure 6.4: Halogenation of 4-mercaptophenol (**36**) gave the disulphide **39** in close to quantitative yields. The halogenated derivatives **37** and **38** were not obtained. Reagents and conditions: a) I_2, Et_2O, H_2O, rt; b) Br_2, Et_2O, H_2O, rt.

A new strategy was outlined using an *ortho*-halogenated phenol which could react with a suitable sulphur derivative in the *para*-position (Figure 6.5). The method of Miura *et al.* should give the *ortho*-halogenated derivative of **10**, but the prospects of low yields and a mixture of isomers made this approach less appealing [60, 86]. However, Kita *et al.* have reported the *para*-selective thiocyanation of various types of phenols in good to excellent yields using $PhICl_2$ and $Pb(SCN)_2$ [129, 130]. Thus, $PhICl_2$ was synthesised [131, 132], and the two 2-halophenols **40** and **41** were subjected to thiocyanation using the *in situ* generated [$PhI(SCN)_2$] reagent (Figure 6.6) giving the corresponding thiocyanates **42** and **43** in low chemical yields (7–27 %). Increased chemical yields of **42** and **43** (>50 %) were obtained in thiocyanations of the respective halogenated phenols **40** and **41** using NH_4SCN and Br_2 in glacial acetic acid [133].

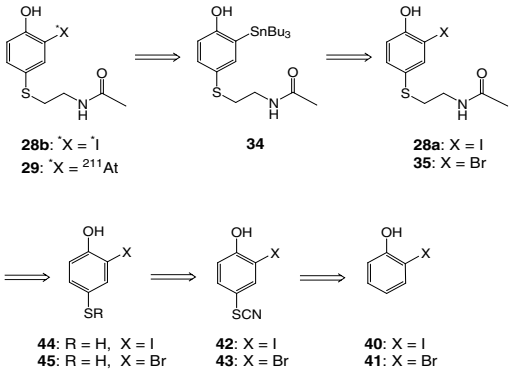

Figure 6.5: Second retrosynthetic analysis of the stannylated precursor **34**.

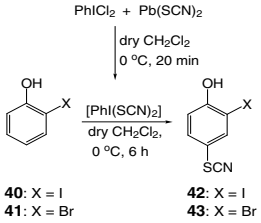

Figure 6.6: Reaction scheme for thiocyanation of **40** and **41** using $PhICl_2$ and $Pb(SCN)_2$ yielding **42** and **43**, respectively (from Refs. [129, 131].)

It was assumed that a subsequent alkaline hydrolysis of the halogenated thiocyanates **42** and **43** would give the corresponding thiols **44** and **45** [134, 135]. Thus, thiocyanates **42** and **43** were allowed to react with aqueous NaOH in MeOH, but under these conditions the corresponding methylthiolethers 2-halo-4-methylsulphanylphenol emerged. However, changing the solvent to aqueous Na_2CO_3 resulted in the dihalogenated disulphides **37** and **38** in high chemical yields (80–95 %). Subsequent $NaBH_4$ reductions of **37** and **38** aiming at the corresponding thiols **44** and **45** were inefficient, however treating **37** and **38** with Ph_3P in the presence of water rapidly gave **44** and **45** in high yields [32, 134]. To avoid rapid oxidation of the thiols in air, the crude product containing **44** or **45** was immediately refluxed in 2-methyl-2-oxazoline and xylene according to the Wehrmeister reaction [126, 127] to give the corresponding halogenated cysteaminylphenols **28a** or **35** in >56 % yield.

Great efforts were made in stannylating the halogenated cysteaminylphenols **28a** and

35, however, both palladium(0)-catalysed stannylations with $R_6Sn_2/(Ph_3P)_4Pd$ (R = Me, Bu) and reactions using *n*-BuLi/Bu_3SnCl were discouraging (Figure 6.7). The stannylated cysteaminylphenol **34** was not identified in the palladium(0)-catalysed reactions. Similar results were obtained with the *O*-acetylated analogue **46** (Figure 6.7). These results were probably due to inhibition by the sulphur atom [136]. In the *n*-BuLi/Bu_3SnCl reactions a rapid hydrolysis was observed, mainly yielding *N*-acetyl-4-*S*-CAP **11** and minimal amounts of **34** (∼6 %). Hydrogen for iodine substitution was also observed when trying to obtain a precursor incorporating the less reactive trimethylsilyl leaving group (**47**, Figure 6.7). Hydrolysis was verified by ^{1}H-NMR and ^{13}C-NMR when quenching the reaction with D_2O gave no incorporation of deuterium in the *ortho*-position. Consequently, it was assumed that hydrolysis was caused by the slightly acidic amide *N*-H hydrogen reacting with the 3-lithio intermediate giving *N*-acetyl-4-*S*-CAP **11**. Thus, protection of the amide function using CH_3MgBr or $(BOC)_2O$ followed by lithiation, stannylation and deprotection steps might improve the

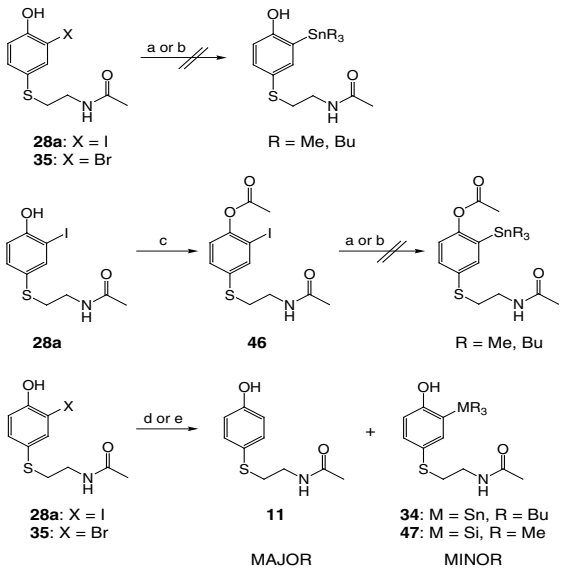

Figure 6.7: Summary of different reactions performed in the efforts of synthesising the stannylated precursor **34** or an analogue. Reagents and conditions: a) $(Ph_3P)_4Pd$, Bu_6Sn_2, toluene, 115 °C; b) $(Ph_3P)_4Pd$, Me_6Sn_2, toluene, 115 °C; c) Ac_2O, 4-DMAP, pyridine, rt; d) *i*) *n*-BuLi, THF, -78 °C; *ii*) Bu_3SnCl, THF, -78 °C; *iii*) sat. $NH_4Cl_{(aq)}$, rt; e) *i*) *n*-BuLi, THF, -78 °C; *ii*) Me_3SiCl, THF, -78 °C; *iii*) sat. $NH_4Cl_{(aq)}$, rt.

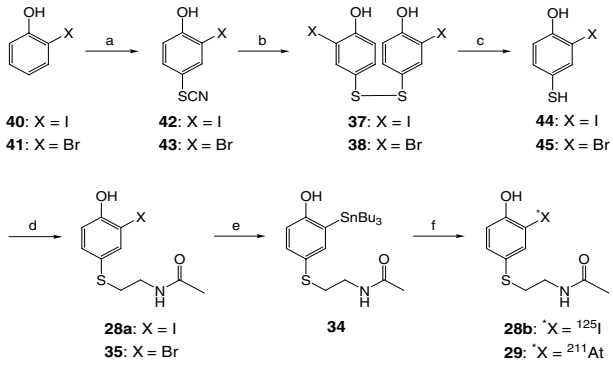

Figure 6.8: Reaction scheme for synthesis of the stannylated precursor **34** and the ^{125}I- and ^{211}At-labelled cysteaminylphenols **28b** and **29**, respectively. Reagents and conditions: a) NH_4SCN, Br_2, glacial acetic acid, 10 °C; b) $NaOH_{(aq)}$, $Na_2CO_{3(aq)}$, 35 °C; c) Ph_3P, dioxane, H_2O, rt; d) 2-methyl-2-oxazoline, xylene, 160 °C; e) *i*) *n*-BuLi, THF, -78 °C; *ii*) Bu_3SnCl, THF, -78 °C; *iii*) sat. $NH_4Cl_{(aq)}$, rt; f) $Na^{125}I$ or ^{211}At, NCS, AcOH, MeOH, rt.

yield of **34**. Protection of the phenolic hydroxyl group may also be considered. However, it was decided to proceed with the available amount of **34** to evaluate *in vivo* stability and biological properties of **28b** and **29**, as such experiments would be decisive for the need of more precursor **34**.

The final synthetic route to precursor **34** and its radiohalogenated derivatives **28b** and **29** is depicted in Figure 6.8. All reactions were first established using the brominated derivatives (spectroscopic data are summarised in Appendix C). In general, the brominated derivatives were obtained in higher chemical yields compared to their iodinated analogues. However, the non-radioactive iodide **28a** was required as a reference compound in the radio-HPLC characterisations of **28b** and **29**. Detailed descriptions of reactions and spectroscopic data of the iodinated derivatives leading to precursor **34** are described in Paper **IV**.

Synthesis of *N*-[2-(4-hydroxy-phenylsulphanyl)ethyl]-4-tributylstannylbenzamide (48) and its iodo derivative 30a

The synthesis of *N*-[2-(4-hydroxy-phenylsulphanyl)ethyl]-4-tributylstannylbenzamide (**48**) and its iodo derivative **30a** is depicted in Figure 6.9. The cysteaminylphenol **11** was synthesised *via* the Wehrmeister reaction. The 4-mercaptophenol **36** was refluxed in 2-methyl-2-oxazoline to give acetamide **11**, followed by a reduction to the corresponding amine **10**

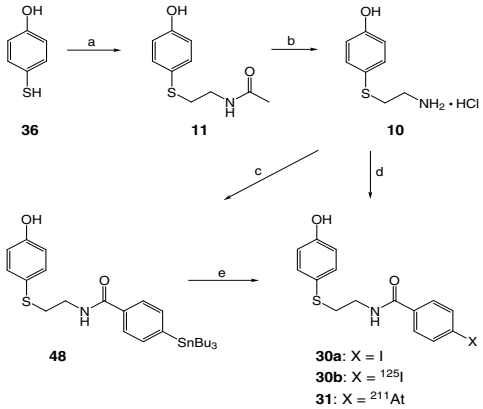

Figure 6.9: Reaction scheme for synthesis of the stannylated precursor **48** and the ^{125}I- and ^{211}At-labelled cysteaminylphenols **30b** and **31**, respectively. Reagents and conditions: a) 2-methyl-2-oxazoline, 130–160 °C; b) conc. $HCl_{(aq)}$, reflux; c) Bu_3SnAr-OTFP **16**, Et_3N, DMF, rt; d) IAr-OTFP **18**, Et_3N, DMF, rt; e) $Na^{125}I$ or ^{211}At, NCS, AcOH, MeOH rt.

according to the procedures of Padgette *et al.* and Prezioso *et al.* [137, 138]. The aromatic activated esters **16** and **18** reacted with the amine **10** to give the corresponding benzamides **48** and **30a** in 34 % and 51 % total yields, respectively. Detailed descriptions of reactions and spectroscopic data of the compounds are found in Paper **IV**.

Synthesis of *N*-[2-(4-hydroxyphenyl)ethyl]acetamide (49) and its iodo derivative 32a

The synthesis of *N*-[2-(4-hydroxyphenyl)ethyl]acetamide (**49**) and the iodinated derivative **32a** is outlined in Figure 6.10. Tyramine **50** was converted into the ester amide **51** through a *N,O*-acetylation, followed by a saponification of the phenolic acetyl group to give amide **49**. The amide **49** underwent direct electrophilic iodination yielding **32a** using a general labelling procedure. The non-radioactive iodide **32a** was identified by LC-MS analysis of the reaction mixture, and the HPLC retention time was used to identify the peak of the radio-iodinated derivative **32b** on radio-HPLC. Reactions and spectroscopic data of the compounds are described in detail in Paper **IV**.

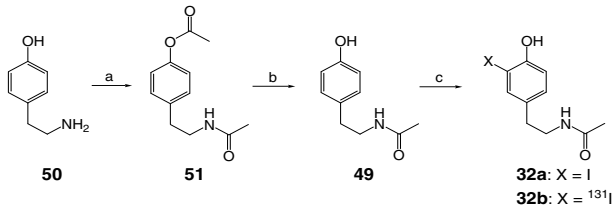

Figure 6.10: Reaction scheme for synthesis of the ^{131}I-labelled tyramine derivative **32b**. Reagents and conditions: a) Ac_2O, 4-DMAP, pyridine, rt; b) $NaHCO_{3(aq)}$, MeOH, rt; c) KI or $Na^{131}I$, NCS, AcOH, MeOH, rt.

Synthesis of *N*-[2-(4-hydroxyphenyl)ethyl]-4-tributylstannylbenzamide (52) and its iodo derivative 33a

The synthesis of *N*-[2-(4-hydroxyphenyl)ethyl]-4-tributylstannylbenzamide (**52**) and its iodo derivative **33a** is outlined in Figure 6.11. Precursor **52** and the iodinated derivative **33a** were synthesised using the methods of Wilbur *et al.* [118]. Tyramine **50** reacted with the aromatic activated esters **16** and **18** to give the corresponding benzamides **52** and **33a** in 63 % and 58 % yields, respectively. Detailed descriptions of the reactions and spectroscopic data of the compounds are found in Paper **IV**.

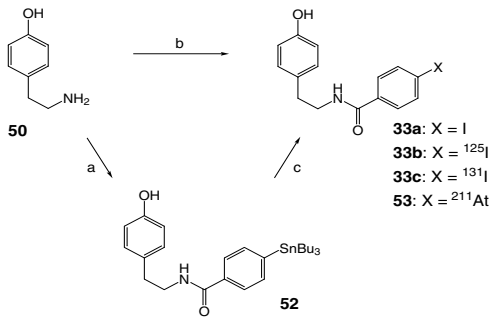

Figure 6.11: Reaction scheme for synthesis of the stannylated precursor **52** and the ^{125}I-, ^{131}I- and ^{211}At-labelled tyramine derivatives **33b**, **33c** and **53**. Reagents and conditions: a) Bu_3SnAr-OTFP **16**, Et_3N, DMF, rt; b) IAr-OTFP **18**, Et_3N, DMF, rt; c) $Na^{125}I$ or $Na^{131}I$ or ^{211}At, NCS, AcOH, MeOH, rt.

6.2.2 Radiolabelling and purification

Precursors **34**, **48**, **49** and **52** were radiohalogenated using the general labelling procedure described in Paper **IV** (with minor modifications for ^{211}At). Radiohalogenations with *X = ^{125}I, ^{131}I or ^{211}At were performed under acidic conditions using NCS as oxidising agent in a solution of MeOH/AcOH (9:1) for 5–30 min (Figures 6.8–6.11). The radioiodinated derivatives **28b**, **30b**, **32b** and **33b,c** were obtained in 80–95 % integrated radiochemical yields, while the yields of the astatinated derivatives **29**, **31** and **53** were in the range 50–90 % (Table 6.1). Compound **49** was radiolabelled *via* a direct electrophilic iodination to give **32b**. Hence, an astatinated derivative of compound **49** was not obtained (Section 2.4.1).

The radiohalogenated products were identified on radio-HPLC by co-injection with the corresponding non-radioactive iodinated derivative. Radio-HPLC purification and isolation gave the radiohalogenated products in 30–85 % isolated radiochemical yields. Isolated products were concentrated *in vacuo*, transferred into PBS, pH adjusted and sterile filtered prior to use (Paper **IV**). Preparations were made by combining two or three compounds labelled with different radionuclides in each biodistribution study.

Table 6.1: Integrated radiochemical yields estimated by radio-HPLC.

Radiohalogenated compound		**Integrated radiochemical yield**
N-[2-(4-hydroxy-3-[^{125}I]iodo-phenylsulphanyl)ethyl]acetamide	**28b**	80 %
N-[2-(4-hydroxy-3-[^{211}At]astato-phenylsulphanyl)ethyl]acetamide	**29**	50 %
N-[2-(4-hydroxy-phenylsulphanyl)ethyl]-4-[^{125}I]iodobenzamide	**30b**	80 %
N-[2-(4-hydroxy-phenylsulphanyl)ethyl]-4-[^{211}At]astatobenzamide	**31**	70 %
N-[2-(4-hydroxy-3-[^{131}I]iodophenyl)ethyl]acetamide	**32b**	90 %
N-[2-(4-hydroxyphenyl)ethyl]-4-[^{125}I]iodobenzamide	**33b**	95 %
N-[2-(4-hydroxyphenyl)ethyl]-4-[^{131}I]iodobenzamide	**33c**	95 %
N-[2-(4-hydroxyphenyl)ethyl]-4-[^{211}At]astatobenzamide	**53**	90 %

6.3 Biology

6.3.1 Preliminary biodistribution studies

Preliminary biodistribution studies were were conducted at the University of Washington, Seattle, USA (Paper **IV**). One group of normal Balb/c nude mice (male) were injected the radioiodinated acetamides **28b** and **32b**, and another group were injected the radioiodinated benzamides **30b** and **33c**. The injection volume contained approximately 370 kBq of each radioiodinated compound. Animals were sacrificed 0.5 h, 2 h and 6 h post-injection while under xylazine/ketamine anesthesia.

6.3.2 Biodistribution studies in the HHMSX model

Biodistribution studies in a melanoma model were conducted at the Norwegian Radium Hospital using experimental procedures identical to those described in Paper **II**. Animal studies were carried out in Balb/c nude mice (male) bearing the malignant melanoma xenograft HHMSX (melanotic). The mice (weight 28–37 g) were injected 100 μL of preparation I) **28b** and **29**, II) **30b** and **31** or III) **32b**, **33b** and **53** into a lateral tail vein (Table 6.2). At 0.5 h, 2 h, 6 h and 16 h post-injection, four animals were sacrificed by cardiectomy while under hypnorm/dormicum anesthesia.

Table 6.2: Properties of radiolabelled cysteaminylphenols and tyramine derivatives studied in Balb/c nude mice bearing the HHMSX melanoma model.

Preparation	**Radiohalogenated compound**	**Activity injected/ 100 μL**	$\mathbf{t_R}$
I	**28b**	130 kBq	11.5 min
I	**29**	110 kBq	12.9 min
II	**30b**	100 kBq	14.3 min
II	**31**	160 kBq	16.6 min
III	**32b**	80 kBq	9.4 min
III	**33b**	80 kBq	13.9 min
III	**53**	230 kBq	14.6 min

6.4 Results and discussion

Preliminary biodistribution studies

Preliminary biodistribution studies were performed with the ^{125}I- or ^{131}I-labelled derivatives **28b**, **30b**, **32b** and **33c** in normal Balb/c nude mice. The studies were conducted to evaluate the *in vivo* stability of the radioiodinated compounds, as well as the distribution and clearance from non-target tissues (Paper **IV**). The results indicated that all the radioiodinated derivatives showed high stability to enzymatic deiodination *in vivo*. Both the cysteaminylphenols **28b** and **30b** and the corresponding tyramine derivatives **32b** and **33c** seemed to undergo a very fast metabolism and renal excretion, resulting in low concentrations of radioactivity in non-target tissues 6 h post-injection. Biodistribution data are presented in Tables D.1 and D.2 (Appendix D), and the results are summarised in Paper **IV**.

Biodistribution studies in the melanotic melanoma model HHMSX

The prospects of high tumour to non-target tissue dose ratios for the radioiodinated derivatives **28b**, **30b**, **32b** and **33c** encouraged a new series of biodistribution studies in mice bearing the

human malignant melanoma xenograft HHMSX. The astatinated derivatives **29**, **31** and **53** were included in the studies to evaluate their potential in targeted radiotherapy of malignant melanoma. Biodistribution data are presented in Tables D.3–D.6 (Appendix D), and the results are summarised in Figures 6.12 and 6.13.

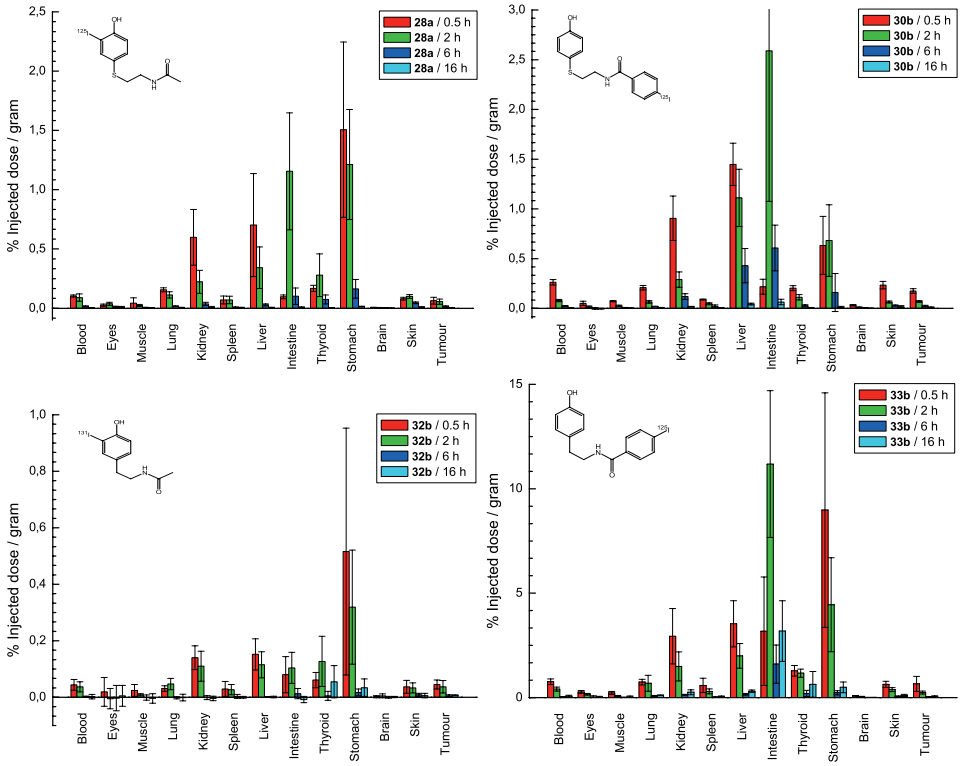

Figure 6.12: Results of the biodistribution studies of **28b**, **30b**, **32b** and **33b** in Balb/c nude mice bearing the HHMSX melanoma model. Gastric and intestinal values include their contents.

Generally, the concentration of radioiodine (% ID/g) measured in all organs and tissues were significantly lower than the values reported for **28b**, **30b** and **32b** in the preliminary biodistribution studies. This observation was not expected since the use of internal standards should have eliminated differences in the detection instruments, as well as in the different amounts of radioactivity injected in the mice. However, the results revealed the same trends in the distribution of the radioiodinated compounds between different organs, producing

proportionally similar organ-to-organ uptake ratios as reported in Paper **IV**. Consequently, the new results were compared and evaluated strictly in terms of uptake ratios.

Free radioiodide is primarily localised in thyroid and stomach, and preferentially in thyroid, yielding thyroid-to-stomach uptake ratios above unity [27]. In these studies the uptake in thyroid was significantly lower than in stomach ($P < 0.05$), verifying the *in vivo* stability towards dehalogenation of **28b**, **30b**, **32b** and **33b,c** reported in Paper **IV**. Similarly, the trends of very rapid renal excretion and clearance were confirmed (Tables D.3–D.6).

The results did not indicate any specific accumulation of **28b**, **30b**, **32b** or **33b** in the melanotic melanoma model HHMSX, giving approximately the same amount of detected radioiodine in tumour as in blood and healthy skin (Table 6.3). The only compounds showing steadily increasing tumour-to-blood and tumour-to-muscle dose ratios were **30b** and **32b**, however, the values were low and the potential tumour-accumulation over time was not convincing. Given these results, the postulated difference in melanocyte incorporation between cysteaminylphenols and tyramine derivatives could neither be demonstrated nor evaluated in this study using the HHMSX melanoma model.

Table 6.3: Melanoma/non-target tissue dose ratios of **28b**, **30b**, **32b** and **33b** in Balb/c nude mice bearing the melanotic melanoma xenograft HHMSX.

	28b	**30b**	**32b**	**33b**	**29**	**31**	**53**
Tumour/Blood							
0.5 h	0.6	0.7	1.0	0.8	1.2	0.7	1.4
2 h	0.6	0.9	1.0	0.5	1.9	3.1	1.7
6 h	0.9	1.0	1.7	0.8	2.3	2.8	2.2
16 h	1.3	2.5	3.5	0.7	2.0	NA	1.8
Tumour/Muscle							
0.5 h	1.5	2.4	1.9	2.9	2.8	2.5	3.3
2 h	2.3	2.8	4.1	3.0	3.6	5.3	3.6
6 h	2.0	3.8	NA	2.4	3.9	5.3	4.2
16 h	2.0	5.0	NA	1.7	4.6	NA	2.8
Tumour/Skin							
0.5 h	0.8	0.7	1.2	1.0	0.6	0.5	0.7
2 h	0.6	1.1	1.1	0.6	0.8	1.1	0.8
6 h	0.3	0.8	0.6	0.5	0.8	0.6	0.7
16 h	0.4	0.6	1.2	0.5	0.6	NA	0.4

NA = not applicable (% ID/g muscle ∼0.)

The best method for evaluating *in vivo* stability of astatinated compounds is by performing co-injected dual label experiments with radioiodine [27]. Radioiodinated and astatinated compounds that are stable to dehalogenation may show very similar distribution *in vivo*. However, free astatide will primarily localise in lungs, spleen, thyroid and stomach while free radioiodide will accumulate in thyroid and stomach. Thus, large differences between the concentrations of the radiohalogens in these tissues are good indicators of *in vivo* instability of

astatinated compounds. In the HHMSX biodistribution studies of the astatinated derivatives **29**, **31** and **53**, high amounts of ^{211}At were detected in lungs, spleen, thyroid and stomach (Figure 6.13). This result indicated that most, if not all, of the detected ^{211}At was present as free astatide. Hence, it was concluded that the astatinated derivatives **29**, **31** and **53** were unstable *in vivo*.

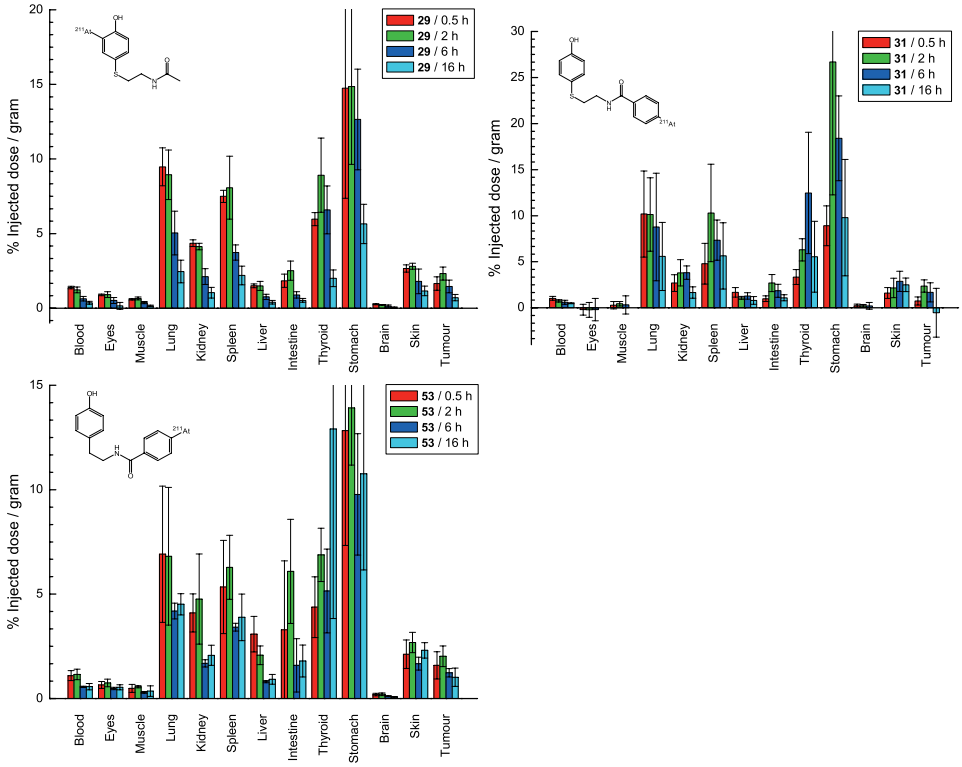

Figure 6.13: Results of the biodistribution studies of **29**, **31** and **53** in Balb/c nude mice bearing the HHMSX melanoma model. Gastric and intestinal values include their contents.

Given these results, the amounts of intact **29**, **31** and **53** undergoing tumour-accumulation would be low, and it is impossible to distinguish between tumour uptake of the astatinated cysteaminylphenol derivatives and of the free astatide. Consequently, the HHMSX tumour uptake ratios of **29**, **31** and **53** could not be further evaluated. However, the tumour/non-target tissue dose ratios have been included in Table 6.3 for comparison.

The carbon–astatine bond is weaker than the carbon–iodine bond. Thus, a situation

showing high *in vivo* stability of radioiodinated compounds and extensive deastatination of the corresponding astatinated analogues often occur. A different chemical approach yielding more stable astatine-compounds might involve the use of carborane-cages giving astatinated boron cage molecules [16].

Conclusion

Biodistribution data of **28b**, **29**, **30b**, **31**, **32b**, **33b** and **53** were analysed using a coarse method based on organ uptake ratios. Nevertheless, it was revealed that these radiohalogenated cysteaminylphenol and tyramine derivatives did not possess the biological properties required for diagnostic and therapeutic radiopharmaceuticals for malignant melanoma. The astatinated compounds **29**, **31** and **53** were unstable to deiodinase enzymes *in vivo*. The radioiodinated compounds **28b**, **30b**, **32b** and **33b** showed high *in vivo* stability, but biodistribution studies did not indicate tumour accumulation in the HHMSX melanoma model. Thus, a new series of HHMSX biodistribution studies with these compounds to obtain a more detailed analysis of the organ uptake values (% ID/g), were not considered justified.

Chapter 7

Benzamide derivatives

7.1 Introduction

In the work with benzamide derivatives the aim was to synthesise an astatinated analogue of the promising benzamide [*I]IMBA **14**. It was suggested that the astatinated analogue would show a melanoma-seeking behaviour and a sigma-receptor affinity similar to **14**, facilitating targeted α-particle radiotherapy of malignant melanoma and its metastases.

In the literature, [*I]IMBA **14** was synthesised using the $Tl(TFA)_3/I^-$ method [104, 109, 139]. Generally, electrophilic aromatic thallations with $Tl(TFA)_3$ in TFA are rarely used in synthetic organic chemistry due to limited versatility and harsh reaction conditions. The reaction mechanism is complex [32], and it is difficult to control yields and isomeric products of the *in situ* thallation [14, 24]. It is also a matter of controversy whether the halodethallation may give the radioiodinated or astatinated products without the addition of a carrier [14, 24, 104, 109, 112, 140, 141].

Thus, an improved method for synthesising no-carrier-added radioiodinated and astatinated derivatives of **14** was required. The chosen strategy was to synthesise a stannylated precursor of **14**, facilitating regiospecific astatination to give the target molecule *N*-(2-diethylaminoethyl)-3-[^{211}At]astato-4-methoxybenzamide ([^{211}At]AMBA **54**, Figure 7.1).

7.2 Chemistry

7.2.1 Synthesis of *N*-(2-diethylaminoethyl)-3-(tri-*n*-butylstannyl)-4-methoxybenzamide (55) and its iodo derivative 14a

The synthesis of the stannylated precursor *N*-(2-diethylaminoethyl)-3-(tri-*n*-butylstannyl)-4-methoxybenzamide (**55**) and its iodo derivative **14a** is depicted in Figure 7.1. The

method was based on the ATE-synthesis described by Zalutsky *et al.* [142]. The 3-bromo-4-methoxybenzoic acid (**56**) was converted into its stannylated derivative **57** using *n*-BuLi/Bu_3SnCl. The benzoic acid **57** reacted with *N*-hydroxysuccinimide using *N,N'*-dicyclohexylcarbodiimide as a coupling reagent. The resulting activated ester **58** reacted with 2-(diethylamino)ethylamine to give the stannylated benzamide **55** in 65 % total chemical yield [112]. Detailed descriptions of reactions and spectroscopic data are found in Papers **I**–**II**.

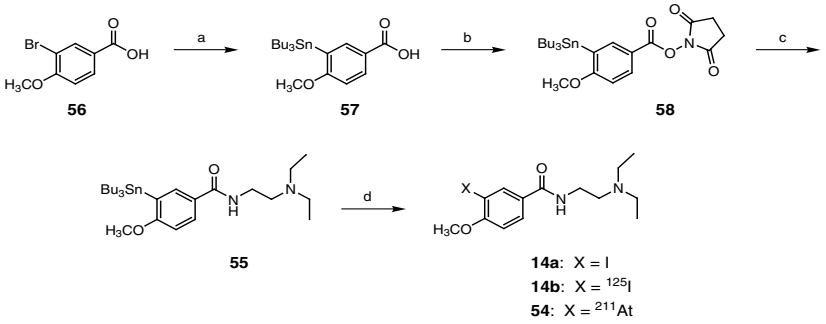

Figure 7.1: Reaction scheme for synthesis of the stannylated precursor **55** and the radiolabelled products [^{125}I]IMBA **14b** and [^{211}At]AMBA **54**. Reagents and conditions: a) *i*) *n*-BuLi, THF, -78 °C; *ii*) Bu_3SnCl, THF, -78 °C; *iii*) sat. $NH_4Cl_{(aq)}$, rt; b) NHS, DCC, THF, rt; c) 2-(diethylamino)ethylamine, $CHCl_3$, rt; d) KI or Na^{125}I or ^{211}At, NCS, AcOH, MeOH, rt.

7.2.2 Radiolabelling and purification

Precursor **55** was radiohalogenated with $^*X = {}^{125}I$ or ^{211}At using the labelling procedure described in Papers **I**–**II**. Radiohalogenations were performed under acidic conditions using NCS as oxidising agent in a solution of MeOH/AcOH (9:1) for 5–15 min (Figure 7.1). Radio-HPLC analysis showed [^{125}I]IMBA **14b** and [^{211}At]AMBA **54** in 70–90 % integrated radiochemical yields. The products **14b** and **54** were obtained in 55–60 % isolated yields and ≥99 % radiochemical purities [112]. The radiohalogenated benzamides were identified on radio-HPLC by co-elution with the non-radioactive IMBA **14a**. The isolated products were concentrated *in vacuo*, dissolved in PBS, pH adjusted and sterile filtered prior to use. Preparations for biodistribution studies were made by combining solutions of **14b** and **54** (Papers **II**–**III**).

7.3 Biology

7.3.1 Biodistribution studies in the HHMSX model

Biodistribution studies were conducted at the Norwegian Radium Hospital using Balb/c nude mice (male) bearing the melanotic melanoma xenograft HHMSX (Paper **II**). The animals were injected 100 μL of a preparation of **14b** (120 kBq) and **54** (430 kBq) in PBS. At 0.5 h, 2 h, 6 h and 16 h post-injection, three or four animals were sacrificed by cardiectomy while under hypnorm/dormicum anesthesia.

7.3.2 Biodistribution studies in the SESX model

Biodistribution studies were conducted at the Norwegian Radium Hospital using Balb/c nude mice (female) bearing the amelanotic melanoma xenograft SESX (Paper **III**). The animals were injected 100 μL of a preparation of **14b** (110 kBq) and **54** (450 kBq) in PBS. At 1 h, 4 h and 16 h post-injection, three animals were killed by cervical dislocation [112].

7.4 Pharmacology

Pharmacology experiments were performed at the Department of Pharmacology, University of Oslo. Preparations of SESX cell membranes for radioligand binding assays were made from frozen tumour nodules as described in Paper **III**. To avoid complications with necrotic tissue, cells were harvested from small tumours weighing 0.1–0.25 g. Radioligand binding assays were performed with the selective σ_1-receptor ligand [^{3}H]-(+)-pentazocine in the absence (total binding) or presence (non-specific binding) of haloperidol. The corresponding K_d and B_max values were determined by analysis of specific binding data (Paper **III**). Pharmacology experiments with HHMSX cell membranes were conducted for comparison, and the results are summarised in Table 7.1.

Table 7.1: Results of pharmacological binding studies of the SESX and HHMSX melanoma models. B_max is the total number of σ_1-receptors and K_d is the equilibrium dissociation constant.

Melanoma model	$\boldsymbol{B}_\mathrm{max}$ **(mol/mg protein)**	$\boldsymbol{K}_\mathrm{d}$ **(nM)**
SESX	$(1.5 \pm 0.3) \times 10^{-12}$	6.8 ± 0.9
HHMSX	$(242 \pm 12) \times 10^{-15}$	16.3 ± 0.3

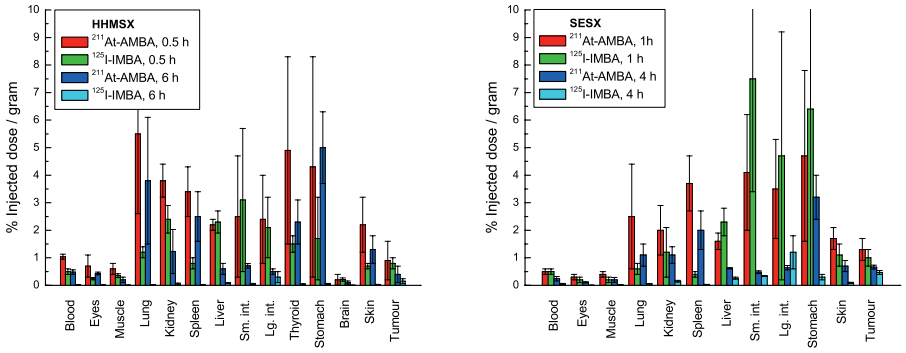

Figure 7.2: Results of the biodistribution studies of **14b** and **54** in Balb/c nude mice bearing the melanoma xenografts HHMSX (left) and SESX (right). Gastric and intestinal values include their contents.

7.5 Results and discussion

Paired label biodistribution studies of the benzamides [^{125}I]IMBA **14b** and [^{211}At]AMBA **54** were conducted in Balb/c nude mice bearing the melanotic melanoma xenograft HHMSX (Paper **II**) or the amelanotic melanoma xenograft SESX (Paper **III**). The studies were performed to evaluate *in vivo* stability of the astatinated benzamide **54**, distribution and clearance from non-target tissues, as well as uptake of **14b** and **54** in pigmented and non-pigmented melanomas. Biodistribution data are presented in Tables D.7 and D.8 (Appendix D), and the results are summarised in Figure 7.2.

Both studies showed low uptake values of ^{211}At in the neck and other tissues with affinity for free astatide. In the HHMSX study the thyroid gland was excised and the accumulated radioactivity was measured, yielding moderate and steadily decreasing uptake values of ^{211}At (mean values from 4.9 %ID/g to 1.1 %ID/g). In contrast, enzymatic deastatination should give increasing uptake values in thyroid and other non-target tissues during the first 4 h post-injection [27]. Consequently, it was assumed that the ^{211}At detected in lungs, spleen, stomach and thyroid primarily was due to uptake of unmetabolised **54** and other ^{211}At-labelled metabolites rather than free astatide. Although some decomposition of **54** might have taken place, no extensive enzymatic deastatination *in vivo* was observed.

Table 7.2: Melanoma/non-target tissue dose ratios of **14b** and **54** in Balb/c nude mice bearing the melanotic melanoma xenograft HHMSX and the amelanotic melanoma xenograft SESX.

	HHMSX				**SESX**		
	0.5 h	**2 h**	**6 h**	**16 h**	**1 h**	**4 h**	**16 h**
Tumour/Blood							
14b	1.6	3.6	10.7	12.0	2.0	9.4	8.6
54	0.9	1.5	0.8	1.4	2.6	2.8	1.5
Tumour/Muscle							
14b	2.3	10.0	50.0	30.0	5.0	23.5	NA
54	1.5	5.0	4.4	4.0	3.3	3.3	3.8
Tumour/Skin							
14b	1.1	2.5	5.4	8.6	0.9	5.2	4.3
54	0.4	0.5	0.3	0.4	0.8	0.9	0.5

NA = not applicable (% ID/g muscle ∼0.)

Tumour accumulation in the melanotic melanoma model HHMSX

The tumour uptake mechanism of the benzamides **14b** and **54** in the pigmented melanoma model HHMSX should go *via* the melanin synthesis and the σ_1-receptors expressed on the HHMSX cell membranes. However, pharmacology experiments revealed a very low density of σ_1-receptors on these cell membranes (Table 7.1), indicating that the melanin synthesis will be the primary uptake mechanism of **14b** and **54** in this melanoma model.

Results from the biodistribution studies in mice bearing the melanotic melanoma model HHMSX showed slightly higher tumour uptake values for **54** than **14b** (0.9 % ID/g and 0.5 % ID/g after 2 h, respectively). However, the iodinated benzamide **14b** demonstrated faster clearance from non-target tissues which gave rise to higher melanoma/non-target tissue dose ratios (Table 7.2). Thus, the proposed diagnostic value of the ^{123}I-labelled IMBA in scintigraphic imaging of malignant melanomas was confirmed in this study [48, 104, 109]. The melanoma/non-target tissue dose ratios also indicated a small tumour accumulation of **54**, but the low tumour uptake combined with a slow clearance from most non-target tissues suggested limited prospects of using **54** in targeted radiotherapy of malignant melanomas (Paper **II**).

However, it is difficult to evaluate the melanoma-seeking properties of **14b** and **54** using the results obtained with the HHMSX melanoma xenograft. While Mohammed *et al.* reported a maximum tumour uptake of 6.7 % ID/g with [^{131}I]IMBA in the murine melanoma model B16 [104], the tumour uptake values were significantly lower for both **14b** and **54** in the HHMSX melanoma model. It is assumed that the different tumour uptake values of [*I]IMBA mainly reflect different physiological properties of the murine B16 and the human HHMSX melanoma models. Consequently, a final conclusion considering the melanoma-seeking properties of **54** could not be made.

A standard reference melanoma model for biodistribution studies in mice is highly warranted, facilitating comparison of tumour uptake values and comparison of the potential of different melanoma-seeking agents. Widespread use of the murine B16 melanoma model suggests that this model should be used when investigating new melanoma-seeking agents, but this melanoma model was not available for this work.

Tumour accumulation in the amelanotic melanoma model SESX

Amelanotic melanomas are characterised by melanocytes with no melanin synthesis. Hence, it has been proposed that uptake of iodobenzamides goes *via* sigma-receptors expressed on the melanoma cell membranes [109]. It has been shown that [^{131}I]IMBA has moderate affinity for the σ_1-receptor subgroup ($K_i = 249 \pm 17$ nM) [48], but the compound has not previously been used for specific targeting of σ_1-receptors *in vivo*. It is not known whether astatinated benzamides have a similar affinity for σ_1-receptors as their iodinated analogues. On the other hand, it is generally assumed that iodinated and astatinated analogues should have similar *in vivo* behaviour, implying that **54** should have affinity for σ_1-receptor binding sites.

Pharmacology experiments showed a high density of σ_1-receptors and a high-affinity binding on the SESX cell membranes. Biodistributions studies in mice bearing the amelanotic melanoma model SESX showed a small uptake in tumour for both **54** and **14b** 1 h post-injection (1.3 %ID/g and 1.0 %ID/g, respectively) [112]. However, only **14b** showed high melanoma/non-target tissue dose ratios, indicating tumour accumulation and tumour retention at the σ_1-receptors (Table 7.2). Thus, the promising prospects of using **14b** in specific targeting of σ_1-receptors were demonstrated (Paper **III**).

In contrast, the slow non-target tissue clearance of **54** hampered a corresponding evaluation of the σ_1-receptor affinity of this benzamide (Table 7.2). The results did not show a preferential accumulation of the astatinated analogue in amelanotic melanomas compared to normal tissues, indicating that **54** can not be used as a radioligand in specific σ_1-receptor targeted radiotherapy (Paper **III**).

Comparison of the HHMSX and SESX studies

Figure 7.3 shows that the tumour uptake values of **14b** and **54** in the pigmented HHMSX and the non-pigmented SESX melanoma models were almost the same. This result indicates that targeting of σ_1-receptors may be of greater significance in melanoma uptake of benzamides than previously assumed.

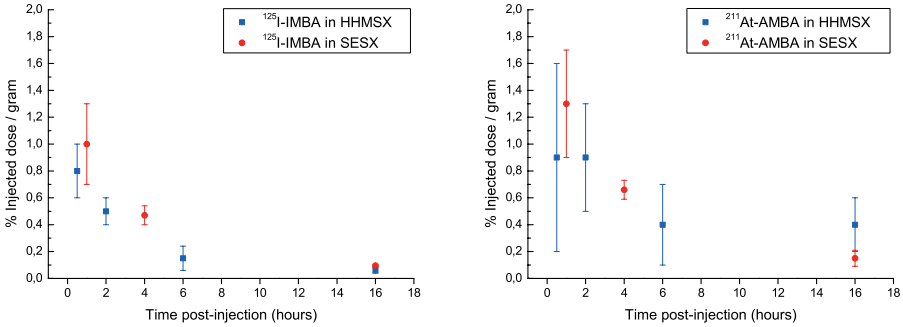

Figure 7.3: Tumour uptake values of [^{125}I]IMBA **14b** (left) and [^{211}At]AMBA **54** (right) in Balb/c nude mice bearing the melanoma xenografts HHMSX and SESX.

Conclusion

The astatinated benzamide **54** was considered stable to enzymatic deastatination *in vivo*, but inefficient as a melanoma-seeking agent for targeted radiotherapy of the melanotic and amelanotic melanoma models HHMSX and SESX. The reported high contrast for scintigraphic imaging of malignant melanoma was confirmed with **14b** in both melanoma models. The results indicated that **14b** may be used for simple and efficient targeting of cancerous tissues expressing a high density of σ_1-receptors. Consequently, targeting of σ_1-receptors on melanoma cell membranes may supplement the more complex uptake mechanism related to melanin biosynthesis.

Chapter 8

Malignant melanoma: Future challenges

The main challenge in this field is to develop an efficient and specific melanoma-seeking agent. In order to achieve this, it is imperative to identify the biologically active part(s) of chemical structures responsible for melanoma uptake.

There is also a need for a better general understanding of the mechanisms by which melanoma-seeking agents bind to melanotic tissue. The use of a standard reference model for pigmented melanomas would enable proper comparison of the melanoma-seeking properties of different agents. Thus, characterisation and development of such a standard system is highly required.

However, it is questionable whether the results obtained with melanoma-seeking agents in a standard melanoma model will give results generally valid for clinical use, or whether the results only will be representative for that specific melanoma model. For future investigations it is important to find the pigmented melanoma model which gives the most representative results compared to the clinical situation in humans.

Part III

BONE-RELATED CANCER

Chapter 9

Bone-related cancer

Primary bone cancers are rare (less than 1 % of all malignant tumours), although quite frequent among children under age 15 [1, 34]. However, almost 50 % of all soft tissue tumours eventually spread to bone, making bone metastases a main problem in clinical oncology [143, 144].

Generally, bone-related cancers are associated with skeletal pain, pathological fractures, spinal cord compression, suppression of bone marrow function, hypercalcemia and finally death. Besides palliative therapy to reduce pain, current treatment modalities includes surgery, external beam irradiation, hormone therapy and chemotherapy. The therapeutic efficiency is often limited due to severe side-effects, and the number of patients with bone metastases achieving complete curation is negligible. Alternative therapeutic methods for tumour control and pain palliation are therefore highly required.

The development of new bone-seeking radiopharmaceuticals for targeted radiotherapy is based on the well-known mechanisms of bone physiology and pathology.

9.1 Bone, osteosarcoma and bone metastasis

Bone tissue consists essentially of mineral (mainly hydroxyapatite $Ca_{10}(PO_4)_6(OH)_2$), organic matrix, cells and water. The bone tissue is organised in an outer part consisting of tightly packed bone tissue (cortical or compact bone) and an inner part consisting of porous bone structures (trabecular or spongy bone) containing the red bone marrow [145, 146]. Bone homeostasis is controlled by osteoblasts (bone-forming cells), osteoclasts (bone-resorbing cells) and osteocytes (mature bone cells). Normally, there is an equilibrium between the osteoblasts and osteoclasts maintaining the bone tissue. Generally, the remodulation of trabecular bone is faster than that of cortical bone tissue [147].

Osteosarcoma is a primary malignant bone cancer originating from osseous tissue cells.

It is usually of osteoblastic nature, forming a primitive tumoural bone matrix (osteoid). Treatment is often problematic due to location (e.g. spine, skull, pelvis) and micrometastatic spread to other organs, e.g. lungs.

Bone metastases are dominated by skeletal metastases arising from breast, prostate or lung cancer [148]. Tumours metastasised to osseous tissue stimulate the osteoblastic and osteoclastic activities, resulting in increased bone-turnover [147].

9.2 Bone-seeking radiopharmaceuticals

Bone-seeking radiopharmaceuticals with therapeutic properties are attractive alternatives to external beam irradiation. The concept is based on the enhanced and selective uptake of bone-seeking agents in tissues of high osteoblastic activity (e.g. in sclerotic lesions), combined with radionuclides emitting short range radiation with high cytotoxicity. Hence, bone-seeking radiopharmaceuticals may deliver high radiation doses to tumours with relative sparing of healthy tissues, particularly the red bone marrow.

Therapeutic radiopharmaceuticals for bone pain palliation have been used successfully for more than 30 years [149]. Nevertheless, only three bone-seeking radiopharmaceuticals are currently approved by the FDA[1] for routine clinical application in humans (Figure 9.1). The ^{32}P-sodium orthophosphate (**59**) was extensively used in the 1970s, but has been widely replaced by $^{89}SrCl_2$ (Metastron® **60**) and ^{153}Sm-EDTMP (Quadramet® **61**). The latter

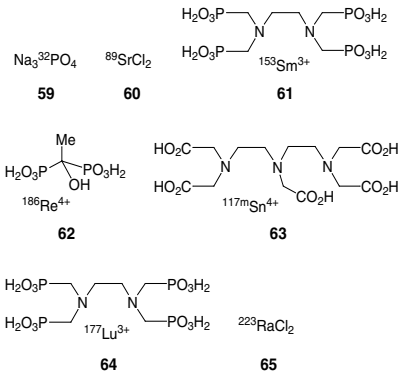

Figure 9.1: Bone-seeking radiopharmaceuticals, of which agents **59**–**61** are approved by the FDA.

[1] U.S. Food and Drug Administration.

agents are equally efficient, reporting significant pain relief in 70–80 % of patients, but less radiotoxic to the red bone marrow than $Na_3{}^{32}PO_4$ [2, 149, 150].

Radiation-induced bone marrow suppression is the limiting factor when administrating high radiation doses of bone-seeking radiopharmaceuticals, especially of agents emitting high-energetic β^--particles (e.g. $Na_3{}^{32}PO_4$, $^{89}SrCl_2$) [151, 152]. Consequently, new bone-seeking agents have been labelled with radionuclides emitting medium- to low-energy β^--particles and radionuclides decaying by electron capture (e.g. ^{153}Sm-EDTMP **61**, ^{186}Re-HEDP **62**, ^{117m}Sn-DTPA **63**, ^{177}Lu-EDTMP **64**) [17, 153–161]. Dense irradiation of bone tissues and sparing of red bone marrow may also be achieved using α-emitting radionuclides (e.g. $^{223}RaCl_2$ **65**) [149, 162–165].

9.2.1 Bisphosphonates

Bisphosphonates is a group of bone-seeking agents extensively used in diagnosis and treatment of different bone-related diseases [166–168]. They have specific affinity for bone matrix, and accumulate in recently formed bone tissues in regions of high bone turnover [147]. Bisphosphonates are also characterised by a high *in vivo* stability, favourable kinetics and low toxicity.

All bisphosphonates contain a metabolically stable P–C–P structure **66** (Figure 9.2). The phosphonate groups and the R_1 side chain are essential for the chemisorption to hydroxyapatite, while R_2 determines the pharmacological properties of the compound. Thus, R_2 is the key for making radiolabelled bisphosphonates for radiotherapeutic applications as this side chain does not interfer with the bone-seeking properties [147].

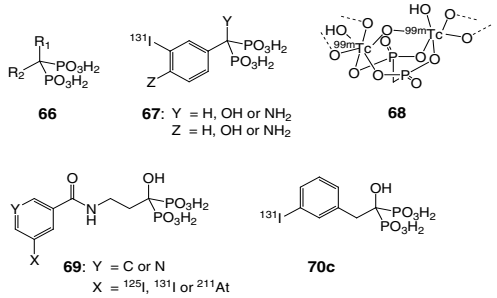

Figure 9.2: Examples of bisphosphonates investigated as bone-seeking agents. The structure of the ^{99m}Tc-MDP complex **68** is indicated (from Refs. [169, 170]).

Eisenhut *et al.* were first to evaluate the potential of ^{131}I-labelled bisphosphonates for treatment of bone metastases [171–174]. Several benzylidenebisphosphonates **67** were synthesised (Figure 9.2), showing bone affinity and selectivity comparable to other bone-seeking agents, e.g. ^{99m}Tc-methylene diphosphonate (^{99m}Tc-MDP **68**). However, the *in vivo* stability was low, with considerable deiodination and subsequent uptake of ^{131}I-iodide in the thyroid. A slightly higher bone affinity and selectivity was found with radiohalogenated aromatic amidobisphosphonates **69** [175, 176].

Recently, Årstad *et al.* synthesised and characterised a series of new ^{131}I-labelled arylalkylidenebisphosphonates, of which 1-hydroxy-(*m*-[^{131}I]iodophenyl)ethylidene-1,1-bisphosphonic acid ([^{131}I]HIPEBA **70c**, Figure 9.2) showed high *in vivo* stability, negligible uptake in thyroid and a bone affinity superior to both $^{89}SrCl_2$ **60** and ^{153}Sm-EDTMP **61** [177, 178]. Thus, it is assumed that [^{131}I]HIPEBA **70c** may find use in diagnosis as well as in curative and palliative treatment of bone-related cancers [178].

9.3 Aim of study

The objective of this study was to evaluate the prospective use of the radioiodinated bisphosphonate [*I]HIPEBA **70** in targeted radiotherapy of bone-related cancer in humans. The specific aim was to characterise the initial pharmacokinetics of [^{123}I]HIPEBA **70b** in an animal model resembling humans with respect to skeletal growth patterns as well as liver and kidney functions.

Chapter 10

Methods

10.1 Radioactivity measurements

Radioactivity measurements of radioiodine and preparations of [*I]HIPEBA **70** were carried out with a VDC-304 dose calibrator (Veenstra Instrumenten bv). Scintigraphic imaging of [^{123}I]HIPEBA **70b** in pigs was performed using a mobile Picker CX 250 compact gamma-camera equipped with a general purpose collimator (Paper **V**).

10.2 Chromatography

The radio-HPLC system for purification and isolation of [*I]HIPEBA **70** was developed by Årstad [177]. The system was based on a PLRP-S 100 Å styrene-divinylbenzene column (stationary phase) and a polar mobile phase run under isocratic conditions. A proper sample preparation prior to radio-HPLC was critical to avoid clogging of the column. The best results were obtained when the reaction mixture was added aqueous phosphoric acid and mixed in an ultrasound bath for ∼10 min before injection on the column [177]. Detailed specifications of the radio-HPLC system, instruments and detectors are found in Paper **V**.

10.3 Animals

Healthy young pigs (3 months) of both genders were transported to the large animal facility at the Center for Comparative Medicine, University of Oslo, one day prior to the experiment (Paper **V**). Housing and all procedures involving animals were performed according to protocols approved by the animal care and use committee, in compliance with the National Committee for Animal Experiment's guidelines on animal welfare [113, 114]. The animals were anaesthetised as described in Paper **V**.

10.4 The FNOMIP method

The new scintigraphic image analysis method FNOMIP ("fixed number of most intense pixels") was developed by Skretting in connection with the experiment described in Paper **V** [179, 180]. The FNOMIP method ensures that a selective region of interest (SROI) has a constant size and covers the same anatomical structure at all time points during a study, thus correcting for small movements and for different animal positions in static studies. The method is illustrated in Figure 10.1. This method enables generation of dynamic uptake curves using the total number of counts in a SROI covering a specific anatomical structure (Paper **V**).

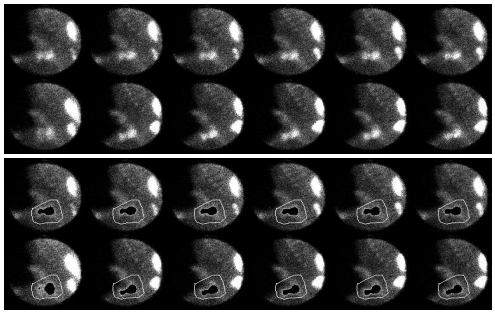

Figure 10.1: Illustration of the FNOMIP method. Upper frame shows the original images, while the lower frame shows the automatically generated selective regions of interest (black regions) of the knee of a pig administrated [^{123}I]HIPEBA **70b**. Note the movement of the knee between image 6–8.

10.5 The OLINDA/EXM code

The OLINDA/EXM personal computer code performs dose calculations and kinetic modeling of radiopharmaceuticals [181]. The estimated radiation dose to different organs of the human body can be calculated from user-supplied biokinetic data obtained from animal or human studies (Paper **V**).

Chapter 11

Bisphosphonate derivatives

11.1 Introduction

Previous biodistribution studies with [*I]HIPEBA **70** in healthy and tumour-bearing rodents have demonstrated a potential for this radioiodinated bisphosphonate as a bone-seeking agent in diagnosis and targeted radiotherapy of bone-related cancer [177, 178]. To provide a basis for future clinical trials in humans, [*I]HIPEBA **70** should be investigated in an animal model more closely resembling humans with respect to skeletal growth patterns, liver and kidney functions.

In this study, the ^{123}I-labelled HIPEBA was synthesised and its initial pharmacokinetic properties investigated in young pigs using gamma-camera imaging.

11.2 Chemistry

The silylated bisphosphonate 1-hydroxy-(*m*-trimethylsilylphenyl)ethylidene-1,1-bisphosphonic acid (**71**) was provided by Årstad, and was radiolabelled and isolated according to literature procedures (Figure 11.1) [177].

Precursor **71** was radioiodinated under acidic conditions using NCS as an oxidis-

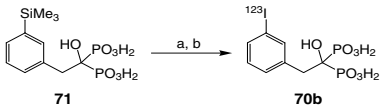

Figure 11.1: Radioiodination of the silylated precursor **71** yielding [^{123}I]HIPEBA **70b**. Reagents and conditions: a) Na^{123}I, NCS, AcOH, TFA, rt; b) $H_3PO_{4(aq)}$, ultrasound, rt.

ing agent, yielding the radioiodinated product 1-hydroxy-(*m*-[^{123}I]iodophenyl)ethylidene-1,1-bisphosphonic acid ([^{123}I]HIPEBA **70b**). Purification by radio-HPLC yielded the radioiodinated bisphosphonate **70b** in >95 % integrated radiochemical yield. However, the yield of isolated material was only 35–40 %. The final preparation consisted of 1.3 GBq [^{123}I]HIPEBA **70b** in 15.7 mL of sterile filtered phosphate buffer (50 mM, pH 7.1, added 2 % EtOH). The radioiodination is depicted in Figure 11.1, and detailed descriptions of the procedure are found in Paper **V**.

11.3 Biology

The following experiment in pigs was approved by the Committee of Ethics for the use of Animals in Research in Norway.

Biodistribution studies were conducted at the Center for Comparative Medicine, University of Oslo, using four 3 months old pigs (two of each gender) weighing 17–21 kg (Paper **V**). The animals were anaesthetised using Stresnil vet/Ketalar/Pentotal, then two of the pigs (one of each gender) were administered [^{123}I]HIPEBA **70b** (204 MBq and 234 MBq, respectively) while the other two pigs were administered the reference compound ^{99m}Tc-MDP **68** (126 MBq and 107 MBq, respectively). The pigs were sacrified after 8 h by injection of Pentotal.

11.4 Imaging and analysis

Biodistribution and biodynamics of [^{123}I]HIPEBA **70b** ($t_{1/2}$ 13.2 h, 159 keV γ in 83.3 %) and ^{99m}Tc-MDP **68** ($t_{1/2}$ 6.02 h, 141 keV γ in 87.2 %) were investigated using a mobile gamma-camera. Dynamic imaging studies were carried out during the first 30 min post-injection, followed by static imaging studies for 5 min at specific time intervals up to 7.5 h (Paper **V**).

The analysis of bone deposition patterns was based on a visual comparison of static images obtained with **70b** and **68**. Dynamic curves for uptake in knee were obtained using the FNOMIP method [179, 180].

11.5 Radiation dose estimates in humans

Estimated absorbed radiation doses for administration of the ^{131}I-labelled HIPEBA **70c** ($t_{1/2}$ 192.48 h, mean β^--energy 0.182 MeV) and ^{153}Sm-EDTMP **61** ($t_{1/2}$ 46.27 h, mean β^--energy 0.225 MeV) in humans were obtained using the OLINDA/EXM code (adult male model) [181]. The input values for the surfaces of trabecular and cortical bone in humans were obtained from data on "Reference man" [182], and the calculations were made under the assumption that accumulated **70c** was not released from bone surfaces. It was assumed that 100 % of **70c**

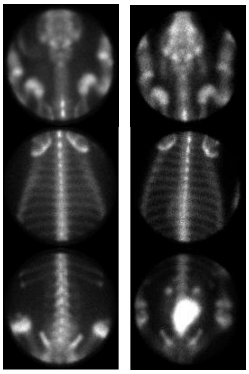

Figure 11.2: Static images showing the uptake of [^{123}I]HIPEBA **70b** (left) and ^{99m}Tc-MDP **68** (right) in head and neck, thorax and pelvis of the pigs 4 h post-injection.

and 80 % of **61** were adsorbed on bone surfaces. To facilitate a direct comparison between **70c** and **61**, the estimated dose values of **61** were converted to correct for the difference in half-lives (Paper **V**).

11.6 Results and discussion

Biodistribution studies were conducted in healthy young pigs to compare the initial pharmacokinetic properties of [^{123}I]HIPEBA **70b** with those of the standard bone scintigraphic agent ^{99m}Tc-MDP **68** (Paper **V**). The results are summarised in Figure 11.2.

Visual inspection of static gamma-camera images of the neck 4 h post-injection showed no accumulation of **70b** in the thyroid (Figure 11.2). This result verified the *in vivo* stability reported for this radioiodinated bisphosphonate in previous studies [177, 178]. However, thyroid blocking agents may be used as a precaution in clinical studies with [*I]HIPEBA **70** in humans.

Dynamic studies of the knee revealed that the bone uptake patterns of **70b** and **68** were indistinguishable during the first 0.5 h post-injection. However, **70b** showed a higher bone accumulation than **68** at later time points, and the uptake increased throughout the experiment. The lower bone accumulation of **68** was due to a rapid renal excretion (Figure 11.2) which reduced the amount of **68** available for uptake in bone. In contrast, a negligible renal excretion of **70b** indicated that almost all the injected activity would end up in bone tissue. These observations were also consistent with the different biological half-lives calculated for

Table 11.1: Estimated absorbed radiation doses for injection of [^{131}I]HIPEBA **70c** and ^{153}Sm-EDTMP **61** in humans. The values were obtained using the OLINDA/EXM code (adult male model). The dose values for **61** have been converted[a] to enable direct comparison with **70c**.

	[^{131}I]**HIPEBA**	^{153}Sm-**EDTMP**$_{\text{converted}}$
Organ	**Dose (mSv/MBq)**	**Dose (mSv/MBq)**[a]
Red bone marrow	4.51	4.66
Osteogenic cells	16.7	24.34
Ovaries	0.24	0.025
Testes	0.13	0.012
Thyroid	0.24	0.029
Effective whole body dose	0.86	0.82

[a] Converted ^{153}Sm-EDTMP dose = Estimated ^{153}Sm-EDTMP dose * $T_{1/2}(^{131}I)$ / $T_{1/2}(^{153}Sm)$

the blood/extravascular compartments (Paper **V**).

The results indicated that [*I]HIPEBA **70** may have favourable properties as a bone-seeking agent in targeted radiotherapy of osseous bone metastases and osteosarcomas in humans. Thus, the radiotherapeutic prospects of the ^{131}I-labelled HIPEBA **70c** were estimated and compared to the bone-seeking radiopharmaceutical ^{153}Sm-EDTMP **61** using the OLINDA/EXM code. The estimated radiation doses for **70c** and **61** were very similar for red bone marrow, osteogenic cells and for the effective whole body dose (Table 11.1). However, the estimated doses to more distant critical organs were larger for **70c** due to emission of photons with higher energies and yields.

Conclusion

The results obtained with [^{123}I]HIPEBA **70b** in pigs indicated high *in vivo* stability and a bone uptake comparable to ^{99m}Tc-MDP **68**. Estimated radiotherapeutic properties of [^{131}I]HIPEBA **70c** were comparable to the FDA-approved ^{153}Sm-EDTMP **61**. Negligible renal uptake and excretion of [*I]HIPEBA **70** facilitate diagnostic scintigraphic imaging of the pelvis and is particularly advantageous for targeted radiotherapy, minimising the radiation doses to kidneys and bladder walls. Hence, future investigations of the biodynamics of [*I]HIPEBA **70** in humans are justified.

Chapter 12

Bone-related cancer: Future prospects

High accumulation of HIPEBA in bone combined with an almost negligible renal excretion indicate that [^{123}I]HIPEBA and [^{124}I]HIPEBA may be used in diagnosis of bone-forming malignancies in SPECT and PET, respectively. The compounds are particularly advantageous for investigations of the pelvis, and may thus be used as a supplement to current bone-seeking agents with considerable renal excretion (e.g. ^{99m}Tc-MDP, ^{153}Sm-EDTMP).

The HIPEBA may also have a future in palliative and curative treatment of bone metastases using therapeutic radionuclides like ^{131}I and ^{211}At. The [^{131}I]HIPEBA has a much more favourable half-life than $^{89}SrCl_2$ and ^{153}Sm-EDTMP, and is more easily available at low cost provided that a kit for *in situ* ^{131}I-labelling is developed. A more strongly focused dose to micrometastases containing bone tissue may be obtained using the ^{211}At-labelled analogue of HIPEBA. The rapid distribution and bone accumulation of HIPEBA are advantageous with regard to the relatively short half-life of ^{211}At. Thus, the ^{211}At-labelled analogue may have potential in treatment of osseous micrometastases, while [^{131}I]HIPEBA would be more efficient for metastatic lesions where pathologically enhanced bone formation is inhomogenously distributed. Treatment of bone-related cancers may also benefit from using [^{131}I]HIPEBA in combination with other bone-seeking radiopharmaceuticals emitting high-LET radiation, e.g. $^{223}RaCl_2$. The radiation dose to red bone marrow will be the limiting factor in humans, unless stem cell support is offered.

References

[1] Cancer Registry of Norway. Institute of Population-based Cancer Research. Cancer in Norway 2004. http://www.kreftregisteret.no/forekomst_og_overlevelse_2004/kreft_i_norge_2004web.pdf.

[2] W. A. Volkert and T. J. Hoffman. Therapeutic Radiopharmaceuticals. *Chem. Rev.*, 99:2269–2292, 1999.

[3] H. Lundqvist V. Tolmachev, J. Carlsson. A Limiting Factor for the Progress of Radionuclide-based Cancer Diagnostics and Therapy. *Acta Oncol.*, 43:264–275, 2004.

[4] T. E. Wheldon and J. A. O'Donoghue. The radiobiology of targeted radiotherapy. *Int. J. Radiat. Biol.*, 58:1–21, 1990.

[5] E. J. Hall. *Radiobiology for the Radiologist.* ISBN 0-397-51248-1. J.B. Lippincott Company, 4. edition, 1994.

[6] A. C. Perkins. *In vivo* molecular targeted radiotherapy. *Biomed. Imaging Interv. J.*, 1:1–7, 2005.

[7] J. Sweit. Radionuclides and carrier molecules for therapy. *Phys. Med. Biol.*, 41:1905–1914, 1996.

[8] C. A. Hoefnagel, S. E. M. Clarke, M. Fischer, J. F. Chatal, V. J. Lewington, S. Nilsson, L. Troncone, and M. R. Vieira. Radionuclide therapy practice and facilities in Europe. *Eur. J. Nucl. Med.*, 26:277–282, 1999.

[9] S. K. Imam. Advancements in cancer therapy with alpha-emitters: a review. *Int. J. Radiation Oncology Biol. Phys.*, 51:271–278, 2001.

[10] M. R. McDevitt, G. Sgouros, R. D. Finn, J. L. Humm, J. G. Jurcic, S. M. Larson, and D. A. Scheinberg. Radioimmunotherapy with alpha-emitting nuclides. *Eur. J. Nucl. Med.*, 25:1341–1351, 1998.

[11] P. M. Pathare, D. K. Hamlin, D. S. Wilbur, M. W. Brechbiel, and L. A. Bray. Synthesis and radiolabeling of a biotin-CHX-B chelate for Bi-213. *J. Labelled Compd. Radiopharm.*, 41:595–603, 1998.

[12] S. G. Gouin, J.-F. Gestin, L. Monrandeau, F. Segat-Dioury, J. C. Meslin, and D. Deniaud. Synthesis and metal complexation properties of Ph-DTPA and Ph-TTHA: novel radionuclide chelating agents for use in nuclear medicine. *Org. Biomol. Chem.*, 3:454–461, 2005.

[13] G. Henriksen, P. Hoff, J. Alstad, and R. H. Larsen. ^{223}Ra for endoradiotherapeutic applications prepared from an immobilized ^{227}Ac/^{227}Th source. *Radiochim. Acta*, 89:661–666, 2001.

[14] H. H. Coenen, S. M. Moerlein, and G. Stöcklin. No-Carrier-Added Radiohalogenation Methods with Heavy Halogens. *Radiochim. Acta*, 34:47–68, 1983.

[15] M. R. Zalutsky and G. Vaidyanathan. Astatine-211-Labeled Radiotherapeutics: An Emerging Approach to Targeted Alpha-Particle Radiotherapy. *Curr. Pharm. Design*, 6:1433–1455, 2000.

[16] M. J. Adam and D. S. Wilbur. Radiohalogens for imaging and therapy. *Chem. Soc. Rev.*, 34:153–163, 2005.

[17] S. C. Srivastava, H. L. Atkins, G. T. Krishnamurthy, I. Zanzi, E. B. Silberstein, G. Meinken, L. F. Mausner, F. Swailem, T. D'Alessandro, C. J. Cabahug, Y. Lau, T. Park, and S. Madajewicz. Treatment of Metastatic Bone Pain with Tin-117m Stannic Diethylenetriaminepentaacetic Acid: A Phase I/II Clinical Study. *Clin. Cancer Res.*, 4:61–68, 1998.

[18] S. J. Adelstein, A. I. Kassis, L. Bodei, and G. Mariani. Radiotoxicity of Iodine-125 and Other Auger-Electron-Emitting Radionuclides: Background to Therapy. *Cancer Biother. Radiopharm.*, 18:301–316, 2003.

[19] T. C. Karagiannis. Targeted cancer therapy with ultra-short range Auger electron emitting isotopes (Electronic letter). http://caonline.amcancersoc.org/cgi/eletters/56/4/226, 2006.

[20] M. Glaser, S. K. Luthra, and F. Brady. Applications of positron-emitting halogens in PET oncology (Review). *Int. J. Oncol.*, 22:253–267, 2003.

[21] S. Palm, J. L. Humm, R. Rundqvist, and L. Jacobsson. Microdosimetry of astatine-211 single-cell irradiation: Role of daughter polonium-211 diffusion. *Med. Phys.*, 31:218–225, 2004.

[22] O. R. Pozzi and M. R. Zalutsky. Radiopharmaceutical Chemistry of Targeted Radiotherapeutics, Part 1: Effects of Solvent on the Degradation of Radiohalogenation Precursors by ^{211}At α-Particles. *J. Nucl. Med.*, 46:700–706, 2005.

[23] O. R. Pozzi and M. R. Zalutsky. Radiopharmaceutical Chemistry of Targeted Radiotherapeutics, Part 2: Radiolytic Effects of ^{211}At α-Particles Influence *N*-Succinimidyl-3-^{211}At-Astatobenzoate Synthesis. *J. Nucl. Med.*, 46:1393–1400, 2005.

[24] H. H. Coenen, J. Mertens, and B. Mazière. *Radioiodination reactions for pharmaceuticals.* ISBN 1-4020-4560-3. Springer, 2006.

[25] D. S. Wilbur. Radiohalogenation of Proteins: An Overview of Radionuclides, Labeling Methods, and Reagents for Conjugate Labeling. *Bioconjugate Chem.*, 3:433–470, 1992.

[26] K. Berei and L. Vasáros. Organic chemistry of astatine. In S. Patai and Z. Rappoport, editors, *The Chemistry of Functional Groups, Supplement D*, chapter 10, pages 405–440. John Wiley & Sons Ltd., 1983.

[27] D. S. Wilbur, M.-K. Chyan, D. K. Hamlin, B. B. Kegley, R. Risler, P. M. Pathare, J. Quinn, R. L. Vessella, C. Foulon, M. Zalutsky, T. J. Wedge, and M. F. Hawthorne. Reagents for Astatination of Biomolecules: Comparison of the in Vivo Distribution and Stability of Some Radioiodinated/Astatinated Benzamidyl and *nido*-Carboranyl Compounds. *Bioconjugate Chem.*, 15:203–223, 2004.

[28] R. H. Seevers and R. E. Counsell. Radioiodination Techniques for Small Organic Molecules. *Chem. Rev.*, 82:575–590, 1982.

[29] C. Galli. Aromatic Iodination: Evidence of Reaction Intermediate and of the σ-Complex Character of the Transition State. *J. Org. Chem.*, 56:3238–3245, 1991.

[30] S. M. Moerlein and H. H. Coenen. Regiospecific No-Carrier-Added Radiobromination and Radioiodination of Aryltrimethyl Group IVb Organometallics. *J. Chem. Soc., Perkin Trans. I*, pages 1941–1947, 1985.

[31] M. Argentini. Labelling with iodine. A review of the literature. Federal Institute for Reactor Research, Wuerenlingen, Switzerland., 1982.

[32] J. March. *Advanced Organic Chemistry; Reactions, Mechanisms, and Structure.* ISBN 0-471-60180-2. John Wiley & Sons, Inc., 4. edition, 1992.

[33] Cancer Research UK. UK Malignant Melanoma statistics. http://info.cancerresearchuk.org/cancerstats/types/melanoma.

[34] The Norwegian Radium Hospital. http://www.radiumhospitalet.no/.

[35] B. S. Larsson. Interaction Between Chemicals and Melanin. *Pigment Cell Res.*, 6:127–133, 1993.

[36] K. Jimbow, T. Iwashina, F. Alena, K. Yamada, J. Pankovich, and T. Umemura. Exploitation of Pigment Biosynthesis Pathway as a Selective Chemotherapeutic Approach for Malignant Melanoma. *J. Invest. Dermatol.*, 100:231S–238S, 1993.

[37] P. A. Riley. Melanin. *Int. J. Biochem. Cell Biol.*, 29:1235–1239, 1997.

[38] S. I. Fox. *Human Physiology.* ISBN 0-07-111584-6. McGraw-Hill Companies, Inc., 9. edition, 2005.

[39] E. J. Land and P. A. Riley. Spontaneous Redox Reactions of Dopaquinone and the Balance between the Eumelanic and Pheomelanic Pathways. *Pigment Cell Res.*, 13:273–277, 2000.

[40] E. J. Land, S. Ito, K. Wakamatsu, and P. A. Riley. Rate Constants for the First Two Chemical Steps of Eumelanogenesis. *Pigment Cell Res.*, 16:487–493, 2003.

[41] S. Ito. A Chemist's View of Melanogenesis. *Pigment Cell Res.*, 16:230–236, 2003.

[42] A. Slominski, D. J. Tobin, S. Shibahara, and J. Wortsman. Melanin Pigmentation in Mammalian Skin and Its Hormonal Regulation. *Physiol. Rev.*, 84:1155–1228, 2004.

[43] G. Prota. Pigment Cell Research: What Directions? *Pigment Cell Res.*, 10:5–11, 1997.

[44] P. A. Riley. Melanogenesis and melanoma. *Pigment Cell Res.*, 16:548–552, 2003.

[45] G. Ronsisvalle, A. Marrazzo, O. Prezzavento, A. Cagnotto, T. Mennini, C. Parenti, and G. M. Scoto. Opioid and sigma receptor studies. New developments in the design of selective sigma ligands. *Pure Appl. Chem.*, 73:1499–1509, 2001.

[46] C. S. John, B. J. Vilner, B. C. Geyer, T. Moody, and W. D. Bowen. Targeting Sigma Receptor-binding Benzamides as *in Vivo* Diagnostic and Therapeutic Agents for Human Prostate Tumors. *Cancer Res.*, 59:4578–4583, 1999.

[47] C. S. John, W. D. Bowen, T. Saga, S. Kinuya, B. J. Vilner, J. Baumgold, C. H. Paik, R. C. Reba, R. D. Neumann, V. M. Varma, and J. G. McAfee. A Malignant Melanoma Imaging Agent: Synthesis, Characterization, In Vitro Binding and Biodistribution of Iodine-125-(2-Piperidinylaminoethyl)-4-Iodobenzamide. *J. Nucl. Med.*, 34:2169–2175, 1993.

[48] M. Eisenhut, W. E. Hull, A. Mohammed, W. Mier, D. Lay, W. Just, K. Gorgas, W. D. Lehmann, and U. Haberkorn. Radioiodinated *N*-(2-Diethylaminoethyl)benzamide Derivatives with High Melanoma Uptake: Structure-Affinity Relationships, Metabolic Fate, and Intracellular Localization. *J. Med. Chem.*, 43:3913–3922, 2000.

[49] C. S. John, W. D. Bowen, S. J. Fisher, B. B. Lim, B. C. Geyer, B. J. Vilner, and R. L. Wahl. Synthesis, *in Vitro* Pharmacologic Characterization, and Preclinical Evaluation of N-[2-(1'-Piperidinyl)Ethyl]-3-Iodo-4-Methoxybenzamide (P[^{125}I]MBA) for Imaging Breast Cancer. *Nucl. Med. Biol.*, 26:377–382, 1999.

[50] V. Cavaliers, H. Everaert, C. S. John, T. Lahoutte, and A. Bossuyt. Sigma Receptor Scintigraphy with *N*-[2-(1'-Piperidinyl)Ethyl]-3-^{123}I-Iodo-4-Methoxybenzamide of Patients with Suspected Primary Breast Cancer: First Clinical Results. *J. Nucl. Med.*, 43:1647–1649, 2002.

[51] K. T. Wheeler, L.-M. Wang, C. A. Wallen, S. R. Childers, J. M. Cline, P. C. Keng, and R. H. Mach. Sigma-2 receptors as a biomarker of proliferation in solid tumours. *Br. J. Cancer*, 82:1223–1232, 2000.

[52] M. Friebe, A. Mahmood, C. Bolzati, A. Drews, B. Johannsen, M. Eisenhut, D. Kraemer, A. Davison, and A. G. Jones. [^{99m}Tc]Oxotechnetium(V) Complexes of Amine-Amide-Dithiol Chelates with Dialkylaminoalkyl Substituents as Potential Diagnostic Probes for Malignant Melanoma. *J. Med. Chem.*, 44:3132–3140, 2001.

[53] C. A. Hoefnagel. Role of nuclear medicine in melanoma. *Eur. J. Nucl. Med.*, 25:1567–1574, 1998.

[54] Y. Miao, M. Hylarides, D. R. Fisher, T. Shelton, H. Moore, D. W. Wester, A. R. Fritzberg, C. T. Winkelmann, T. Hoffman, and T. P. Quinn. Melanoma Therapy via Peptide-Targeted α-Radiation. *Clin. Cancer Res.*, 11:5616–5621, 2005.

[55] P. A. Riley, C. J. Cooksey, C. I. Johnson, E. J. Land, A. M. Latter, and C. A. Ramsden. Melanogenesis-targeted anti-melanoma pro-drug development: Effect of side-chain variations on the cytotoxicity of tyrosinase-generated ortho-quinones in a model screening system. *Eur. J. Cancer*, 33:135–143, 1997.

[56] A. M. Jordan, T. H. Khan, H. M. I. Osborn, A. Photiou, and P. A. Riley. Melanocyte-Directed Enzyme Prodrug Therapy (MDEPT): Development of a Targeted Treatment for Malignant Melanoma. *Bioorg. Med. Chem.*, 7:1775–1780, 1999.

[57] A. M. Jordan, T. H. Khan, H. Malkin, H. M. I. Osborn, A. Photiou, and P. A. Riley. Melanocyte-Directed Enzyme Prodrug Therapy (MDEPT): Development of Second Generation Prodrugs for Targeted Treatment of Malignant Melanoma. *Bioorg. Med. Chem.*, 9:1549–1558, 2001.

[58] K. Ishiwata, K. Kubota, R. Kubota, R. Iwata, T. Takahashi, and T. Ido. Selective 2-[18F]fluorodopa uptake for melanogenesis in murine metastatic melanomas. *J. Nucl. Med.*, 32:95–101, 1991.

[59] K. Ishiwata, M. Shiono, K. Kubota, K. Yoshino, J. Hatazawa, T. Ido, C. Honda, M. Ichihashi, and Y. Mishima. A unique in vivo assessment of 4-[10B]borono-L-phenylalanine in tumor tissues for boron neutron capture therapy of malignant melanomas using positron emission tomography and 4-borono-2-[18F]fluoro-L-phenylalanine. *Melanoma Res.*, 2:171–179, 1992.

[60] S. Miura, T. Ueda, K. Jimbow, S. Ito, and K. Fujita. Synthesis of cysteinylphenol, cysteaminylphenol, and related compounds, and in vivo evaluation of antimelanoma effect. *Arch. Dermatol. Res.*, 279:219–225, 1987.

[61] S. Ito, T. Kato, K. Ishikawa, T. Kasuga, and K. Jimbow. Mechanism of selective toxicity of 4-S-cysteinylphenol and 4-S-cysteaminylphenol to melanocytes. *Biochem. Pharmacol.*, 36:2007–2011, 1987.

[62] N. J. Lant, P. McKeown, L. R. Kelland, P. M. Rogers, and D. J. Robins. Synthesis and antimelanoma activity of analogues of N-acetyl-4-S-cysteaminylphenol. *Anticancer Drug Des.*, 15:295–302, 2000.

[63] J. Yukitake, H. Otake, S. Inoue, K. Wakamatsu, and S. Ito. Comparison of *in vivo* anti-melanoma effect of enantiomeric α-methyl- and α-ethyl-4-*S*-cysteaminylphenol. *Melanoma Res.*, 14:115–120, 2004.

[64] B. S. Larsson, B. Larsson, and A. Roberto. Boron Neutron Capture Therapy for Malignant Melanoma: An Experimental Approach. *Pigment Cell Res.*, 2:356–360, 1989.

[65] U. Mårs, V. Tolmachev, and A. Sundin. Positron Emission Tomography of Experimental Melanoma with [^{76}Br]5-Bromo-2-Thiouracil. *Nucl. Med. Biol.*, 27:845–849, 2000.

[66] V. Tolmachev, A. Orlova, and A. Sundin. Preparation of [^{76}Br]5-bromo-2-thiouracil, a positron-emitting melanoma localizing agent. *J. Radioanal. Nucl. Chem.*, 251:406–412, 2002.

[67] A. M. Potts. Uveal Pigment and Phenothiazine Compounds. *Trans. Am. Ophthalmol. Soc.*, 60:517–552, 1962.

[68] E. M. Link, I. Brown, R. N. Carpenter, and J. S. Mitchell. Uptake and Therapeutic Effectiveness of ^{125}I- and ^{211}At-Methylene Blue for Pigmented Melanoma in an Animal Model System. *Cancer Res.*, 49:4332–4337, 1989.

[69] E. M. Link, A. S. Michalowski, and F. Rösch. 211At-Methylene Blue in Targeted Radiotherapy of Disseminated Melanoma. *Pigment Cell Res.*, 7:358–362, 1994.

[70] I. Brown, R. N. Carpenter, E. M. Link, and J. S. Mitchell. Potential diagnostic and therapeutic agents for malignant melanoma: Synthesis of heavy radiohalogenated derivatives of methylene blue by electrophilic and nucleophilic methods. *J. Radioanal. Nucl. Chem. Letters*, 107:337–351, 1986.

[71] P. J. Blower and N. J. Carter. Rapid preparation of iodine-123-labelled methylene blue and toluidine blue: potential new agents for parathyroid scintigraphy. *Nucl. Med. Comm.*, 11:413–420, 1990.

[72] E. M. Link and R. N. Carpenter. 211At-methylene blue for targeted radiotherapy of human melanoma xenografts: treatments of cutaneous tumours and lymph node metastases. *Cancer Res.*, 52:4385–4390, 1992.

[73] E. M. Link, D. C. Costa, D. Lane, P. J. Blower, and M. F. Spittle. Radioiodinated methylene blue for diagnosing early melanoma metastases. *The Lancet*, 348:753, 1996.

[74] P. J. Blower, K. Clark, and E. M. Link. Radioiodinated Methylene Blue for Melanoma Targeting: Chemical Characterisation and Tumour Selectivity of Labelled Components. *Nucl. Med. Biol.*, 24:305–310, 1997.

[75] E. M. Link, P. J. Blower, D. C. Costa, D. M. Lane, D. Lui, R. S. D. Brown, P. J. Ell, and M. F. Spittle. Early detection of melanoma metastases with radioiodinated methylene blue. *Eur. J. Nucl. Med.*, 25:1322–1329, 1998.

[76] K. Hasegawa, S. Ito, S. Inoue, K. Wakamatsu, H. Ozeki, and I. Ishiguro. Dihydro-1,4-benzothiazine-6,7-dione, the Ultimate Toxic Metabolite of 4-*S*-Cysteaminylphenol and 4-*S*-Cysteaminylcatechol. *Biochem. Pharmacol.*, 53:1435–1444, 1997.

[77] G. Prota, M. d'Ischia, and D. Mascagna. Melanogenesis as a targeting strategy against metastatic melanoma: a reassessment. *Melanoma Res.*, 4:351–358, 1994.

[78] F. Alena, K. Jimbow, and S. Ito. Melanocytotoxicity and Antimelanoma Effects of Phenolic Amine Compounds in Mice *in Vivo*. *Cancer Res.*, 50:3743–3747, 1990.

[79] S. Inoue, S. Ito, K. Wakamatsu, K. Jimbow, and K. Fujita. Mechanism of growth inhibition of melanoma cells by 4-*S*-cysteaminylphenol and its analogues. *Biochem. Pharmacol.*, 39:1077–1083, 1990.

[80] M. Tandon, P. D. Thomas, M. Shokravi, S. Singh, S. Samra, D. Chang, and K. Jimbow. Synthesis and Antitumour Effect of the Melanogenesis-based Antimelanoma Agent *N*-Propionyl-4-*S*-cysteaminylphenol. *Biochem. Pharmacol.*, 55:2023–2029, 1998.

[81] S. Inoue, K. Hasegawa, K. Wakamatsu, and S. Ito. Comparison of antimelanoma effects of 4-*S*-cysteaminylphenol and its homologues. *Melanoma Res.*, 8:105–112, 1998.

[82] N. J. Lant, P. McKeown, M. C. Timoney, L. R. Kelland, P. M. Rogers, and D. J. Robins. Synthesis and antimelanoma activity of analogues of N-acetyl-4-S-cysteaminylphenol substituted with two methyl groups alpha to the nitrogen. *Anticancer Drug Des.*, 16:49–55, 2001.

[83] J. Yukitake, H. Otake, S. Inoue, K. Wakamatsu, C. Olivares, F. Solano, K. Hasegawa, and S. Ito. Synthesis and selective *in vitro* anti-melanoma effect of enantiomeric α-methyl- and α-ethyl-4-*S*-cysteaminylphenol. *Melanoma Res.*, 13:603–609, 2003.

[84] T. Miura, K. Jimbow, and S. Ito. The *in vivo* antimelanoma effect of 4-S-cysteaminylphenol and its N-acetyl derivative. *Int. J. Cancer*, 46:931–934, 1990.

[85] F. Alena, T. Iwashina, A. Gili, and K. Jimbow. Selective *in Vivo* Accumulation of *N*-Acetyl-4-*S*-cysteaminylphenol in B16F10 Murine Melanoma and Enhancement of Its *in Vitro* and *in Vivo* Antimelanoma Effect by Combination of Buthionine Sulfoximine. *Cancer Res.*, 54:2661–2666, 1994.

[86] S. Singh, K. Jimbow, P. Kumar, A. J. McEwan, and L. I. Wiebe. Synthesis and radioiodination of 3-(*E*)-(2-iodovinyl)-*N*-acetyl-4-cysteaminylphenol, a putative tyrosinase substrate for imaging neural crest tumours. *J. Labelled Cpd. Radiopharm.*, 41:355–361, 1998.

[87] P. D. Thomas, H. Kishi, H. Cao, M. Ota, T. Yamashita, S. Singh, and K. Jimbow. Selective Incorporation and the Specific Cytocidal Effect as the Cellular Basis for the Antimelanoma Action of Sulphur Containing Tyrosine Analogs. *J. Invest. Dermatol.*, 113:928–934, 1999.

[88] K. Jimbow, T. Miura, S. Ito, and K. Ishikawa. Phenolic Melanin Precursors Provide a Rational Approach to the Design of Antitumor Agents for Melanoma. *Pigment Cell Res.*, 2:34–39, 1989.

[89] J. M. Pankowich, K. Jimbow, and S. Ito. 4-S-Cysteaminylphenol and its Analogues as Substrates for Tyrosinase and Monoamine Oxidase. *Pigment Cell Res.*, 3:146–149, 1990.

[90] P. G. Parsons, D. Favier, M. McEwan, H. Takahashi, K. Jimbow, and S. Ito. Action of cysteaminylphenols on human melanoma cells *in vivo* and *in vitro*: 4-S-cysteaminylphenol binds protein disulphide isomerase. *Melanoma Res.*, 1:97–104, 1991.

[91] K. Yamada and K. Jimbow. Selective *in vivo* and *in vitro* incorporation and accumulation of phenolic thioether amine into malignant melanoma and identification of a (58 kD) binding glycoprotein. *Melanoma Res.*, 2:225–233, 1992.

[92] C. J. Cooksey, K. Jimbow, E. J. Land, and P. A. Riley. Reactivity of orthoquinones involved in tyrosinase-dependent cytotoxicity: differences between alkylthio- and alkoxy-substituents. *Melanoma Res.*, 2:283–293, 1992.

[93] T. Iwashina, K. Jimbow, and L. I. Wiebe. The Synthesis of *N*-Acetyl-4-*S*-Cysteaminyl [U-^{14}C]Phenol as a Basis for the Development of an Antimelanoma and Melanoma-radioimaging Agent. *Appl. Radiat. Isot.*, 45:703–705, 1994.

[94] M. Jimbow, H. Marusyk, and K. Jimbow. The *in vivo* melanocytotoxicity and depigmenting potency of *N*-2,4-acetoxyphenyl thioethyl acetamide in the skin and hair. *Br. J. Dermatol.*, 133:526–536, 1995.

[95] Y. Minamitsuji, K. Toyofuku, S. Sugiyama, K. Yamada, and K. Jimbow. Sulphur Containing Tyrosine Analogs Can Cause Selective Melanocytotoxicity Involving Tyrosinase-Mediated Apoptosis. *J. Invest. Dermatol. Symposium Proceedings*, 4:130–136, 1999.

[96] A. Gili, P. D. Thomas, M. Ota, and K. Jimbow. Comparison of *in vitro* cytotoxicity of *N*-acetyl and *N*-propionyl derivatives of phenolic thioether amines in melanoma and neuroblastoma cells and the relationship to tyrosinase and tyrosine hydroxylase enzyme activity. *Melanoma Res.*, 10:9–15, 2000.

[97] R. A. Murphy, H. F. Kung, M.-P. Kung, and J. Billings. Synthesis and Characterization of Iodobenzamide Analogues: Potential D-2 Dopamine Receptor Imaging Agents. *J. Med. Chem.*, 33:171–178, 1990.

[98] J. M. Michelot, M. F. Moreau, P. G. Labarre, J. C. Madelmont, A. J. Veyre, J. M. Papon, D. F. Parry, J. F. Bonafous, J. Y. Boire, and G. G. Desplanches. Synthesis and evaluation of new iodine-125 radiopharmaceuticals as potential tracers for malignant melanoma. *J. Nucl. Med.*, 32:1573–1580, 1991.

[99] H. Dittmann, H. H. Coenen, F. Zölzer, K. Dutschka, W. Brandau, and C. Streffer. *In Vitro* Studies on the Cellular Uptake of Melanoma Imaging Aminoalkyl-Iodobenzamide Derivatives (ABA). *Nucl. Med. Biol.*, 26:51–56, 1999.

[100] S. M. N. Efange, R. H. Michelson, B. Knusel, F. Hefti, R. J. Boudreau, J. R. Thomas, and J. R. Tennison. Synthesis and Biological Evaluation of Radioiodinated *N*-2-(4-Piperidyl)ethyl Benzamides. *Nucl. Med. Biol.*, 20:527–538, 1993.

[101] B. J. Vilner, C. S. John, and W. D. Bowen. Sigma-1 and Sigma-2 Receptors Are Expressed in a Wide Variety of Human and Rodent Tumor Cell Lines. *Cancer Res.*, 55:408–413, 1995.

[102] L. Maffioli, L. Mascheroni, V. Mongioj, M. Gasparini, M. T. Baldini, E. Seregni, M. R. Castellani, N. Cascinelli, and G.-L. Buraggi. Scintigraphic Detection of Melanoma Metastases with a Radiolabeled Benzamide ([^{123}I]-(S)-IBZM). *J. Nucl. Med.*, 35:1741–1747, 1994.

[103] M. F. Moreau, J. Michelot, J. Papon, M. Bayle, P. Labarre, J. C. Madelmont, D. Parry, J. Y. Boire, N. Moins, H. Seguin, A. Veyre, and L. Mauclaire. Synthesis, Radiolabeling, and Preliminary Evaluation in Mice of Some (*N*-Diethylaminoethyl)-4-Iodobenzamide Derivatives as Melanoma Imaging Agents. *Nucl. Med. Biol.*, 22:737–747, 1995.

[104] A. Mohammed, C. Nicholl, U. Titsch, and M. Eisenhut. Radioiodinated N-(Alkylaminoalkyl)-Substituted 4-Methoxy-, 4-Hydroxy-, and 4-Aminobenzamides: Biological Investigations for the Improvement of Melanoma-Imaging Agents. *Nucl. Med. Biol.*, 24:373–380, 1997.

[105] N. Moins, J. Papon, H. Seguin, D. Gardette, M.-F. Moreau, P. Labarre, M. Bayle, J. Michelot, J.-C. Gramain, J.-C. Madelmont, and A. Veyre. Synthesis, characterization and comparative biodistribution study of a new series of *p*-Iodine-125 benzamides as potential melanoma imaging agents. *Nucl. Med. Biol.*, 28:799–808, 2001.

[106] M. Wolf, U. Bauder-Wüst, A. Mohammed, F. Schönsiegel, W. Mier, U. Haberkorn, and M. Eisenhut. Alkylating benzamides with melanoma cytotoxicity. *Melanoma Res.*, 14:353–360, 2004.

[107] J. M. Michelot, M. F. Moreau, A. J. Veyre, J. F. Bonafous, F. J. Bacin, J. C. Madelmont, F. Bussiere, P. A. Souteyrand, L. P. Mauclaire, and F. M. Chossat. Phase II scintigraphic clinical trial of malignant melanoma and metastases with iodine-125-N-(2-diethylaminoethyl)-4-iodobenzamide. *J. Nucl. Med.*, 33:1260–1266, 1993.

[108] C. S. John, T. Saga, S. Kinuya, N. Le, J. M. Jeong, C. H. Paik, R. C. Reba, V. M. Varma, and J. G. McAfee. An Improved Synthesis of [^{125}I]*N*-(diethylaminoethyl)-4-iodobenzamides: a Potent Ligand for Imaging Malignant Melanoma. *Nucl. Med. Biol.*, 20:75–79, 1993.

[109] C. Nicholl, A. Mohammed, W. E. Hull, B. Bubeck, and M. Eisenhut. Pharmacokinetics of Iodine-123-IMBA for Melanoma Imaging. *J. Nucl. Med.*, 38:127–133, 1997.

[110] G. Henriksen, S. Messelt, E. Olsen, and R. H. Larsen. Optimisation of cyclotron production parameters for the ^{209}Bi(α, 2n)^{211}At reaction related to biomedical use of ^{211}At. *Appl. Radiat. Isot.*, 54:839–844, 2001.

[111] S. Lindegren, T. Bäck, and H. J. Jensen. Dry-distillation of astatine-211 from irradiated bismuth targets: a time-saving procedure with high recovery yields. *Appl. Radiat. Isot.*, 55:157–160, 2001.

[112] E. M. Brevik. Syntesemetoder for renfremstilling av ^{125}I- og ^{211}At-merkete benzamider. Master's thesis, Department of Chemistry, University of Oslo, 2000.

[113] Royal Society/Universities federation for animal welfare (UFAW). Guidelines on the care of laboratory animals and their use for scientific purposes. 1. Housing and care. UFAW, London, UK, 1987.

[114] United Kingdom Coordinating Committee on Cancer Research (UKCCCR). UKCCCR guidelines for the welfare of animals in experimental neoplasia. *Br. J. Cancer*, 58:156–160, 1988.

[115] The National Institutes of Health (NIH). Guide for the care and use of laboratory animals. NIH Publication No. 86-23. Bethesda, US, 1985.

[116] K. M. Hwang, Ø. Fodstad, R. K. Oldham, and A. C. Morgan Jr. Radiolocalization of xenografted human malignant melanoma by monoclonal antibody (9.2.27) to a melanoma-associated antigen in nude mice. *Cancer Res.*, 45:4150–4155, 1985.

[117] V. N. Ivanov, Ø. Fodstad, and Z. Ronai. Expression of ring finger-deleted TRAF2 sensitizes metastatic melanoma cells to apoptosis via up-regulation of p38, TNFα and suppression of NF-κB activities. *Oncogene*, 20:2243–2253, 2001.

[118] D. S. Wilbur, D. K. Hamlin, P. M. Pathare, and S. A. Weerawarna. Biotin Reagents for Antibody Pretargeting. Synthesis, Radioiodination, and *in Vitro* Evaluation of Water Soluble, Biotinidase Resistant Biotin Derivatives. *Bioconjugate Chem.*, 8:572–584, 1997.

[119] J. J. Feigenbaum, M. D. Choubal, K. Payza, J. R. Kanofsky, and D. S. Crumrine. Receptor Inactivation by Dye-Neuropeptide Conjugates: 1. The Synthesis of Cys-Containing Dye-Neuropeptide Conjugates. *Peptides*, 17:991–994, 1996.

[120] K. H. Holm. Personal communication.

[121] H. Masuya, H. Shimadzu, T. Miyawaki, and M. A. Motsenbocker. Preparation of phenothiazines for use in photodynamic therapy and immunoassays. Eur. Pat. Appl., 1992.

[122] N. Leventis, M. Chen, and S. Sotiriou-Leventis. Synthesis of Substituted Phenothiazines Analogous to Methylene Blue by Electrophilic and Nucleophilic Aromatic Substitutions in Tandem. A Mechanistic Perspective. *Tetrahedron*, 53:10083–10092, 1997.

[123] M. Wainwright and R. M. Giddens. Phenothiazinium photosensitisers: choises in synthesis and applications. *Dyes and Pigments*, 57:245–257, 2003.

[124] R. Nishii, K. Kawai, L. G. Flores II, S. Jinnouchi, S. Nagamachi, and S. Tamura. Synthesis and preliminary biodistribution of 3-iodo-4-hydroxyphenyl-L-cystein. *J. Labelled Cpd. Radiopharm.*, 42, Suppl. 1:S795–S797, 1999.

[125] R. Nishii, K. Kawai, L. G. Flores II, H. Kataoka, S. Jinnouchi, S. Nagamachi, Y. Arano, and S. Tamura. A novel radiopharmaceutical for detection of malignant melanoma, based on melanin formation: 3-iodo-4-hydroxyphenyl-L-cysteine. *Nucl. Med. Comm.*, 24:575–582, 2003.

[126] H. L. Wehrmeister. Reactions of Aromatic Thiols with Oxazolines. *J. Org. Chem.*, 28:2587–2588, 1963.

[127] H. L. Wehrmeister. N-(Arylmercaptoalkyl) Amides by Reaction of Thiols with Amino Alcohols and Carboxylic Acid. *J. Org. Chem.*, 28:2589–2591, 1963.

[128] T. W. Greene and P. G. M. Wuts. *Protective groups in organic synthesis*. ISBN 0-471-16019-9. John Wiley & Sons, Inc., 3. edition, 1999.

[129] Y. Kita, T. Okuno, M. Egi, K. Iio, Y. Takeda, and S. Akai. An Effective *p*-Thiocyanation of Phenols Using Phenyliodine Dichloride–Lead(II) Thiocyanate. *Synlett*, pages 1039–1040, 1994.

[130] Y. Kita, Y. Takeda, T. Okuno, M. Egi, K. Iio, K. Kawaguchi, and S. Akai. An Efficient *p*-Thiocyanation of Phenols and Naphthols Using a Reagent Combination of Phenyliodine Dichloride and Lead(II) Thiocyanate. *Chem. Pharm. Bull.*, 45:1887–1890, 1997.

[131] D. Koyunçu, A. McKillop, and L. McLaren. A Simple and Inexpensive Procedure for the Preparation of (Dichloroiodo)arenes. *J. Chem. Research (S)*, page 21, 1990.

[132] A. Varvoglis. Hypervalent Iodine In Organic Synthesis. In A. R. Katritzky, O. Meth-Cohn, and C. W. Rees, editors, *Best Synthetic Methods*, ISBN 0-12-714975-9, chapter 2.2 and 6.4.5. Academic Press, Inc., San Diego, 1997.

[133] R. Q. Brewster and W. Schroeder. *p*-Thiocyanodimethylaniline. *Org. Synth.*, II:574–575, 1943.

[134] J. L. Wardell. Preparation of thiols. In S. Patai, editor, *The chemistry of functional groups; The chemistry of the thiol group*, chapter 4, pages 163–269. John Wiley & Sons Ltd., 1974.

[135] R. J. Laufer. 4-Mercaptophenol. In *Chem. Abstr.*, volume 75, pages 88310–88311. 1971.

[136] T. Matsui, M. Harada, M. Toba, and Y. Yoshimura. Effect of the coexistence of nitrogen compounds on the sulfur tolerance and catalytic activity of Pd and Pt monometallic catalysts supported on high-silica USY zeolite and amorphous silica. *Appl. Catal. A*, 293:137–144, 2005.

[137] S. R. Padgette, H. H. Herman, J. H. Han, S. H. Pollock, and S. W. May. Antihypertensive Activities of Phenyl Aminoethyl Sulfides, a Class of Synthetic Substrates for Dopamine β-Hydroxylase. *J. Med. Chem.*, 27:1354–1357, 1984.

[138] J. A. Prezioso, N. Wang, and W. D. Bloomer. Thymidylate synthase as a target enzyme for the melanoma-specific toxicity of 4-S-cysteaminylphenol and *N*-acetyl-4-S-cysteaminylphenol. *Cancer Chemother. Pharmacol.*, 30:394–400, 1992.

[139] M. M. Edreira and O. R. Pozzi. Iodide benzamides for the in-vivo detection of melanoma and metastases. *Melanoma Res.*, 16:37–43, 2006.

[140] D. L. Gilliland, G. P. Basmadjian, A. P. Marchand, G. H. Hinkle, A. Earlywine, and R. D. Ice. Iodine Labelled Radiopharmaceuticals from Arylthallium bis(trifluoroacetate) Intermediates. *J. Radioanal. Chem.*, 65:107–113, 1981.

[141] G. W. M. Visser and E. L. Diemer. The Synthesis of Organic At-Compounds through Thallium Compounds. *Int. J. Appl. Radiat. Isot.*, 33:389–390, 1982.

[142] M. R. Zalutsky and A. S. Narula. A Method for the Radiohalogenation of Proteins Resulting in Decreased Thyroid Uptake of Radioiodine. *Appl. Radiat. Isot.*, 38:1051–1055, 1987.

[143] R. E. Coleman. The treatment of metastatic bone disease. In O. L. M. Bijvoet, H. A. Fleisch, R. E. Canfield, and R. G. G. Russell, editors, *Bisphosphonate on Bones*, ISBN 0-444-89132-3, pages 349–363. Elsevier Science B.V., Amsterdam, 1995.

[144] A. Stuhaug. Nytt skyts mot benmetastaser. http://www.legemidlerogsamfunn.no/, 2002.

[145] E. Shane and J. P. Bilezikian. Normal bone and mineral homeostasis. In O. L. M. Bijvoet, H. A. Fleisch, R. E. Canfield, and R. G. G. Russell, editors, *Bisphosphonate on Bones*, ISBN 0-444-89132-3, pages 3–21. Elsevier Science B.V., Amsterdam, 1995.

[146] S. Ott. Osteoporosis and Bone Physiology. http://courses.washington.edu/bonephys/, 2007.

[147] H. Fleisch. From the Laboratory to the Patient. Bisphosphonates in bone disease. New York: The Parthenon Publishing Group, 1995.

[148] R. D. Rubens. Bone involvement in solid tumours. In O. L. M. Bijvoet, H. A. Fleisch, R. E. Canfield, and R. G. G. Russell, editors, *Bisphosphonate on Bones*, ISBN 0-444-89132-3, pages 337–347. Elsevier Science B.V., Amsterdam, 1995.

[149] V. J. Lewington. Bone-Seeking Radionuclides for Therapy. *J. Nucl. Med.*, 46:38S–47S, 2005.

[150] V. J. Lewington. A practical guide to targeted therapy for bone pain palliation. *Nucl. Med. Commun.*, 23:833–836, 2002.

[151] L. G. Bouchet, W. E. Bolch, S. M. Goddu, R. W. Howell, and D. V. Rao. Considerations in the Selection of Radiopharmaceuticals for Palliation of Bone Pain from Metastatic Osseous Lesions. *J. Nucl. Med.*, 41:682–687, 2000.

[152] C. K. Lee, D. M. Aeppli, J. Unger, R. J. Boudreau, and S. H. Levitt. Strontium-89 Chloride (Metastron) for Palliative Treatment of Bony Metastases: The University of Minnesota Experience. *Am. J. Clin. Oncol.*, 19:102–107, 1996.

[153] C. Collins, J. F. Eary, G. Donaldson, C. Vernon, N. E. Bush, S. Petersdorf, R. B. Livingston, E. E. Gordon, C. R. Chapman, and F. R. Appelbaum. Samarium-153-EDTMP in bone metastases of hormone refractory prostate carcinoma: a phase I/II trial. *J. Nucl. Med.*, 34:1839–1844, 1993.

[154] Ø. S. Bruland, A. Skretting, Ø. P. Solheim, and M. Aas. Targeted radiotherapy of osteosarcoma using ^{153}Sm-EDTMP. A new promising approach. *Acta. Oncol.*, 35:381–384, 1996.

[155] C. L. Maini, S. Bergomi, L. Romano, and R. Sciuto. ^{153}Sm-EDTMP for bone pain palliation in skeletal metastases. *Eur. J. Nucl. Med. Mol. Imaging*, 31 (Suppl. 1):S171–S178, 2004.

[156] W. Brenner, W. U. Kampen, C. Brümmer, C. von Forstner, M. Zuhayra, N. Czech, C. Muhle, and E. Henze. Bone Uptake Studies in Rabbits Before and After High-Dose Treatment with ^{153}Sm-EDTMP or ^{186}Re-HEDP. *J. Nucl. Med.*, 44:247–251, 2003.

[157] J. M. de Klerk, A. D. van het Schip, B. A. Zonnenberg, A. van Dijk, J. M. Quirijnen, G. H. Blijham, and P. P. van Rijk. Phase 1 study of rhenium-186-HEDP in patients with bone metastases originating from breast cancer. *J. Nucl. Med.*, 37:244–249, 1996.

[158] M. G. E. H. Lam, J. M. H. de Klerk, and P. P. van Rijk. ^{186}Re-HEDP for metastatic bone pain in breast cancer patients. *Eur. J. Nucl. Med. Mol. Imaging*, 31 (Suppl. 1):S162–S170, 2004.

[159] A. Bishayee, D. V. Rao, S. C. Srivastava, L. G. Bouchet, W. E. Bolch, and R. W. Howell. Marrow-Sparing Effects of ^{117m}Sn(4+)Diethylenetriaminepentaacetic Acid for Radionuclide Therapy of Bone Cancer. *J. Nucl. Med.*, 41:2043–2050, 2000.

[160] G. A. R. Solá, M. G. Argüelles, D. L. Bottazzini, J. C. Furnari, I. G. Parada, A. Rojo, and H. V. Ruiz. Lutetium-177-EDTMP for bone pain palliation. Preparation, biodistribution and pre-clinical studies. *Radiochim. Acta*, 88:157–161, 2000.

[161] S. Chakraborty, T. Das, P. R. Unni, H. D. Sarma, G. Samuel, S. Banerjee, M. Venkatesh, N. Ramamoorthy, and M. R. A. Pillai. ^{177}Lu labelled polyaminophosphonates as potential agents for bone pain palliation. *Nucl. Med. Comm.*, 23:67–74, 2002.

[162] G. Henriksen, K. Breistøl, Ø. S. Bruland, Ø. Fodstad, and R. H. Larsen. Antitumor Effect from Bone-seeking, α-Particle-emitting ^{223}Ra Demonstrated in an Experimental Skeletal Metastases Model. *Cancer Res.*, 62:3120–3125, 2002.

[163] G. Henriksen, D. R. Fischer, J. C. Roeske, Ø. S. Bruland, and R. H. Larsen. Targeting of Osseous Sites with α-Emitting ^{223}Ra: Comparison with the β-Emitter ^{89}Sr in Mice. *J. Nucl. Med.*, 44:252–259, 2003.

[164] S. Nilsson, R. H. Larsen, S. D. Fosså, L. Balteskard, K. W. Borch, J.-E. Westlin, G. Salberg, and Ø. S. Bruland. First Clinical Experience with α-Emitting Radium-223 in the Treatment of Skeletal Metastases. *Clin. Cancer Res.*, 11:4451–4459, 2005.

[165] Ø. S. Bruland, S. Nilsson, D. R. Fisher, and R. H. Larsen. High-Linear Energy Transfer Irradiation Targeted to Skeletal Metastases by the α-Emitter ^{223}Radium: Adjuvant or Alternative to Conventional Modalities? *Clin. Cancer Res.*, 12:6250s–6257s, 2006.

[166] O. L. M. Bijvoet, H. A. Fleisch, R. E. Canfield, and R. G. G. Russell. Bisphosphonate on Bones. Elsevier Science B.V., Amsterdam, 1995. ISBN 0-444-89132-3.

[167] L. Widler, K. A. Jaeggi, M. Glatt, K. Müller, R. Bachmann, M. Bisping, A.-R. Born, R. Cortesi, G. Guiglia, H. Jeker, R. Klein, U. Ramseier, J. Schmid, G. Schreiber, Y. Seltenmeyer, and J. R. Green. Highly Potent Geminal Bisphosphonates. From Pamidronate Disodium (Aredia) to Zoledronic Acid (Zometa). *J. Med. Chem.*, 45:3721–3738, 2002.

[168] M. D. Michaelson and M. R. Smith. Bisphosphonates for Treatment and Prevention of Bone Metastases. *J. Clin. Oncol.*, 23:8219–8224, 2005.

[169] K. Libson, E. Deutsch, and B. L. Barnett. Structural Characterization of a ^{99}Tc-Diphosphonate Complex. Implications for the Chemistry of ^{99m}Tc Skeletal Imaging Agents. *J. Am. Chem. Soc.*, 102:2476–2478, 1980.

[170] J. R. Dilworth and S. J. Parrott. The biomedical chemistry of technetium and rhenium. *Chem. Soc. Rev.*, 27:43–55, 1998.

[171] M. Eisenhut. Iodine-131-Labeled Diphosphonates for the Palliative Treatment of Bone Metastases: I. Organ Distribution and Kinetics of I-131 BDP3 in Rats. *J. Nucl. Med.*, 25:1356–1361, 1984.

[172] M. Eisenhut, R. Berberich, B. Kimmig, and E. Oberhausen. Iodine-131-Labeled Diphosphonates for Palliative Treatment of Bone Metastases: II. Preliminary Clinical Results with Iodine-131 BDP3. *J. Nucl. Med.*, 27:1255–1261, 1986.

[173] M. Eisenhut, P. Fritz, B. Kimmig, F. Wingen, and B. Krempien. Iodine-131-Labeled Diphosphonates for the Palliative Treatment of Bone Metastases–III. Considerations of Interaction, Binding and Absorbed Dose. *Appl. Radiat. Isot.*, 37:741–747, 1986.

[174] M. Eisenhut, J. Barber, and D. M. Taylor. ^{131}I Labeled Diphosphonates for the Palliative Treatment of Bone Metastases–IV. Syntheses of Benzylidenediphosphonates and their Organ Distribution in Rats. *Appl. Radiat. Isot.*, 38:535–540, 1987.

[175] K. M. Murud. *Synthesis and preclinical evaluation of radiohalogenated aromatic amidobisphosphonates.* PhD thesis, Faculty of Mathematics and Natural Sciences, University of Oslo, Norway, 1999.

[176] R. H. Larsen, K. M. Murud, G. Akabani, P. Hoff, Ø. S. Bruland, and M. R. Zalutsky. ^{211}At- and ^{131}I-Labeled Biphosphonates with High In Vivo Stability and Bone Accumulation. *J. Nucl. Med.*, 40:1197–1203, 1999.

[177] E. Årstad. *Novel Bisphosphonates in Targeted Radiotherapy.* PhD thesis, Faculty of Mathematics and Natural Sciences, University of Oslo, Norway, 2001.

[178] E. Årstad, P. Hoff, L. Skattebøl, A. Skretting, and K. Breistøl. Studies on the Synthesis and Biological Properties of Non-Carrier-Added [^{125}I and ^{131}I]-Labeled Arylalkylidenebisphosphonates: Potent Bone-Seekers for Diagnosis and Therapy of Malignant Osseous Lesions. *J. Med. Chem.*, 46:3021–3032, 2003.

[179] A. Skretting, T. Bach-Gansmo, and P. Hoff. A method for movement correction based on a fixed optnumber of descending sorted pixels region of interest definition (Abstract). *Nuklearmedizin*, 6:A206–A207, 2006.

[180] A. Skretting. To be published, 2007.

[181] M. G. Stabin, R. B. Sparks, and E. Crowe. OLINDA/EXM: The Second-Generation Personal Computer Software for Internal Dose Assessment in Nuclear Medicine. *J. Nucl. Med.*, 46:1023–1027, 2005.

[182] ICRP Publication 89. Basic anatomical and physiological data for use in radiological protection: reference values. *Ann. ICRP*, 32:1–277, 2002.

Part IV

APPENDIX

Appendix A

Chemical abbreviations

Table A.1: Chemical abbreviations

Azure B	3-dimethylamino-7-methylaminophenothiazin-5-ylium chloride
$(BOC)_2O$	di-*tert*-butyl dicarbonate
Bu_3SnAr-OTFP	4-(tri-*n*-butylstannyl)benzoic acid-2,3,5,6-tetrafluorophenyl ester
Bu_3SnCl	tri-*n*-butyltin chloride
n-BuLi	*n*-butyllitium
Bu_6Sn_2	hexa-*n*-butyldistannane
$(CH_3)_3COK$	potassium *tert*-butoxide
DCC	*N,N'*-dicyclohexylcarbodiimide
4-DMAP	4-dimethylaminopyridine
DMF	*N,N*-dimethylformamide
DMSO	dimethylsulphoxide
DTPA	diethylenetriamine pentaacetic acid
EDC	*N*-(3-dimethylaminopropyl)-*N'*-ethylcarbodiimide hydrochloride
EDTMP	ethylene diamine tetramethylene phosphonate
HEDP	hydroxyethylidene diphosphonate
IAr-OTFP	4-iodobenzoic acid-2,3,5,6-tetrafluorophenyl ester
NCS	*N*-chlorosuccinimide
NHS	*N*-hydroxysuccinimide
PBS	phosphate buffered saline
Ph_3P	triphenylphosphine
$[Ph_3P]_4Pd$	tetrakis(triphenylphosphine)palladium(0)
TFA	trifluoroacetic acid
TFP-OH	2,3,5,6-tetrafluorophenol
THF	tetrahydrofuran
$Tl(TFA)_3$	thallium (III) trifluoroacetate

Appendix B

Glossary of radiochemical and medical terms

Table B.1: Glossary of radiochemical and medical terms

α-particle	a helium nucleus; $^4He^{2+}$
ad libitum	in accordance with desire
amelanotic	non-pigmented; do not produce melanin
amelanotic melanoma	a form of melanoma in which the malignant cells (melanocytes) do not synthesise the pigment melanin
β^--particle	an electron; e^-
β^+-particle	a positron; e^+
epidermis	the outermost layer of the skin
in situ	in position; in the natural or original position or place
in vivo	in the living; in the living body of a plant or animal
in vitro	in glass; outside the living body and in an artificial environment
LET	linear energy transfer; a measure of energy deposition from a charged particle to a medium per unit length
melanin	pigments present in animal or plant structures (as skin or hair); black, dark brown, reddish-brown or yellow
melanocyte	an epidermal cell which produces melanin
melanoma	a highly malignant tumour arising from melanocytes in normal skin or moles
melanosome	melanin-producing organelle found in the melanocytes
melanotic	pigmented; melanin-producing
melanogenesis	the formation of melanin; melanin synthesis
PET	positron emission tomography
RBE	relative biological effectiveness
SPECT	single photon emission computed tomography
xenografts	cells, tissues or organs which are transplanted from one species to another

Appendix C

Additional spectroscopic data

^{1}H- and ^{13}C-NMR spectra were recorded on a Bruker DPX 300 MHz instrument, and the chemical shifts were calibrated using the $CHCl_3$-signal. Electron ionisation mass spectrometry was performed on a Micromass Prospec Q instrument.

Aromatic activated tetrafluorophenyl esters

4-iodobenzoic acid-2,3,5,6-tetrafluorophenyl ester (18): ^{1}H-NMR ($CDCl_3$): δ 7.03 (m, 1 H, Ph$\mathbf{H}_4$); 7.90 (s, 4 H, Ph$\mathbf{H}_{2',3',5',6'}$). ^{13}C-NMR: δ 103.0 103.4 126.6 131.9 138.3 162.2. MS (EI): m/z 396 (M^+ not detected), 231 (100), 203 (20) and 104 (9).

4-tributylstannylbenzoic acid-2,3,5,6-tetrafluorophenyl ester (16): ^{1}H-NMR ($CDCl_3$): δ 0.8–1.6 (m, 27 H, -Sn($C_4\mathbf{H}_9$)$_3$); 7.01 (m, 1 H, Ph$\mathbf{H}_4$); 7.62 (d, 2 H, J = 9 Hz, Ph$\mathbf{H}_{3',5'}$); 8.08 (d, 2 H, J = 9 Hz, Ph$\mathbf{H}_{2',6'}$). ^{13}C-NMR: δ 9.8 13.8 27.4 29.1 129.4 136.8. MS (EI): m/z 559 (M^+ not detected), 503 (100), 447 (32), 391 (54), 196 (8), 161 (8), and 105 (18).

Brominated cysteaminylphenol derivatives

2-bromo-4-thiocyanatophenol (43): ^{1}H-NMR ($CDCl_3$): δ 5.8 (broad, 1 H, Ar-O**H**); 7.06 (d, 1 H, J = 9 Hz, Ph$\mathbf{H}_6$); 7.43 (dd, 1 H, J = 2 and 9 Hz, Ph$\mathbf{H}_5$); 7.71 (d, 1 H, J = 2 Hz, Ph$\mathbf{H}_3$). ^{13}C-NMR: δ 111.5 117.8 128.4 133.2 135.5 152.7. MS (EI): m/z 231 (M^+ 92), 229 (92), 150 (100), 122 (67) and 95 (19).

2,2'-dibromo-4,4'-dimercaptodiphenol (38): ^{1}H-NMR ($CDCl_3$): ^{1}H-NMR ($CDCl_3$): δ 5.6 (broad, 2 H, Ar-O**H**); 6.93 (d, 2 H, J = 9 Hz, Ph$\mathbf{H}_6$); 7.28 (dd, 2 H, J = 2 and 9 Hz, Ph$\mathbf{H}_5$); 7.56 (d, 2 H, J = 2 Hz, Ph$\mathbf{H}_3$). ^{13}C-NMR: δ 110.6 116.8 129.5 132.2 134.4 152.9. MS (EI): m/z 410 (M^+ 57), 408 (100), 406 (50), 205 (99), 204 (62), 203 (92), 125 (21), 124 (31) and 95 (31).

***N*-[2-(4-hydroxy-3-bromo-phenylsulphanyl)ethyl]acetamide (35):** ^{1}H-NMR ($CDCl_3$): δ 1.96 (s, 3 H, -NH(CO)C$\mathbf{H}_3$); 2.94 (t, 2 H, J = 7 Hz, -SC$\mathbf{H}_2$CH_2NH-); 3.40 (q, 2 H, J = 6 Hz, -SCH_2C$\mathbf{H}_2$NH-); 5.80 (broad, 1 H, Ar-O**H**); 6.94 (d, 1 H, J = 9 Hz, Ph$\mathbf{H}_5$); 7.27 (dd, 1 H, J = 2 and 9 Hz, Ph$\mathbf{H}_6$); 7.54 (d, 1 H, J = 2 Hz, Ph$\mathbf{H}_2$). ^{13}C-NMR: δ 23.2 35.5 38.6 111.0 116.8 127.5 133.0 135.3 152.3 170.4. MS (EI): m/z 291 (M^+ 9), 289 (8), 232 (100), 230 (98), 151 (77), 138 (14) and 86 (76).

Appendix D

Biodistribution data

Table D.1: Biodistribution data of **28b** and **32b** in normal Balb/c nude mice.

Organ	**0.5 h**[a]	**2 h**	**6 h**
28b			
Blood	2.0 ± 0.2	0.7 ± 0.4	0.38 ± 0.07
Eye	0.39 ± 0.03	-0.2 ± 0.8	0.04 ± 0.25
Muscle	0.6 ± 0.2	0.21 ± 0.08	0.2 ± 0.2
Lung	1.5 ± 0.2	1.3 ± 0.6	0.31 ± 0.06
Kidney	4.7 ± 0.9	0.6 ± 0.1	0.7 ± 0.7
Spleen	0.6 ± 0.1	0.4 ± 0.2	0.22 ± 0.05
Liver	8.6 ± 0.9	1.9 ± 1.0	0.32 ± 0.09
Stomach[b]	1.3 ± 0.9	4.9 ± 2.9	1.7 ± 0.3
Intestine[b]	4.7 ± 3.6	14.7 ± 0.4	4.7 ± 1.7
Urine	96.5 ± 56.6	43.2 ± 20.1	79.1 ± 23.1
Thyroid	1.2 ± 0.3	3.7 ± 2.0	3.3 ± 3.0
32b			
Blood	2.6 ± 0.1	1.3 ± 0.4	0.4 ± 0.2
Eye	0.57 ± 0.05	0.5 ± 0.2	0.18 ± 0.04
Muscle	0.6 ± 0.2	0.31 ± 0.07	0.1 ± 0.1
Lung	1.8 ± 0.2	1.4 ± 0.4	0.3 ± 0.1
Kidney	6.5 ± 0.5	1.09 ± 0.06	0.4 ± 0.3
Spleen	1.2 ± 0.3	0.8 ± 0.2	0.2 ± 0.1
Liver	4.3 ± 0.4	1.4 ± 0.7	0.16 ± 0.05
Stomach[b]	2.8 ± 1.3	6.5 ± 2.9	2.0 ± 0.8
Intestine[b]	3.8 ± 2.3	7.8 ± 1.4	0.5 ± 0.1
Urine	124.1 ± 79.1	80.7 ± 27.9	42.8 ± 14.3
Thyroid	3.4 ± 0.9	7.9 ± 3.2	4.9 ± 4.7

[a] Values are mean % ID/g ± SD (n = 4).

[b] Gastric and intestinal values include their contents.

Table D.2: Biodistribution data of **30b** and **33c** in normal Balb/c nude mice.

Organ	**0.5 h**[a]	**2 h**	**6 h**
30b			
Blood	1.8 ± 1.2	0.7 ± 0.2	0.2 ± 0.1
Eye	0.49 ± 0.08	-0.04 ± 0.54	-0.04 ± 0.19
Muscle	0.6 ± 0.1	0.22 ± 0.05	0.04 ± 0.02
Lung	4.8 ± 2.3	0.9 ± 0.4	0.27 ± 0.09
Kidney	3.4 ± 1.3	1.2 ± 0.3	0.9 ± 0.5
Spleen	0.8 ± 0.6	0.22 ± 0.05	0.07 ± 0.02
Liver	5.6 ± 1.3	7.0 ± 2.5	3.4 ± 0.6
Stomach[b]	8.5 ± 9.8	5.9 ± 3.6	0.5 ± 0.2
Intestine[b]	3.2 ± 0.9	6.0 ± 8.8	11.5 ± 4.7
Urine	168.2 ± 137.3	22.1 ± 26.9	49.6 ± 8.7
Thyroid	2.2 ± 0.3	1.1 ± 0.3	0.5 ± 0.4
33c			
Blood	3.4 ± 0.9	0.9 ± 0.2	0.3 ± 0.1
Eye	1.0 ± 0.2	0.5 ± 0.2	0.10 ± 0.03
Muscle	1.0 ± 0.1	0.26 ± 0.05	0.05 ± 0.01
Lung	4.1 ± 1.5	1.1 ± 0.2	0.3 ± 0.1
Kidney	6.5 ± 2.3	1.6 ± 0.4	0.8 ± 0.5
Spleen	1.3 ± 0.5	0.52 ± 0.04	0.14 ± 0.05
Liver	4.9 ± 1.3	3.4 ± 1.6	1.0 ± 0.2
Stomach[b]	7.4 ± 6.0	8.3 ± 2.2	1.6 ± 0.5
Intestine[b]	3.2 ± 0.7	5.7 ± 7.6	7.4 ± 2.8
Urine	352.9 ± 316.6	24.9 ± 29.8	41.2 ± 7.4
Thyroid	4.5 ± 0.5	5.9 ± 2.3	2.5 ± 2.1

[a] Values are mean % ID/g ± SD (n = 4).

[b] Gastric and intestinal values include their contents.

Table D.3: Biodistribution of **28b** and **29** in Balb/c nude mice bearing the melanotic melanoma xenograft HHMSX.

Organ	**0.5 h**[a]	**2 h**	**6 h**	**16 h**
28b				
Blood	0.103 ± 0.009	0.09 ± 0.03	0.016 ± 0.005	0.003 ± 0.001
Tumour	0.06 ± 0.03	0.06 ± 0.02	0.014 ± 0.006	0.004 ± 0.003
Muscle	0.04 ± 0.05	0.024 ± 0.008	0.007 ± 0.001	0.002 ± 0.003
Lung	0.16 ± 0.02	0.11 ± 0.03	0.017 ± 0.003	0.006 ± 0.002
Kidney	0.6 ± 0.2	0.2 ± 0.1	0.04 ± 0.01	0.009 ± 0.007
Spleen	0.07 ± 0.03	0.07 ± 0.03	0.009 ± 0.003	0.005 ± 0.003
Liver	0.7 ± 0.4	0.3 ± 0.2	0.029 ± 0.008	0.007 ± 0.002
Large intestine[b]	0.10 ± 0.02	1.2 ± 0.5	0.10 ± 0.07	0.009 ± 0.003
Urine	62.6 ± 41.9	15.2 ± 7.5	8.5 ± 5.0	0.6 ± 0.4
Thyroid	0.17 ± 0.03	0.3 ± 0.2	0.08 ± 0.04	0.004 ± 0.002
Stomach[b]	1.5 ± 0.7	1.2 ± 0.5	0.16 ± 0.08	0.015 ± 0.003
Skin	0.08 ± 0.01	0.10 ± 0.02	0.046 ± 0.007	0.010 ± 0.003
Tail	0.30 ± 0.06	0.17 ± 0.07	0.17 ± 0.05	0.05 ± 0.05
Eye	0.027 ± 0.009	0.04 ± 0.01	0.013 ± 0.004	0.011 ± 0.005
Heart	0.05 ± 0.02	0.05 ± 0.02	0.011 ± 0.002	0.002 ± 0.002
Femur	0.04 ± 0.02	0.04 ± 0.01	0.010 ± 0.009	0.000 ± 0.004
Brain	0.007 ± 0.001	0.005 ± 0.002	0.003 ± 0.002	0.001 ± 0.001
Small intestine[b]	4.4 ± 3.3	1.5 ± 1.2	0.2 ± 0.1	0.012 ± 0.003
29				
Blood	1.39 ± 0.08	1.2 ± 0.2	0.6 ± 0.2	0.4 ± 0.1
Tumour	1.7 ± 0.4	2.3 ± 0.4	1.5 ± 0.4	0.7 ± 0.2
Muscle	0.59 ± 0.05	0.7 ± 0.1	0.37 ± 0.08	0.15 ± 0.05
Lung	9.5 ± 1.3	8.9 ± 1.7	5.0 ± 1.5	2.5 ± 0.8
Kidney	4.4 ± 0.2	4.1 ± 0.2	2.1 ± 0.5	1.0 ± 0.4
Spleen	7.5 ± 0.4	8.1 ± 2.1	3.7 ± 0.5	2.2 ± 0.6
Liver	1.5 ± 0.1	1.5 ± 0.3	0.8 ± 0.2	0.4 ± 0.1
Large intestine[b]	1.8 ± 0.4	2.5 ± 0.6	0.9 ± 0.2	0.5 ± 0.1
Urine	32.7 ± 25.0	7.8 ± 2.7	24.8 ± 5.9	5.2 ± 0.9
Thyroid	6.0 ± 0.4	8.9 ± 2.5	6.6 ± 1.6	2.0 ± 0.6
Stomach[b]	14.8 ± 7.4	14.9 ± 5.2	12.7 ± 3.4	5.6 ± 1.3
Skin	2.7 ± 0.2	2.8 ± 0.2	1.8 ± 0.8	1.2 ± 0.3
Tail	2.3 ± 0.1	2.0 ± 0.1	1.5 ± 0.5	0.7 ± 0.2
Eye	0.89 ± 0.05	0.9 ± 0.2	0.5 ± 0.2	0.2 ± 0.2
Heart	2.9 ± 0.4	2.9 ± 0.4	1.5 ± 0.4	0.7 ± 0.2
Femur	1.4 ± 0.1	1.4 ± 0.3	0.7 ± 0.2	0.5 ± 0.2
Brain	0.27 ± 0.04	0.22 ± 0.02	0.14 ± 0.07	0.04 ± 0.04
Small intestine[b]	2.7 ± 0.4	2.5 ± 0.6	1.1 ± 0.3	0.6 ± 0.2

[a] Values are mean % ID/g ± SD (n = 4).

[b] Gastric and intestinal values include their contents.

Table D.4: Biodistribution of **30b** and **31** in Balb/c nude mice bearing the melanotic melanoma xenograft HHMSX.

Organ	**0.5 h**[a]	**2 h**	**6 h**	**16 h**
30b				
Blood	0.26 ± 0.03	0.08 ± 0.01	0.023 ± 0.006	0.004 ± 0.001
Tumour	0.17 ± 0.02	0.069 ± 0.008	0.023 ± 0.007	0.010 ± 0.004
Muscle	0.071 ± 0.005	0.025 ± 0.008	0.006 ± 0.003	0.002 ± 0.002
Lung	0.21 ± 0.02	0.06 ± 0.01	0.020 ± 0.001	0.007 ± 0.002
Kidney	0.9 ± 0.2	0.29 ± 0.08	0.12 ± 0.03	0.017 ± 0.003
Spleen	0.088 ± 0.003	0.046 ± 0.009	0.02 ± 0.01	0.005 ± 0.002
Liver	1.4 ± 0.2	1.1 ± 0.3	0.4 ± 0.2	0.043 ± 0.009
Large intestine[b]	0.22 ± 0.08	2.6 ± 1.5	0.6 ± 0.2	0.06 ± 0.03
Urine	55.5 ± 28.0	51.7 ± 18.2	14.1 ± 2.8	0.38 ± 0.09
Thyroid	0.20 ± 0.03	0.11 ± 0.03	0.03 ± 0.01	0.004 ± 0.002
Stomach[b]	0.6 ± 0.3	0.7 ± 0.4	0.2 ± 0.2	0.01 ± 0.01
Skin	0.23 ± 0.04	0.06 ± 0.01	0.028 ± 0.005	0.02 ± 0.01
Tail	1.1 ± 0.7	0.3 ± 0.2	0.16 ± 0.09	0.11 ± 0.08
Eye	0.05 ± 0.02	0.017 ± 0.007	0.000 ± 0.008	-0.003 ± 0.003
Heart	0.17 ± 0.02	0.045 ± 0.004	0.016 ± 0.006	0.003 ± 0.002
Femur	0.06 ± 0.01	0.024 ± 0.006	0.004 ± 0.008	0.001 ± 0.004
Brain	0.031 ± 0.006	0.009 ± 0.005	0.003 ± 0.001	0.001 ± 0.001
Small intestine[b]	7.4 ± 0.8	2.3 ± 0.8	1.1 ± 0.4	0.03 ± 0.02
31				
Blood	1.0 ± 0.2	0.8 ± 0.1	0.6 ± 0.2	0.49 ± 0.06
Tumour	0.7 ± 0.4	2.4 ± 0.7	1.7 ± 1.0	-0.5 ± 2.6
Muscle	0.3 ± 0.4	0.4 ± 0.2	0.3 ± 1.0	ND[c]
Lung	10.2 ± 4.7	10.1 ± 4.0	8.8 ± 5.8	5.6 ± 3.7
Kidney	2.7 ± 0.9	3.8 ± 1.4	3.8 ± 0.7	1.7 ± 0.6
Spleen	4.8 ± 2.2	10.3 ± 5.3	7.3 ± 2.2	5.6 ± 3.6
Liver	1.7 ± 0.5	1.1 ± 0.2	1.3 ± 0.4	0.8 ± 0.4
Large intestine[b]	1.0 ± 0.3	2.7 ± 0.9	1.9 ± 0.7	1.1 ± 0.3
Urine	47.1 ± 23.7	39.3 ± 33.9	55.8 ± 21.3	13.0 ± 2.9
Thyroid	3.3 ± 0.8	6.3 ± 1.2	12.5 ± 6.6	5.6 ± 3.8
Stomach[b]	8.9 ± 2.2	26.7 ± 14.4	18.4 ± 4.6	9.8 ± 6.3
Skin	1.6 ± 0.6	2.2 ± 1.1	2.9 ± 1.1	2.5 ± 0.7
Tail	2.8 ± 0.8	1.9 ± 0.9	1.6 ± 0.3	0.8 ± 0.2
Eye	-0.2 ± 0.6	-0.2 ± 0.8	-0.2 ± 1.2	ND
Heart	1.6 ± 0.3	3.1 ± 1.2	2.6 ± 1.1	ND
Femur	0.9 ± 0.6	1.7 ± 0.6	1.3 ± 1.9	ND
Brain	0.2 ± 0.2	0.2 ± 0.1	0.2 ± 0.4	ND
Small intestine[b]	5.5 ± 0.6	1.8 ± 0.4	1.2 ± 0.4	0.9 ± 0.3

[a] Values are mean % ID/g ± SD (n = 4).

[b] Gastric and intestinal values include their contents.

[c] ND = not detected.

Table D.5: Biodistribution of **32b** in Balb/c nude mice bearing the melanotic melanoma xenograft HHMSX.

Organ	**0.5 h**[a]	**2 h**	**6 h**	**16 h**
32b				
Blood	0.04 ± 0.02	0.04 ± 0.02	0.003 ± 0.001	0.002 ± 0.008
Tumour	0.05 ± 0.02	0.04 ± 0.02	0.005 ± 0.004	0.007 ± 0.001
Muscle	0.02 ± 0.02	0.009 ± 0.004	-0.001 ± 0.009	-0.004 ± 0.017
Lung	0.03 ± 0.01	0.05 ± 0.02	-0.002 ± 0.004	-0.001 ± 0.012
Kidney	0.14 ± 0.04	0.11 ± 0.05	-0.001 ± 0.007	-0.004 ± 0.008
Spleen	0.03 ± 0.03	0.03 ± 0.02	0.003 ± 0.007	0.000 ± 0.003
Liver	0.15 ± 0.06	0.12 ± 0.05	0.001 ± 0.001	0.001 ± 0.003
Large intestine[b]	0.08 ± 0.06	0.10 ± 0.06	0.01 ± 0.02	-0.008 ± 0.011
Urine	70.9 ± 14.2	6.7 ± 4.2	0.3 ± 0.3	0.7 ± 0.8
Thyroid	0.06 ± 0.03	0.13 ± 0.09	0.005 ± 0.016	0.06 ± 0.06
Stomach[b]	0.5 ± 0.4	0.3 ± 0.2	0.02 ± 0.01	0.03 ± 0.03
Skin	0.04 ± 0.02	0.03 ± 0.02	0.009 ± 0.005	0.006 ± 0.008
Tail	0.10 ± 0.03	0.07 ± 0.03	0.008 ± 0.007	0.021 ± 0.008
Eye	0.02 ± 0.05	-0.005 ± 0.036	-0.003 ± 0.045	0.005 ± 0.037
Heart	0.02 ± 0.02	0.02 ± 0.02	0.002 ± 0.010	0.005 ± 0.010
Femur	-0.004 ± 0.026	0.03 ± 0.02	0.006 ± 0.006	0.01 ± 0.03
Brain	0.002 ± 0.004	0.005 ± 0.007	0.000 ± 0.003	0.001 ± 0.002
Small intestine[b]	0.6 ± 0.5	0.2 ± 0.1	0.006 ± 0.007	0.001 ± 0.006

[a] Values are mean % ID/g ± SD (n = 4).

[b] Gastric and intestinal values include their contents.

Table D.6: Biodistribution of **33b** and **53** in Balb/c nude mice bearing the melanotic melanoma xenograft HHMSX.

Organ	**0.5 h**[a]	**2 h**	**6 h**	**16 h**
33b				
Blood	0.8 ± 0.1	0.4 ± 0.1	0.04 ± 0.01	0.07 ± 0.04
Tumour	0.7 ± 0.4	0.24 ± 0.07	0.03 ± 0.01	0.05 ± 0.03
Muscle	0.23 ± 0.07	0.08 ± 0.02	0.013 ± 0.006	0.03 ± 0.05
Lung	0.7 ± 0.1	0.7 ± 0.4	0.08 ± 0.02	0.11 ± 0.02
Kidney	2.9 ± 1.3	1.5 ± 0.7	0.14 ± 0.02	0.3 ± 0.1
Spleen	0.6 ± 0.3	0.3 ± 0.1	0.02 ± 0.01	0.05 ± 0.03
Liver	3.5 ± 1.1	2.0 ± 0.6	0.16 ± 0.04	0.31 ± 0.06
Large intestine[b]	3.1 ± 2.6	11.2 ± 3.5	1.6 ± 0.9	3.2 ± 1.4
Urine	312.9 ± 51.1	33.6 ± 15.3	8.0 ± 1.1	11.5 ± 3.3
Thyroid	1.3 ± 0.3	1.2 ± 0.2	0.2 ± 0.1	0.6 ± 0.6
Stomach[b]	9.0 ± 5.6	4.4 ± 2.2	0.2 ± 0.1	0.5 ± 0.3
Skin	0.6 ± 0.1	0.4 ± 0.1	0.06 ± 0.02	0.10 ± 0.05
Tail	1.3 ± 0.3	0.6 ± 0.1	0.23 ± 0.08	0.21 ± 0.04
Eye	0.27 ± 0.07	0.16 ± 0.04	0.03 ± 0.06	0.02 ± 0.04
Heart	0.5 ± 0.1	0.21 ± 0.06	0.03 ± 0.01	0.03 ± 0.03
Femur	0.3 ± 0.1	0.2 ± 0.1	0.01 ± 0.01	0.02 ± 0.03
Brain	0.081 ± 0.007	0.04 ± 0.02	0.007 ± 0.004	0.008 ± 0.001
Small intestine[b]	12.2 ± 10.8	5.6 ± 3.9	0.4 ± 0.2	1.7 ± 0.3
53				
Blood	1.1 ± 0.2	1.2 ± 0.3	0.56 ± 0.03	0.6 ± 0.2
Tumour	1.6 ± 0.7	2.0 ± 0.5	1.2 ± 0.2	1.0 ± 0.4
Muscle	0.5 ± 0.2	0.56 ± 0.05	0.29 ± 0.05	0.4 ± 0.3
Lung	6.9 ± 3.3	6.8 ± 3.3	4.2 ± 0.4	4.5 ± 0.5
Kidney	4.1 ± 0.9	4.8 ± 2.2	1.7 ± 0.2	2.1 ± 0.5
Spleen	5.3 ± 2.2	6.3 ± 1.5	3.4 ± 0.2	3.9 ± 1.1
Liver	3.1 ± 0.9	2.1 ± 0.4	0.81 ± 0.06	0.9 ± 0.2
Large intestine[b]	3.3 ± 3.3	6.1 ± 2.5	1.6 ± 1.3	1.8 ± 0.8
Urine	285.9 ± 102.0	28.9 ± 10.7	15.6 ± 4.6	16.9 ± 9.1
Thyroid	4.4 ± 1.5	6.9 ± 1.3	5.2 ± 2.0	12.9 ± 9.1
Stomach[b]	12.8 ± 5.5	13.9 ± 2.7	9.8 ± 2.9	10.8 ± 4.6
Skin	2.1 ± 0.7	2.7 ± 0.5	1.7 ± 0.3	2.3 ± 0.4
Tail	2.5 ± 0.8	2.2 ± 0.2	1.3 ± 0.2	1.6 ± 0.3
Eye	0.7 ± 0.2	0.7 ± 0.2	0.48 ± 0.06	0.5 ± 0.1
Heart	2.2 ± 0.7	2.7 ± 0.6	1.22 ± 0.05	1.3 ± 0.4
Femur	1.1 ± 0.3	1.4 ± 0.7	0.61 ± 0.03	0.8 ± 0.4
Brain	0.19 ± 0.06	0.21 ± 0.07	0.12 ± 0.03	0.08 ± 0.02
Small intestine[b]	8.3 ± 7.9	3.2 ± 0.9	1.0 ± 0.1	1.2 ± 0.3

[a] Values are mean % ID/g ± SD (n = 4).

[b] Gastric and intestinal values include their contents.

Table D.7: Biodistribution of **14b** and **54** in Balb/c nude mice bearing the melanotic melanoma xenograft HHMSX.

Organ	**0.5 h**[a]	**2 h**[a]	**6 h**[b]	**16 h**[b]
14b				
Blood	0.5 ± 0.1	0.14 ± 0.03	0.014 ± 0.002	0.005 ± 0.001
Tumour	0.8 ± 0.2	0.5 ± 0.1	0.15 ± 0.09	0.06 ± 0.02
Muscle	0.35 ± 0.07	0.05 ± 0.03	0.003 ± 0.004	0.002 ± 0.002
Lung	1.2 ± 0.2	0.18 ± 0.03	0.022 ± 0.007	0.006 ± 0.001
Kidney	2.4 ± 0.5	0.60 ± 0.08	0.05 ± 0.03	0.013 ± 0.005
Spleen	0.8 ± 0.2	0.09 ± 0.02	0.011 ± 0.004	0.004 ± 0.003
Liver	2.3 ± 0.4	0.42 ± 0.04	0.08 ± 0.02	0.03 ± 0.01
Large intestine[c]	2.1 ± 1.1	3.4 ± 2.2	0.3 ± 0.2	0.008 ± 0.001
Urine	183.1 ± 109.1	107.6 ± 15.0	20.5 ± 18.4	0.10 ± 0.03
Thyroid	1.5 ± 0.3	0.4 ± 0.1	0.04 ± 0.02	0.004 ± 0.001
Stomach[c]	1.7 ± 1.5	0.6 ± 0.1	0.05 ± 0.02	0.006 ± 0.002
Skin	0.7 ± 0.1	0.20 ± 0.04	0.028 ± 0.007	0.007 ± 0.004
Tail	1.7 ± 0.5	0.5 ± 0.2	0.14 ± 0.08	0.2 ± 0.2
Eye	0.24 ± 0.04	0.05 ± 0.02	0.008 ± 0.003	0.003 ± 0.005
Heart	0.5 ± 0.1	0.098 ± 0.005	0.009 ± 0.002	0.004 ± 0.002
Femur	0.4 ± 0.1	0.07 ± 0.02	0.004 ± 0.004	0.003 ± 0.004
Brain	0.21 ± 0.06	0.023 ± 0.005	0.002 ± 0.001	0.001 ± 0.001
Small intestine[c]	3.1 ± 2.6	0.6 ± 0.4	0.05 ± 0.02	0.007 ± 0.002
54				
Blood	1.04 ± 0.09	0.6 ± 0.2	0.48 ± 0.08	0.29 ± 0.09
Tumour	0.9 ± 0.7	0.9 ± 0.4	0.4 ± 0.3	0.4 ± 0.2
Muscle	0.6 ± 0.2	0.18 ± 0.09	0.2 ± 0.1	0.1 ± 0.1
Lung	5.5 ± 2.9	2.8 ± 0.9	3.8 ± 2.3	2.0 ± 0.9
Kidney	3.8 ± 0.6	2.1 ± 1.0	1.23 ± 0.8	0.9 ± 0.3
Spleen	3.4 ± 0.9	3.8 ± 1.5	2.5 ± 0.9	1.9 ± 0.9
Liver	2.2 ± 0.2	0.8 ± 0.3	0.6 ± 0.2	0.30 ± 0.03
Large intestine[c]	2.4 ± 1.6	2.5 ± 0.6	0.5 ± 0.1	0.5 ± 0.1
Urine	137.0 ± 70.4	149.1 ± 27.6	28.1 ± 17.2	5.0 ± 1.5
Thyroid	4.9 ± 3.4	3.4 ± 2.0	2.3 ± 0.8	1.1 ± 0.2
Stomach[c]	4.3 ± 4.0	11.2 ± 5.4	5.0 ± 1.3	4.4 ± 1.3
Skin	2.2 ± 1.0	2.0 ± 0.5	1.3 ± 0.5	1.1 ± 0.6
Tail	3.0 ± 1.7	1.2 ± 0.3	0.9 ± 0.2	0.6 ± 0.2
Eye	0.7 ± 0.4	0.5 ± 0.3	0.43 ± 0.05	0.3 ± 0.3
Heart	1.2 ± 0.3	1.9 ± 0.9	0.8 ± 0.1	0.9 ± 0.5
Femur	0.6 ± 0.3	0.5 ± 0.2	0.4 ± 0.1	0.4 ± 0.1
Brain	0.2 ± 0.2	0.16 ± 0.05	0.10 ± 0.06	0.10 ± 0.03
Small intestine[c]	2.5 ± 2.2	1.1 ± 0.2	0.71 ± 0.08	0.6 ± 0.2

[a] Values are mean % ID/g ± SD (n = 4).

[b] Values are mean % ID/g ± SD (n = 3).

[c] Gastric and intestinal values include their contents.

Table D.8: Biodistribution of **14b** and **54** in Balb/c nude mice bearing the amelanotic melanoma xenograft SESX.

Organ	**1 h**[a]	**4 h**	**16 h**
14b			
Blood	0.5 ± 0.1	0.05 ± 0.02	0.011 ± 0.001
Skin	1.1 ± 0.4	0.09 ± 0.02	0.022 ± 0.005
Heart	0.7 ± 0.7	0.03 ± 0.01	0.008 ± 0.003
Lung	0.6 ± 0.2	0.056 ± 0.005	0.018 ± 0.006
Liver	2.3 ± 0.5	0.26 ± 0.04	0.103 ± 0.004
Kidney	1.2 ± 0.9	0.15 ± 0.03	0.052 ± 0.004
Spleen	0.4 ± 0.1	0.032 ± 0.006	0.010 ± 0.003
Stomach[b]	6.4 ± 7.3	0.3 ± 0.1	0.02 ± 0.01
Small intestine[b]	7.5 ± 4.1	0.34 ± 0.02	0.03 ± 0.01
Eye	0.2 ± 0.1	0.001 ± 0.002	0.002 ± 0.004
Tumour	1.0 ± 0.3	0.47 ± 0.07	0.095 ± 0.006
Muscle	0.2 ± 0.1	0.02 ± 0.01	0.000 ± 0.000
Femur	0.2 ± 0.1	0.04 ± 0.04	0.001 ± 0.002
Urine	–	–	0.11 ± 0.09
Large intestine[b]	4.7 ± 4.5	1.2 ± 0.6	0.02 ± 0.02
54			
Blood	0.5 ± 0.1	0.24 ± 0.08	0.10 ± 0.04
Skin	1.7 ± 0.4	0.7 ± 0.2	0.3 ± 0.1
Heart	1.2 ± 0.2	0.6 ± 0.1	0.23 ± 0.04
Lung	2.5 ± 1.9	1.1 ± 0.4	0.8 ± 0.1
Liver	1.6 ± 0.3	0.62 ± 0.02	0.210 ± 0.009
Kidney	2.0 ± 0.9	1.1 ± 0.3	0.42 ± 0.05
Spleen	3.7 ± 1.0	2.0 ± 0.7	0.8 ± 0.2
Stomach[b]	4.7 ± 3.1	3.2 ± 0.8	1.2 ± 0.4
Small intestine[b]	4.1 ± 2.1	0.48 ± 0.05	0.17 ± 0.05
Eye	0.3 ± 0.1	0.11 ± 0.02	0.05 ± 0.04
Tumour	1.3 ± 0.4	0.66 ± 0.07	0.15 ± 0.06
Muscle	0.4 ± 0.1	0.20 ± 0.09	0.04 ± 0.02
Femur	0.5 ± 0.2	0.29 ± 0.08	0.13 ± 0.03
Urine	–	–	1.3 ± 0.6
Large intestine[b]	3.5 ± 1.8	0.64 ± 0.08	0.2 ± 0.1

[a] Values are mean % ID/g ± SD (n = 3).

[b] Gastric and intestinal values include their contents.

List of Figures

List of Tables